MONITEQ

Monitoring Environmental Quality
Moniteq Ltd., 630 Rivermede Road, Concord, Ontario, Canada L4K 2H7 (416) 669-5334 Telex: 06-964776

FEASIBILITY OF USING GASPILS AND OTHER METHODS OF REMOTELY MEASURING METHANE IN COAL MINES AND PREPARATION OF A CONCEPTUAL DESIGN FOR A SUITABLE INSTRUMENT (UP-M-513)

FINAL REPORT
DSS Contract #14SQ.23440-4-9278

Prepared for:

CANMET, Energy, Mines & Resources
Cape Breton Coal Research Lab
210 George Street
Sydney, Nova Scotia
B1P 1J3

CONTRACT SERIAL NUMBER: 1SQ85-00021

REQUISITION NUMBER 23440-4-9278

CONTRACTOR: MONITEQ Ltd.

TR 86-135
April 1986

136 pp

MICROMEDIA
AUG 15 1986

TABLE OF CONTENTS

EXECUTIVE SUMMARY

1.0 INTRODUCTION.. 1-1

1.1 Remote Detection Techniques........................... 1-1

  1.1.1 Raman Scattering.................................. 1-1
  1.1.2 Absorption Techniques............................. 1-2

1.2 Systems for Remote Detection of Methane............... 1-2

  1.2.1 USBM: Raman Scattering............................ 1-2
  1.2.2 Westinghouse: Differential Absorption............. 1-3
  1.2.3 Homer Research Lab: Differential Absorption.. 1-3
  1.2.4 MONITEQ Ltd.: Gas Filter Correlation.............. 1-3

2.0 DEPLOYMENT SCENARIOS.................................. 2-1

2.1 System Requirements................................... 2-1

2.2 Path Averaged Techniques.............................. 2-2

2.3 Triangulation Techniques.............................. 2-2

2.4 Time of Flight Techniques............................. 2-3

3.0 DIFFERENTIAL ABSORPTION............................... 3-1

3.1 Path Averaged Sensors................................. 3-1

3.2 Stability Requirements................................ 3-1

3.3 Range Resolved DIAL S/N Analyses...................... 3-3

4.0 RAMAN TECHNIQUES 4-1

4.1 Theory and Required Signal to Noise Level 4-1

- 4.1.1 Signal Level 4-1
- 4.1.2 Effect of Background 4-2
- 4.1.3 Signal to Noise Ratio Requirements in the Absence of Background 4-3
- 4.1.4 Calibration 4-4

4.2 Laser Source 4-4

4.3 System Performance - Signal Levels and Signal to Noise Ratio Calculations 4-7

- 4.3.1 Methane 4-7
- 4.3.2 Nitrogen 4-8

4.4 System Performance versus Laser Figure of Merit 4-8

- 4.4.1 Requirements of the Laser 4-8

4.5 Size and Efficiency of Laser Sources 4-10

- 4.5.1 Commercial 4-10
- 4.5.2 Future Sources 4-11

5.0 OPTICAL INSTRUMENTATION CONCEPTS 5-1

5.1 Optical Overview 5-1

5.2 Range Response Function 5-2

5.3 Colour Separation and Stray Light 5-4

- 5.3.1 Laser Rejection Requirement 5-5
- 5.3.2 Interference Filters 5-6
- 5.3.3 Long Pass Filters 5-7
- 5.3.4 Angle of Incidence Effect 5-7
- 5.3.5 Recommendation 5-8

5.4 Other Sources of Stray Light 5-8

- 5.4.1 Ambient Light 5-8
- 5.4.2 Fluorescence in Coal Dust 5-8

5.5 Detector Selection 5-9

5.6 Receiver Focal Length 5-10

6.0 ELECTRONICS SUBSYSTEM.............................. 6-1

6.1 Electronics Overview................................ 6-1

6.2 System Accuracy and Dynamic Range Requirements........ 6-2

6.3 Time Resolution Requirements........................ 6-4

6.4 Digitizer Recommendations........................... 6-5

  6.4.1 Commercial Transient Recorders................ 6-6
  6.4.2 Custom Digitizer Implementation............... 6-7
  6.4.3 Custom Design - Power, Size Requirements...... 6-8
  6.4.4 Summary....................................... 6-8

6.5 Synchronization..................................... 6-8

7.0 RECOMMENDATIONS FOR FURTHER WORK..................... 7-1

7.1 System Specifications and Implementation............. 7-2

APPENDIX 1: Description of Program Used for SNR Calculation

APPENDIX 2: Summary of Opto-Electronics Ltd. Photodiodes

APPENDIX 3: Long Pass Filter Characteristics

APPENDIX 4: Collected Literature Separate Volume

REFERENCES

LIST OF TABLES

1.1 Comparison of Cross-Sections of Different Processes for Methane at S.T.P........................ 1-5

1.2 Methane Cross-Sections Relative to Q Branch of Nitrogen Fundamental................................ 1-5

1.3 Methane Absorption Coefficients.......................... 1-5

2.1 Design Goals... 2-4

2.2 Summary of Key Instrument Requirements................ 2-5

3.1 Path Averaged Performance Extrapolation.............. 3-6

3.2 Change in Detector Power vs Range and Concentration... 3-7

4.1 Instrumental Parameters for a Raman Methanometer...... 4-12

4.2 Reduction in Signal to Noise Ratio due to Background.. 4-12

4.3 Alternative Signal to Noise Ratio Requirements for the Desired System.............................. 4-13

4.4 Summary of Available Lasers and Sources.............. 4-14

4.5 Laser Figure of Merit at the Maximum Permissible Exposure.................................... 4-16

4.6 Laser Figure of Merit for Selected Lasers............. 4-17

4.7 Commercial Laser Efficiency............................ 4-18

5.1 Rejection Ratio for Methane versus Atmospheric Transmittance........................... 5-11

5.2 Rejection Ratio for Nitrogen versus Atmospheric Transmittance........................... 5-12

5.3 Filter Centre Wavelengths and Absorptive Filters...... 5-13

5.4 Wavelength Shift versus Cone Angle.................... 5-14

5.5 Hamamatsu Photomultiplier Tubes....................... 5-14

5.6 Effective Focal Length................................. 5-15

6.1 Detailed Signal Estimates.................................. 6-9
6.2 Response Time and Sampling Rate.......................... 6-11
6.3 Commercial Transient Recorders and Digital Oscilloscopes.......................... 6-12
6.4 Custom Digitizer Designs Power Consumption and Size.................................. 6-13
7.1 System Performance.................................. 7-4
7.2 Optical System Components.................................. 7-5
7.3 Detector Specifications.................................. 7-7
7.4 Electronics Specification.................................. 7-7

LIST OF FIGURES

1.1 Averaged Relative Normalized Differential Raman Scattering Cross-Sections for Important Gases as Function of Raman Wavenumber Shift................ 1-6

1.2 Measured Absorption Spectra and Their Assignment of the 2 3 Overtone Band of CH4 Molecules in the 1.63-1.69 um Region at 60 Torr Pressure.......... 1-6

1.3 Measured Absorption Spectra and Their Assignment of the 2 + 2 3 Combination Band of CH4 Molecules in the 1.31-1.35 um Region at 300 Torr Pressure... 1-7

1.4 Transmission of the Atmosphere from 0.2 to 15 um...... 1-7

2.1 Schematic Diagram of a Triangulation System........... 2-6

2.2 Schematic Diagram of a Depth Resolved Collinear System... 2-6

4.1 Schematic Diagram of the Transmitter/Receiver Aperture... 4-19

4.2 Reduction of MPE for Repetitively Pulsed or Multiple Exposures from Scanning Lasers, Individual Pulse or Exposure Less than 10 us......... 4-20

4.3 Signal and Signal to Noise Ratio (SNR) versus Range for Methane..................................... 4-21

4.4 Signal and Signal to Noise Ratio (SNR) versus Methane Concentration............................... 4-22

4.5 Signal and Signal to Noise Ratio (SNR) versus Range for Nitrogen.................................... 4-23

4.6 System Performance versus Laser Figure of Merit....... 4-24

4.7 Schematic Diagram of Laser Diode Pumped Nd:YAG Laser... 4-26

5.1 Overview of a Typical Optical System.................. 5-16

5.2 Zones of Different Range Response..................... 5-17

5.3 Normalized Range Response............................. 5-18

5.4 Alternate Interference Filter Deployment Scenarios.... 5-19

5.5 Raman Notch Filter.................................. 5-20

5.6 Fluorescence from Coal.............................. 5-21

5.7 Quantum Efficiency and Radiant Response of Photocathodes.................................. 5-22

6.1 Electronics System Block Diagram.................... 6-14

6.2 Response to Two Gaussian Gas Plumes................. 6-15

EXECUTIVE SUMMARY

In Phase I of this work, various techniques and technologies which could be applied to the remote sensing of methane in underground coal mines were examined. Use of remote sensing systems is advantageous in an underground mining environment as they would allow an operator to measure methane concentrations in areas in which access with an in-situ sampler is either impossible or requires the use of cumbersome extension probes.

The Phase I report examined a number of techniques which are being investigated by several institutes for the remote measurement of methane. The systems were evaluated with respect to their capabilities in each of three key areas. These being:

a) portability,

b) ability to measure over the desired concentration range, and

c) the ability to range resolve the concentration data.

The report concluded that none of the systems which were being developed were capable, in the short term, of meeting the specifications in all three of the key areas. The report did, however, identify the differential absorption and Raman scattering techniques as having the greatest potential for the desired application. A summary of the Phase I work has been included in this report.

In this second phase, the differential absorption and Raman scattering techniques are examined in greater depth. The analysis of the differential absorption technique showed that non-range resolved systems were incapable of achieving the desired concentration and range specifications. Since the performance of a range resolved system will be poorer, this technique was determined to be unsuitable for methane detection in an underground coal mine. On the other hand, an analysis of the Raman scattering technique illustrates that the desired concentration and ranging requirements can be achieved. A conceptual design based on the Raman technique is presented. The availability of a suitable UV source is critical. Unfortunately, commercially available sources with sufficient output power are relatively large and do not meet the key requirement of system portability. Furthermore, it is unlikely that these commercial sources will undergo a substantial reduction in size in the foreseeable future. Recent developments such as the diode pumped Nd:YAG laser, however, do offer promise for compact and powerful sources in the near future.

The optical system requirements depend on colour separation, that is the rejection of radiation at the laser wavelength. The use of a dielectric long pass cut on filter, in series with bandpass filters at the Raman wavelengths, is recommended.

The most stringent requirement for the design of the electronics subsystem is the rapid signal processing necessitated by a time of flight measurement technique. Range resolving the concentration data within one metre requires that the return signal be digitally sampled at the rate of 4 to 6 ns. For an experimental laboratory system a digital oscilloscope is recommended.

Specifications for a Raman based methanometer are presented. A recommendation is made to develop a system based on a diode pumped Nd:YAG system.

SOMMAIRE

Au cours de la Phase I des travaux, plusieurs techniques et technologies qui pourraient s'appliquer à la télédétection des émissions de méthane dans les mines de charbon souterraines ont été étudiées. L'emploie des systèmes de télédétection dans le milieu minier souterrain est avantageux puisqu'ils permettraient à un opérateur de mesurer les concentrations de méthane dans les endroits où l'accès avec un échantillonneur in-situ est soit impossible, ou nécessite l'utilisation de sondes rallongées encombrantes.

Le rapport sur la Phase I présente un certain nombre de techniques de télédétection du méthane qui font présentement l'objet d'études dans plusieurs instituts. Les systèmes ont été évalués quant à leur capacité dans chacun des trois domaines clefs suivants:

a) capacité d'être portable;

b) capacité de mesurer au-delà de l'intervalle de variation de la concentration souhaitée; et

c) la capacité de déterminer le taux de concentration en fonction de la distance de la ligne de visée à l'aide des données de concentration.

On en est arrivé à la conclusion dans le présent rapport qu'aucun des systèmes mis au point n'a été capable, à court terme, de remplir les spécifications désirées dans les trois domaines clefs. Toutefois, les techniques d'absorption différentielle et de diffusion Raman ont été identifiées comme étant les techniques qui offrent le plus de potentiel pour l'utilisation recherchée. Un résumé des travaux de la Phase I est présenté dans ce rapport.

Au cours de cette deuxième phase, les techniques d'absorption différentielle et de diffusion Raman sont étudiées plus à fond. L'étude de la technique d'absorption différentielle a démontré que les systèmes, n'ayant pas la capacité de déterminer le taux de concentration en fonction de la distance de

la ligne de visée, étaient incapables d'atteindre les spécifications de concentration et de calibrage souhaitées. Puisque le rendement d'un système capable de déterminer le taux de concentration en fonction de la distance de la ligne de visée serait moins efficace, cette technique a été jugée peu appropriée à la détection du méthane dans une mine de charbon souterraine. Toutefois, l'étude de la technique de diffusion Raman démontre que les spécifications de concentration et de calibrage souhaitées peuvent être atteintes. Un plan conceptuel basé sur la technique de Raman est aussi présenté dans ce rapport. Il est important d'avoir une source adéquate de UV disponible. Malheureusement, les sources disponibles dans le commerce avec suffisamment de puissance d'émission sont d'une taille relativement importante et ne satisfont pas à l'une des exigences clefs, soit d'être portatif. Par ailleurs, il est peu probable que ces sources commerciales puissent subir une réduction importante de leur taille dans un avenir prévisible. Les derniers développements technologiques visant à mettre au point des sources de UV plus compactes et puissantes, tel le laser à YAG:Nd exité par pompage diode, semblent prometteurs toutefois.

Les exigences d'un système optique dépendent de la séparation des couleurs, c'est-à-dire le rejet du rayonnement au niveau des longueurs d'ondes du laser. L'utilisation d'un long coupe-bande dialectrique sur filtre, en série avec des filtres à passe-bande au niveau des longueurs d'ondes Raman est recommandée.

La plus difficile des exigences à satisfaire lors de la conception d'un sous-ensemble électronique est le traitement rapide du signal requis pour effectuer la technique de mesure du temps de vol. Pour déterminer le taux de concentration en fonction de la distance de la ligne de visée des données de concentration obtenues pour une longueur d'un mètre, il faut échantillonner numériquement le signal de retour à une vitesse de 4 à 6 nanosecondes. L'emploie d'un oscilloscope numérique avec un système d'essai en laboratoire est également recommandé.

En outre, les spécifications pour un méthanomètre Raman sont présentées dans le rapport. Enfin, on y fait une recommandation dont l'objet est la mise au point d'un nouveau système conçu d'après un système à YAG:Nd excité par pompage diode.

1.0 INTRODUCTION

1.1 Remote Detection Techniques

Generally there are three basic techniques which can be utilized for the remote detection of methane. These are Raman scattering, absorption, and resonance fluorescence techniques. All three of these are molecular specific. A comparison of the optical cross-sections for each of the techniques is shown in Table 1.1. In general, Raman scattering techniques have the smallest cross-section while absorption techniques are characterized by some of the largest cross-sections. Although resonance fluorescence techniques offer the largest cross-section at low concentrations, the cross-section is reduced at higher concentrations due to quenching. Additionally, the quenching process is quite complex and its effect on the measurement accuracy is not totally predictable, with the result that concentration measurements can be unreliable. For these reasons, resonance fluorescence techniques are not widely used for accurate concentration measurements and are not discussed further.

Instead, the conclusion presented in the Phase 1 report was that the Raman scattering technique offered the best promise of making the remote range-resolved methane concentration measurement, and as such is the technique which is investigated in depth in this report.

1.1.1 Raman Scattering

The methane molecule has a tetrahedral geometry with four fundamental vibrations; a totally symmetric (A1), a doubly degenerate (E) and two triply degenerate (F2) (Ref. 1). All four vibrations are Raman active and a comparison of their Raman scattering cross-sections, relative to nitrogen gas is shown in Table 1.2. For nitrogen excited at 337 nm the Raman differential cross-section (Q branch) is:

$$\frac{d\sigma}{d\Omega} = 3.8 \times 10^{-30}\ \text{cm}^2/\text{sr.mol.} \tag{1-1}$$

The data shows that the cross-section at the vibrational band at $2914\ \text{cm}^{-1}$ is eight times greater than nitrogen and is therefore a good choice for detection of methane. A comparison of the Raman scattering cross-section for other key gases, relative to nitrogen gas, is shown in Figure 1.1. The figure illustrates that there is little potential for interference from other gases which may be present in the atmosphere.

1.1.2 Absorption Techniques

In addition to two active vibrations in the infrared region ($\nu 3$ and $\nu 4$), methane has a number of overtone and combination bands in the near infrared region. The strongest of these are the $2\nu 3$ overtone and ($\nu 2 + 2\nu 3$) combination bands. A summary of these bands is shown in Table 1.3 and detailed absorption spectra are presented in Figures 1.2 and 1.3.

In general, absorption techniques used for the remote detection of methane can be divided into two categories. Techniques which measure the absorption of methane at two wavelengths, one on an absorption line and the other at a reference (or off absorption line), are classified as differential absorption techniques. A second technique, gas filter correlation, uses a spectrally matched gas filter to measure for absorption due to methane across a relatively large bandwidth. Both techniques are limited to operation within the spectral regions of high atmospheric transparency (see Figure 1.4).

Systems which employ a differential absorption measurement are the more common of the absorption techniques. This is due in part to the availability of narrow band sources, such as lasers, which can be used to provide the necessary off and on absorption line radiation. Gas filter correlation techniques require a relatively broadband radiation source and therefore are generally deployed in passive configuration due to the unavailability of powerful active sources in this wavelength region.

1.2 Systems for Remote Detection of Methane

A number of systems which have been developed specifically for the remote detection of methane were uncovered during the course of this study. A brief review of each is included in the following sections.

1.2.1 USBM: Raman Scattering (Ref. 7 and 8)

A laboratory system which utilizes the Raman scattering technique for the remote detection of methane has been developed by the USBM (United States Bureau of Mines). The system is comprised of a pulsed nitrogen laser source operating at 337.1 nm, associated collecting optics and a photomultiplier tube for signal detection. A digital storage oscilloscope is used for signal processing.

The laser source is operated with a pulse width of approximately 350 ps which is sufficiently narrow to provide a time of flight range resolution of less than 1 metre. The laser pulse energy of approximately 70 uJ is sufficient to allow methane concentration measurements of between 0.3% and 5% at distances of 15 metres*. A summary of the system performance can be found in Table 1.4. A detailed examination of the Raman scattering technique is provided later in this report.

Dr. C. Litton of USBM has verbally indicated that measurements at 30 metres have recently been performed.

1.2.2 Westinghouse: Differential Absorption (Ref. 9)

Westinghouse Inc. has developed a differential absorption system which relies upon radiation reflected off the coal face to provide a total path absorption (non-range resolved) measurement. A broadband xenon pulsed flash lamp (0.1 W) is collimated by a 12 cm parabolic mirror and the reflected light from the coal face is detected by a 15 cm receiver arranged at 45 degrees from the transmitter. The collected light is divided into two paths and is filtered to allow for measurements on and off the absorption line of methane. Two bandpass filters, one centred at 3.37 um with a HPBW (half power bandwidth) of 0.33 um and a second centred at 2.87 um with a HPBW of 1.47 um, are used to filter the collected radiation. Two thermoelectric (TE) cooled PbSe detectors are used to detect the filtered radiation. A summary of the system performance is tabulated in Table 1.4.

1.2.3 Homer Research Lab.: Differential Absorption (Ref. 10)

Homer Research Lab. have developed a differential absorption system which is capable of providing spatially resolved concentration measurements using an Er:YAG laser source in a triangulation configuration. The tunable Er:YAG laser is operated at 1.6451 um to detect methane at the 2 ν3 overtone band. An intra-cavity etalon is used to tune the laser on and off the absorption peak.

Reflected light from Mie particulates within the two volumes intercepted by the transmitted light beam at distances R and R- ΔR, is collected and detected by two uncooled germanium detectors which are spatially displaced in the lens focal plane. The detection signal is amplified and processed and the signal is displayed on a digital oscilloscope and concentration is calculated using a computer.

Including power supplies, the entire system can be fitted into two suitcase size containers. The system, however, is currently capable of making range resolved measurements only at a fixed range. The mechanical modifications required to incorporate a source or optics scanning device have not yet been developed.

1.2.4 MONITEQ Ltd.: Gas Filter Correlation

The MONITEQ GASPILS sensor was developed as an airborne remote sensor for detecting underground natural gas pipelne leaks. The instrument employs the gas filter correlation (GFC) technique to detect leaks by measuring for the presence of methane above the earth's surface. In its current configuration, the instrument uses the earth's blackbody emission as a radiation source and therefore only provides an integrated path measurement. To account for variations in the methane concentration due to sensor altitude the GASPILS is equipped with a second optional channel to measure N2O. Since N2O is a common atmospheric gas and not present in pipeline leaks it is possible to eliminate variations due to sensor altitude by ratioing the methane to N2O.

Upwelling radiation from the earth's surface enters the instrument through an entrance lens, where it is focussed on to the chopper wheel containing the target and reference gas cells. The chopper wheel consists of an electronics blanking sector, a reference gas sector and a target gas sector. In the GASPILS system, there are two target gas sectors, one for N2O and for CH4. The blanking and reference sectors are common to both the N2O and CH4 optical trains. The radiation from the chopper wheel is passed through a second lens, where it is collimated and passed through a passband filter to eliminate stray radiation. The radiation is focussed on to a liquid nitrogen cooled HgCdTe detector by a third lens.

The signals from the detectors are fed first through a pre-amp, a post-amp, a 12 bit A/D converter and then on to a digital integrator where they are summed to obtain 16 bit accuracy. These values are then input to the system software (Z-80 based) where they are processed through various algorithms to compensate for radiance variations and to calculate the gas and radiance signals. The processed data is then output in both analog and digital formats.

Table 1.1: Comparison of Cross-Sections of Different Processes for Methane at S.T.P.

Process	Cross-Section (cm**-2/sr.mol.)
Raman	
- UV + visible	1E-31
Resonance Fluorescence	
- UV + visible	1E-14 to 1E-17
- infrared	1E-18 to 1E-23
Absorption	
- infrared	1E-17 to 1E-21

Table 1.2: Methane Cross-Sections Relative to Q Branch of Nitrogen Fundamental (Ref. 2)

Band	Raman Shift cm**-1	Relative Values of Cross-Section
1	2914	8.0
3	3018.9	4.5
2	1533.3	0.24
4	1306	0.008

Table 1.3: Methane Absorption Coefficients

Band	Line	(um)	(cm**-1 atm**-1)	Ref.
ν 3	P(7)	3.3913	ca 8.8	3
2ν3	Q Branch	1.6654	ca .1	4
2ν3 + ν2	Q Branch	1.3312	ca .05	4

SYSTEM:	USBM	Westinghouse	Homer Research Lab
Technique:			
- Measurement	Raman Scattering	Differential Absorption	Differential Absorption
- Spatial Resolution	Collinear	N/A	Off-Axis
Methane Detection:			
- Maximum Conc.	5%	5%	4%
- Accuracy	+/- 0.3%	+/- 0.5%	+/- 0.3%
- Range	15 m	10 m	10 m
- Resolution	1 m	N/A	0.3 m
System Specifications:			
- Source	Pulsed N_2 Laser	Xenon Pulsed Flash Lamp	Er-YAG Pulsed Laser
- Detector(s)	Photomultiplier Tube	TE Cooler PbSe	Uncooled Germanium
- Size	Not Portable	Portable	Semi-Portable
Comments:	Laser Power Exceeds Safety Requirements	No Spatial Resolution	Fixed Spatial Resolution

Table 1.4: Summary of Reported Technologies

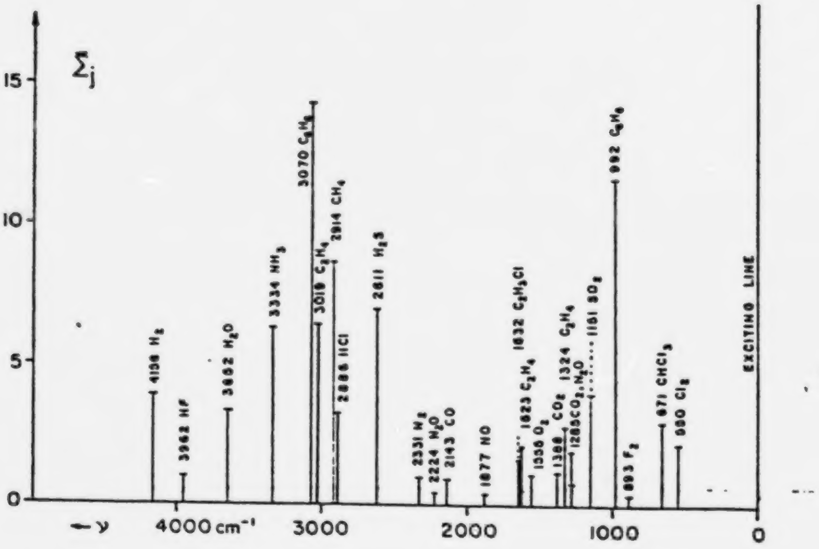

Figure 1.1: Averaged Relative Normalized Differential Raman Scattering Cross-Sections for Important Gases as Function of Raman Wave-number Shift. Dotted lines indicate resonance increase in the near UV.

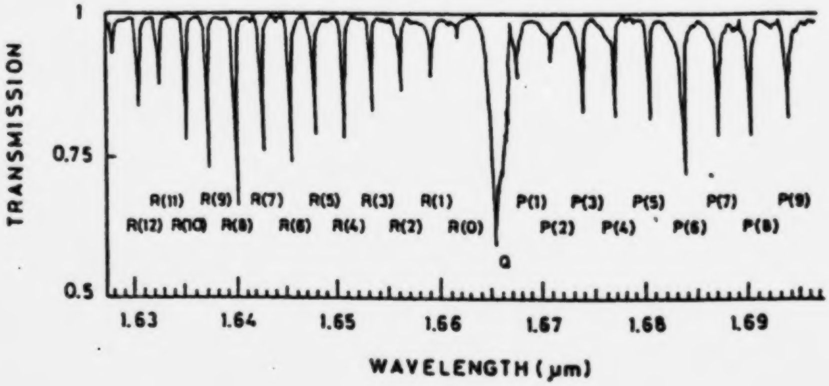

Figure 1.2: Measured Absorption Spectra and Their Assignment of the 2 ν 3 Overtone Band of CH4 Molecules in the 1.63-1.69 μm Region at 60 Torr Pressure (Ref. 4)

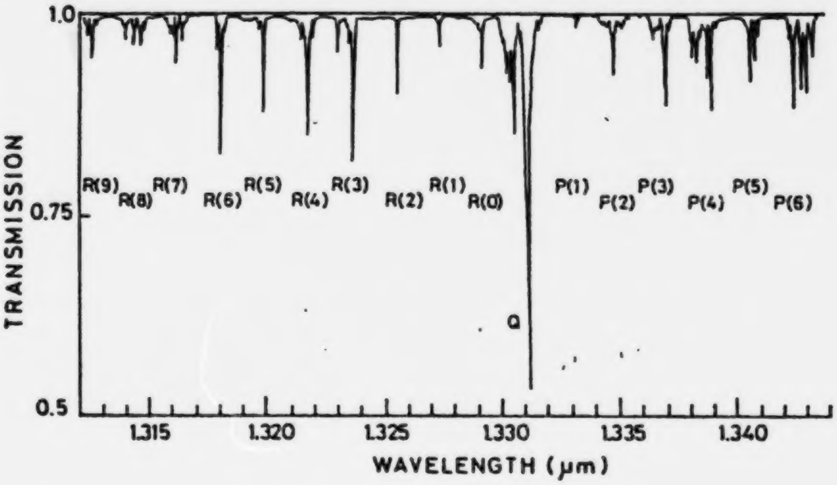

Figure 1.3: Measured Absorption Spectra and Their Assignment of the ν 2 + 2 ν 3 Combination Band of CH4 Molecules in the 1.31-1.35 μm Region at 300 Torr Pressure (Ref. 5)

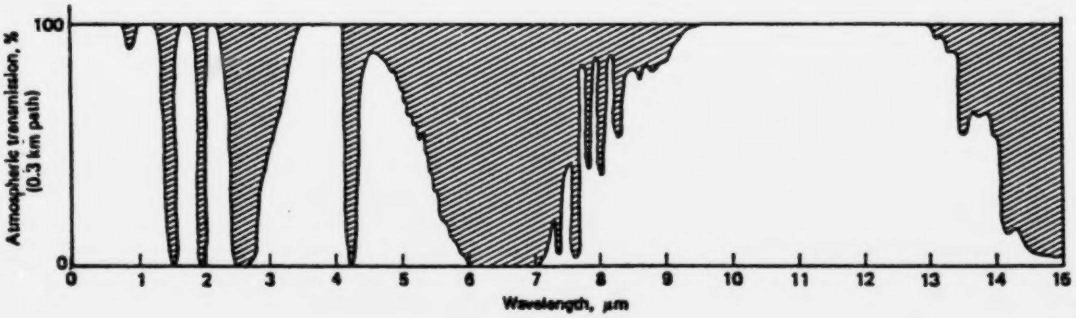

Figure 1.4: Transmission of the Atmosphere from 0.2 to 15 μm. Hatched areas indicate regions of low atmospheric transmission (Ref. 6)

2.0 DEPLOYMENT SCENARIOS

2.1 System Requirements

Table 2.1 has been extracted from the original statement of work and defines the desired requirements for a remote methane monitor. The requirements are based upon a variety of safety and sensor deployment considerations which are either desirable or essential for an instrument which is to be operated in an undergrond coal mining environment. The more critical of these requirements are summarized in Table 2.2 and are discussed below.

It is generally accepted that the lower and upper explosive limits of methane are approximately 5% and 15% respectively. A methane sensor must therefore be capable of detecting the lower (5%) explosive limit with reasonable accuracy. Additionally, from our discussions with Dr. B. Konda, it is our understanding that a mine safety requirement exists for detecting methane concentrations of 1.25%. If this level is reached or exceeded, all electrical equipment must be shut down.

For operation in an underground mine environment the sensor must be insensitive to the extreme variations in temperature, humidity and dust concentrations. Additionally, the instrument must be designed to meet the strict safety requirements for equipment operated in underground coal mines. Specifically the instrument must be designed to be explosion proof and the emitted source radiation must not exceed eye safety exposure limits. The instrument must incorporate automatic fault detecting features to facilitate its ease of use.

The desired minimum and maximum ranges for measurement are 2 and 30 m respectively with a resolution of 1 m. Distances of less than 2 m can be easily monitored using current in-situ techniques, however these techniques are often cumbersome and time consuming for monitoring more remote areas such as roof cavities. Both differential absorption and Raman techniques can be used to make remote measurements. The range and resolution requirements were thought to be satisfied by either triangulation or time of flight. Time of flight techniques are preferred over triangulation techniques because the optical and mechanical arrangement is much simpler which reduces the overall sensor size. Techniques which rely upon backscatter from the mine face or other topographic targets to return the source energy are not capable of range resolution. Although such path averaged measurements could be useful in certain instances, where the distance to the target could be estimated, this type of system does not meet the ranging requirements of this application.

The desired sensor would be hand-held, weigh less than 5 kg and be capable of self-contained battery operation for a minimum of 10 hours. The overall sensor size and power requirements are, however, almost solely a function of the laser source and the requirement of high collection efficiency.

2.2 Path Averaged Techniques

Path averaging techniques are not capable of range resolving the concentration data. However, systems which make a path averaged measurement do have advantages which make them desirable for operation in underground coal mines. Single ended systems rely upon backscatter from topographic targets to return the source energy. Since topographic backscatter is more efficient, returns more energy, than other scattering processes, such as Mie or Raman, the source energy requirements are reduced and path averaged systems are generally smaller and require less overall power than range resolved systems. The temporal bandwidth requirements are similar to triangulation techniques.

There are several applications for a portable averaged system in an underground mine. An example would be the measurement of methane trapped in roof cavities where the majority of the methane would exist within a relatively small area for which the path length (or thickness of the gas layer) could be easily estimated. In this case a path averaged or non-range resolved measurement could be used to make a reasonable estimate of the gas concentration trapped within the cavity. Although there will be concentration uncertainty because of path length errors, such a system would prove useful for detecting high concentrations of trapped gas.

2.3 Triangulation Techniques

Although systems which utilize the triangulation technique (Figure 2.1) have been demonstrated to nearly meet the desired measurement and ranging requirements they are far from being portable. As an example, the system developed by the Homer Research group (Ref. 10) occupies a volume of greater than (0.5 m3) and weighs in excess of (20 kg). In such a system, the field of view of the receiver optics intercepts the volume illuminated by the laser at an angle, θ . Range is determined by the angle θ for a fixed distance between the transmitter and receiver. This system is only capable of a fixed range measurement and modifications to incorporate an optical scanning mechanism would likely increase the size and weight substantially. Because the size of the system is limited by separation between the source and receiver and not by the source size, modifications to significantly reduce the system size are not likely.

There are, however, several applications for this type of semi-portable instrument in an underground mine. For example the sensor could be located in the coal face work zone and be used to continuously scan the open area behind the workers. Alternatively, the sensor could be deployed from a vehicular platform, and used to scan roadways both vertically and longitudinally. In these examples the portability requirements are of less importance than the ranging abilities of the sensor.

2.4 Time of Flight Techniques

Time of flight techniques (Ref. 11) (Figure 2.2) measure a characteristic return signal as a function of the transit time; concentration is determined by signal strength while transit time provides the range information. In general the optical arrangement is collinear and is smaller than triangulation systems. The system size is usually limited by the source and detecton requirements. The technique requires the source to have a narrow pulse width at reasonable repetition rates. The length of the pulse will determine the minimum range which can be resolved.

Table 2.1: Design Goals

MEASUREMENT

Minimum detectable concentration:	0.2% +/- 0.1%
Maximum detectable concentration:	5.0% +/- 0.1% (preferrably to 100% with an accuracy of +/- 0.25% from 5% to 100%)
Location of the methane target:	2 m to 30 m (adaptability to longer distances desirable).
Resolution along the line of sight:	1 m
Dimension across the line of sight:	2 m x 2 m at 30 m
Measurement time:	under 10 seconds
Frequency:	up to 5 measurements in succession during each test and up to 20 test/hour for 10 hours

System must compensate for variation in temperature, moisture, dust, aerosols and other gases.

EQUIPMENT

Power:	battery operated; capable of a minimum 10 hours of continuous use before battery replacement or charging is necessary
Output:	analog; 0-10v DC for chart recorder (optional) digital, 3 digits as follows xx.x
Size:	portable, hand-held
Weight:	5 kg; lighter weight desirable
Indicators:	1 lamp for power; 3 digit LCD for concentration, 1 or more lamps for status.
Maintenance:	all sub-assemblies to be plug-in modules for easy replacement
Standardization & Calibration:	standardization and calibration procedures should be simple and foolproof (fail safe construction)
Malfunction Indicator:	alarms on low battery, out of standardization, faults of basic sub-systems, etc.

OPERATING ENVIRONMENT

Operating temperature:	0 to 40 C
Non-operating temperature:	-20 C to 50 C
Relative humidity:	0 to 100% and aerosols
Dust:	2 to 40 mg/m
Working face conditions:	rock and coal surface is irregular; dry and wet conditions encountered; reflectance of mine face is variable

Table 2.2: Summary of Key Instrument Requirements

Concentration Requirements (% methane)

Desired operating range; lower:	0.2% +/- 0.1%
; upper:	5.0% +/- 0.1%
Mine safety limit:	1.25%
Lower explosive limit:	5%

Range Requirements

Technique	Range 30 m	Resolution 1 m
Path averaged measurement:	likely	not possible
Triangulation configuration:	likely	likely
Time of flight measurement:	likely	likely

Size/Portability Requirements Desired size and weight	Size Hand-held	Weight 5 kg
Path averaged technique:	likely	likely
Triangulation technique:	too large	too large
Time of flight technique:	large	large

Safety/Environmental Requirements

Dust loadings:	2 to 40 mg/m**3
Humidity:	0 to 100% (relative)
Temperature:	0 to 40 C
Explosive proof	
Laser output must not exceed eye safety limits	Varies with laser characteristics

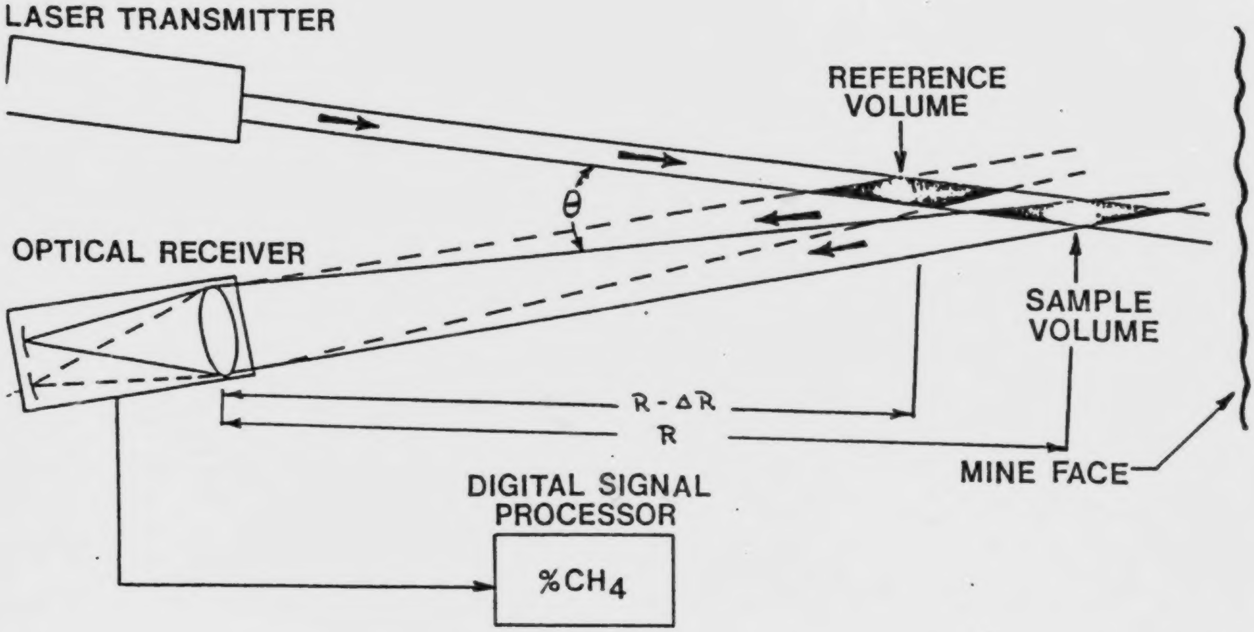
LASER TRANSMITTER
REFERENCE VOLUME
θ
OPTICAL RECEIVER
SAMPLE VOLUME
R - ΔR
R
MINE FACE
DIGITAL SIGNAL PROCESSOR
%CH4

Figure 2.1: Schematic Diagram of a Triangulation System

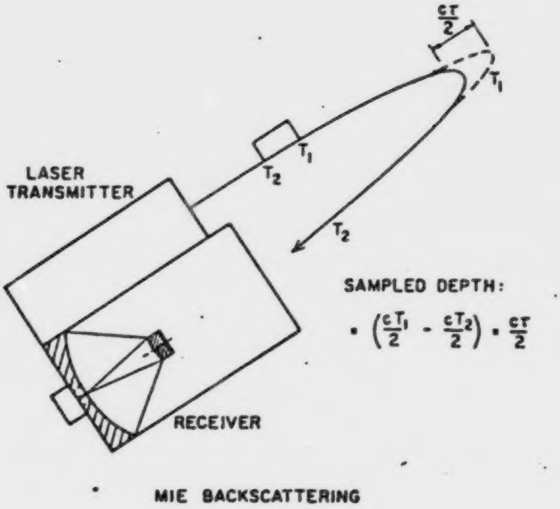
cτ/2
T1
T1
T2
T2
LASER TRANSMITTER
SAMPLED DEPTH:
= (cT1/2 - cT2/2) = cτ/2
RECEIVER
MIE BACKSCATTERING

Figure 2.2: Schematic Diagram of a Depth Resolved Collinear System

3.0 DIFFERENTIAL ABSORPTION

3.1 Path Averaged Sensors

Methane monitors based on infrared absorption methods have been developed for electric face equipment in underground mines (Ref. 12).

The parameters of this particular instrument which utilizes gas sampling can be extrapolated to a remote system. These are given in Table 3.1.

As noted in the Phase I report, the optical depth of the system should be ca 1 for satisfactory performance. At greater optical depth light does not penetrate through the gas volume whereas at lower optical depth the power difference on and off the absorption feature is reduced.

Consequently, in our extrapolation we have examined the 1.33 um absorption band, which can utilize lead sulfide detectors instead of the lead selenide detector which is better suited for the longer wavelength. We note that the transmittance for a path to a 100% reflecting mirror is inappropriate in our example. A coal face is likely to reflect only 10% of the illuminating light, so that the detector must be capable of measuring 10 times less light. Fortunately PbS detectors are at least 10 times more sensitive than PbSe. For a 10 sec measurement period (on and off the absorption), a 3 mm x 3 mm flake is capable of measuring power differences as small as 5E-13 W.

Table 3.2 estimates the power received at such a detector for four concentrations (.2%, .3%, 4%, 5%) for a variety of distances to the wall. We note that there is no difference in signal for the two higher concentrations at 10 and 15 m distances; that is, the 'path averaging' takes place over the first 10 m only and thus is decidedly non-linear, while the signal variaton is due to a 1/R**2 dependence. The corresponding signal to noise ratios are proportional to the source power and are very high. On the other hand the lower concentration values provides full depth penetration although the signal to noise is substantially reduced. In conclusion, then path averaged systems are useful up to a maximum distance of 5-10 m from the wall face; under these conditions a source power of ca 0.25 mW would give a concentration error of +/- .1% at the lower limit and +/- 1% at the higher limit.

3.2 Stability Requirements

Any infrared absorption technique involves the comparison of absorption on and off the absorption profile. Thus prior knowledge of the spectral profile for CH4 in the presence of air is required. This does not exist to date. Extrapolation from measurements made at other pressures of air or in the pure gas are not possible since the bands are complicated and departures from a sum of Lorentzians will be large. This presents two difficulties:

i) The spectrum will have to be measured under the expected field conditions. Fortunately for low concentrations (<10%) the spectrum is not expected to be a sensitive function of temperature, pressure or concentration as the dominant source of perturbations is CH4-air collisions.

ii) Without a knowledge of the spectral profile estimates of the laser frequency stability necessary to achieve a given signal to noise ratio will at best be very approximate.

To illustrate the last point and to estimate the stability requirement of a laser consider the ν_3 band of CH4. At very low pressures the Doppler width of the lines is about 300 MHz. At about 1 atmosphere (pure CH4, not air) the band has a width of the order of 30,000 MHz. If 1% accuracy is required then crudely speaking the laser sources would have to have a stability better than ca 3 MHz at low densities and ca 300 MHz at 1 atm. The less stringent requirement at higher densities is however open to question as the profile is unknown and is certainly more complicated than a simple Gaussian or Doppler broadened line. As an educated guess we will assume that an infrared laser stabilized to +/- 30 MHz would meet the frequency stability requirements for "continuous" lasers appropriate to a triangulation technique for range resolution. For a time of flight infrared technique a 1 ns pulse at best would have a width of ca 200 MHz and thus blanket about 1% of the line at atmospheric pressures. The shot to shot stability would still have to be of the order of 30 MHz for range resolved measurements. An injection locked diode laser temperature stabilized to .001 degree C might achieve 1 mW average power. Such a source might be engineered to meet the frequency stability requirements. It is not at all clear if 1 mW is adequate (refer to Section 3.3).

Comments on Pollution Detection by Absorption Using Mie Scattering and Topographic Targets by Byer and Garbuny (Ref. 11)

The paper of Byer and Garbuny, while it shows that less power is required for an infrared laser system than for a Raman system for the detection of air pollutants, contains a number of approximations that are not applicable to the detection of CH4 in mines. They assume that the particles responsible for Mie scattering are uniformly distributed. This is undoubtedly not the case of coal dust in a mine.

They assume uniform absorption and thus avoid a very difficult deconvolution problem. The received signal, by either range resolved technique depends upon the absorption integrated over the entire path times the local Mie scattering intensity. Thus one must measure the on minus off resonance signal at adjacent locations and subtract these to determine a local CH4 concentration and iterate forward down the optical path. Technically this complicates the picture as:

i) one must now worry more about signal normalization

ii) it changes (degrades) the estimates based on a SNR calculation.

A realistic estimate of laser energy requirements for the detection of CH4 in mines is thus complicated and has not been performed. Furthermore Smith and Carswell (Ref. 13) indicate that there can be serious errors (50%) in estimating extinction using the DIAL technique.

3.3 Range Resolved DIAL S/N Analyses

Ignoring the complication of non-uniform Mie scattering, we can estimate signal to noise ratios. The power received at the detector when the laser source is tuned off of the absorption line is

$$P_1(R) = \varepsilon\left(\frac{A}{R^2}\right) \cdot I_0 \, \frac{\beta(R)}{4\pi} \, V e^{-\int \beta(R)\,dR} \qquad (3.1)$$

where ε is the overall optical/detection system efficiency, A/R**2 the solid angle of acceptance of the collection optics, Io the intensity of the laser light, $\beta(R)$ the attenuation coefficient for Mie scattering and V the scattering volume located at R that is selected either by triangulation or by a time of flight technique. The integral in the exponent is over both the outward and return path. For simplicity we have assumed that the Mie scattering is distributed over 4 π steradians. For the laser tuned to an absorption line the power at the detector is

$$P_2(R) = \varepsilon\left(\frac{A}{R^2}\right) \cdot I_0 \, \frac{\beta(R)}{4\pi} \, V e^{-\int [\beta(R)+\alpha(R)]\,dR} \qquad (3.2)$$

When $\alpha(R)$ is the absorption coefficient of CH4 and is proportional to the concentration of CH4 at the distance R. A range resolved DIAL measurement of $\alpha(R)$ then consists of measuring P1(R) at different R's and then computing

$$\frac{\partial}{\partial R} \ln\left[\frac{P_1(R)}{P_2(R)}\right] = -\alpha(R) \sim \quad \text{concentration.} \qquad (3.3)$$

In fact Io will vary as the laser is changed and thus one really must measure P1(R)/Io1 and P2(R)/Io2. Note in taking the ratio (P2/Io2)//(P1/Io1) that the cancellation of the factor $\varepsilon \frac{A}{R} = \beta(R) \frac{V}{4\pi}$ and of the exponent $\int\beta$ (R)dR while obviously correct mathematically does depend upon being able to determine R correctly experimentally for both P1 and P2. This could place restrictions on the timing for time of flight measurements and upon pointing stability for a triangulation technique. Only field trials will ascertain the severity of these problems. We neglect them in trying to establish a figure of merit for any proposed Dial system.

The weakest signal will be P2 at the largest value of R and it is the difference ΔP2 in this signal at R and R + 1 (for 1 m resolution) that must be compared with detector noise. Consider a time of flight technique. Then ΔP2 is given by

$$\Delta P_2 = \varepsilon(\frac{A}{R^2}) \cdot \frac{\beta(R)}{4\pi} P_0[e^{-2\int_0^{R'} \alpha(R)\,dR}]\, \alpha(R') \qquad (3.4)$$

Here IoV = $\frac{P_o}{a}$ a $\frac{c\tau}{2}$ where a is the area of the laser beam τ the pulse length and Po the peak power of the laser and we have taken $c\tau/2$ as 1 meter. Furthermore we have assumed that P2 was evaluated at R' and R'+1 m. ΔP2 must exceed the detector noise NEP/$\tau^{1/2}$.

Note that ΔP2 has a maximum for a certain value of α but this depends upon the integrated absorption over the path and the value of α at R'. For estimates one could take α(R) a constant and thus ΔP2 will be a maximum for a $\alpha \sim \frac{1}{2R}$.

Provided such conditions can be met we estimate that the energy per pulse, Ep, must be greater than 1E-4 joules for ε = 0.1, A/R**2 = 1E-5, τ = 6 ns, β=1E-3, R = 30 m ($\alpha \cong 1/60$) and NEP = 1E-13 W/Hz$^{1/2}$ in order to have a S/N >1. For a pulse repetition rate of 100 Hz (average laser power 10 mW) one would have a S/N of $(100)^{1/2}$= 10 which is probably marginal considering all the other noise channels and uncertainties.

This analysis has shown that diode sources are inadequate. Estimates of performance for sources which would be satisfactory under conditions of uniform particle loading in a mine must be reevaluated. This requires a rather complicated estimate of expected SNR. We would not recommend that this be pursued as the frequency requirements for the infrared detection are so stringent that it is unlikely a reliable instrument can be constructed for use outside of a research laboratory. Er:YAG systems are not suitable for range resolution because of the long pulse length of the laser.

In conclusion, the performance analysis of path averaged systems illustrate that the maximum useful range for the differential absorption technique is less than 15 metres. Since the performance of a range resolved system will be considerably worse it is obvious that the differential absorption technique is not capable of achieving the desired ranging and concentration specifications. Additionally, the SNR analysis for the differential absorption technique shows that the output power of diode lasers is inadequate to achieve the required SNR levels. A detailed SNR analysis, to determine the suitability of other sources, was not performed because of the stringent laser frequency and stability requirements associated with range resolving a differential absorption measurement.

Table 3.1: Path Averaged Performance Extrapolaton

	Existing NDIR* System	Extrapolation 4.4 m Range to the Wall
Spectral Band (um)	3.43	1.33
Bandwidth (um)	0.17	.07
Concentration Range	0-5%	0-5%
Temperature	-40 C	-20 C
Detector	PbSe	PbS
D*(cm Hz**1/2 W**-1)	1E10	2E10
Integration Time (sec)	30	10
Path Length (cm)	5	440x2=880
Absorption Coefficient cm^{-1}/atm	8.8	.05
Optical Depth (5%)	2.2	2.2
Transmittance (5%)	.11	.11
Noise (%)	.1	.2
Wall Reflectance	100%	10%

*Non-dispersive infrared

Table 3.2: Change in Detector Power versus Range and Concentration

Distance to Wall (m)	Fractional Power at the Detector ($\frac{\Delta P}{Io}$)				SNR Io = 10μW Source	
(R/2)	c=.2%	c=.3%	c=4%	c=5%	c=.2%	c=5%
1	3.5E-06	5.22E-06	5.8E-05	7E-05	7E01	1.4E03
5	6.73E-07	9.85E-07	6.11E-06	6.5E-06	1.4E01	1.3E02
10	3.20E-07	4.58E-07	1.73E-06	1.8E-06	6.4	3.6E01
15	2.04E-07	2.85E-07	7.83E-07	7.9E-07	4.1	1.6E01
20	1.46E-07	1.99E-07	4.42E-07	4.42E-07	2.9	
25	1.11E-07	1.49E-07		2.83E-07	2.2	
30	8.86E-08	1.17E-07		1.96E-07	1.74	

$$\frac{\Delta P}{Io} = \varepsilon\left(\frac{A}{R^2}\right)\ \rho\left(1 - \exp -c\int \alpha(R)\ dR\right)$$

$\rho \sim \varepsilon \sim .1$

$A = \frac{\pi d^2}{4}$ d=15cm

Mie Scattering is neglected

ρ is wall reflectance

ε is detector efficiency

Detector NEP = 5E-13W

Sample Calculation

$$SNR = \left(\frac{\Delta P}{Io}\right) * Io/\text{Detector NEP}$$

$$= (7E{-}05) * (10E{-}06)/5E{-}13 = 1.4E03$$

4.0 RAMAN TECHNIQUES

A review of the literature on Raman effect and its applicability to the measurement of methane in mines was substantially completed during Phase I of this work (Ref. 14). Both systematic and random errors affect the measurement. The systematic errors are due to background light such as: unrejected source light, fluorescence from coal and coal dust that appears in band (i.e. at the CH4 Raman wavelength) and ambient light that is in band. The random noise process is due to shot noise in the signal plus the background which follows Poisson statistics. The theoretical equations are summarized below.

4.1 Theory and Required Signal to Noise Level

4.1.1 Signal Level

We assume an area, A, for the entrance aperture of the receiver then, the Raman signal S_R, (photons) is given by:

$$S_R = F_3 A \left(\frac{1}{R_N} - \frac{1}{R_F}\right) K c \tau \qquad (4.1)$$

where F3 describes a laser figure of merit, RN, RF represent the near and far points of the range interval, c is the concentration (mole fraction) of the target gas and τ is the integration time.

The quantity K describes a number of physical parameters and is given by:

$$K = \left(\frac{d\sigma}{d\Omega}(\lambda_f)\right) \lambda_f^4 \; N_L \qquad (4.2)$$

where $d\sigma/d\Omega$ is the differential Raman cross-section at a reference wavelength λ_f = 488 nm (see Ref. 2).

The values of the differential cross-section for CH4 and N2 are 2.64 E-30 and 3.31 E-31 cm**2/sr. mol. respectively.

N_L is Loschmidt's number, the molecular density at STP, 2.7 E-17 molecules/cm**3.

The laser figure of merit, F3, permits comparison of different sources and is given by:

$$F_3 = \frac{E(\lambda_o)}{hc} (PRF) \frac{T(\lambda o)\, T(\lambda_R)}{\lambda_o^{\,3}} \varepsilon(\lambda_R) \qquad (4.3)$$

where	λ_o	is the laser wavelength (nm)	
	λ_R	is the Raman wavelength	(4.3a)
	$1/\lambda_R=1/\lambda_o-\nu$	where ν is the Raman shift	
	E	is the laser pulse energy (Joules)	
	PRF	is the laser pulse repetition rate (sec)	
	T	is the transmittance of the optical system and the atmosphere at the specified wavelength	
	ε	is the quantum efficiency of the detector are	
	h,c	respectively Planck's constant and the speed of light	

The terms in the equations which have the greatest variation are those associated with the pulse energy and the pulse repetition rate. We must evaluate the dependence of the signal on concentration, c, and range RN, RF while making reasonable assumptions for the other parameters. Table 4.1 summarizes the assumed system parameters and of these, the most arguable asssumption is the assumption of a receiver area which is independent of range.

In a subsequent section we will re-evaluate this assumption. Certainly, the full receiver area can be utilized at the farthest range of 30 m. The other values give conservative estimates. Since these values are not likely to vary by more than a factor of 2-5 in total, we will look at the equivalent variation in the laser figure of merit. That is, the overall system performance depends on a product of these parameters and the laser figure of merit and very large variations are likely in the latter values. In this manner, we are able to examine the dependence of signal and signal to noise ratio on concentration, range and instrumentation parameters.

The random noise is due to the shot noise in detecting the S photoelectrons; this noise is given by S so that the resulting signal to noise ratio is S**0.5.

4.1.2 Effect of Background

Background signals represent systematic errors in the Raman measurement. If the background is much smaller than the signal levels, then the backgroud can of course be ignored. However, this is not likely to be the case and the background must be estimated and removed. That is two signals S1 = S + B and S2 = B must be measured. If we assume that the background B is stable then suitable averaging over m measurements can reduce the noise in S2 to (B/m)**.5, and the measurement is given by S ca S1 - S2. The signal to noise ratio is

$$\sqrt{S}\ F \tag{4.4a}$$

where

$$F = (1 + \frac{B}{S}\,(1+1/m))^{-1/2} \tag{4.4b}$$

We will examine two extreme cases. The first assumes that m is sufficiently large that the error in estimating B is negligible; that is

$$F_1 = (1 + \frac{B}{S})^{-1/2} \tag{4.4c}$$

The second case corresponds to alternating between signal and background measurements has m = 1. That is,

$$F_2 = (1 + 2(\frac{B}{S}))^{-1/2} \tag{4.4d}$$

The distinction between the two depends on the stability of the background; only a deployment in a simulated or actual mine environment will indicate which is more reasonable since there are background terms which depend jointly on dust concentration, and laser pulse energy as well as constant terms. However, each site is likely to require a background measurement.

In Table 4.2 we evaluate the reduction in signal to noise ratio for assumed values of the background to signal ratio.

For a stable background and background to signal ratios of ca 100, the signal to noise ratio is degraded by a factor of ca 10. We note that the signal to noise ratio in the absence of background is proportional to S**.5, so that a background to signal ratio of 100 requires a laser figure of merit 100 times larger than the condition for equal background and signal (B/S = 1). Clearly, the latter case is a design goal. But we recognize the need for a margin of 3 to 4 to account for a background to signal ratio of up to 8 at low signal levels, i.e., low concentration.

In the following sections we will only calculate the SNR = S**.5 recognizing that conservatively a factor ca 10 may be required if there is a great deal of fluorescence from coal.

4.1.3 Signal to Noise Ratio Requirements in the Absence of Background

The theoretical analysis above clearly shows that the signal to noise ratio scales as the square root of concentration. We have therefore re-interpreted the desired system performance (Table 4.3). We distinguish between the absolute and relative error in deriving the required signal to noise ratio. These errors must be obtained after accounting for background.

We note that if this performance can be obtained at the farthest range it can easily be obtained at the nearest range. Although two scenarios are given, we will mostly discuss performance in the context of the more stringent requirement.

4.1.4 Calibration

The accuracy of calibration of a Raman methanometer depends critically on the assumption that the receiver cross-sectional area is independent of range. In practice, the enormous depth of field required makes this highly unlikely (see Section 5.2). However, calibration can be accomplished by using nitrogen as a calibration signal. Since the differential cross-section (and therefore the Raman signal) from methane is 8 times that of nitrogen, nitrogen Raman signals from air provide a calibration level equivalent to 10% methane. Strictly speaking, there will be some slight variation in the system performance at the Raman wavelengths of the two gases.

The overall noise generated by such a normalization is given by

$$\left(\frac{\Delta C}{C}\right)^2 = \frac{1}{S(\text{methane})} + \frac{1}{S(\text{nitrogen})} = \frac{1}{S(\text{methane})}\left(1+\frac{S(\text{methane})}{S(\text{nitrogen})}\right) \qquad (4.5)$$

The error contribution is largest for the lowest concentrations of methane since the first term is just the shot noise calculated in Section 4.1.1.

4.2 Laser Source

We have evaluated laser sources with respect to availability, eye safety and performance.

Table 4.4 summarizes specifications of commercially available laser sources. The lasers were selected independent of their operating wavelength. However a laser pulse length of less than 6 ns is required to achieve the 1 m resolution requirement via the time of flight technique (refer to Figure 2.2). The table is extracted from Laser Focus Buyers Guide (Ref. 15). The laser systems include gas lasers such as the nitrogen laser which has the advantage of high repetition rate and excimer lasers (XeCl, XeF) which have high average power but which use toxic gases. Two solid state systems are included based on Nd:YAG and Ruby lasers. The Nd:YAG system includes the laser fundamental as well as doubled, tripled and quadrupled configurations.

Eye Safety Requirements and Aperture Size of the Receiver

Eye safety requirements (Ref. 16, ANSI Z136-1980) are based upon the maximum permissible exposure (energy per unit area) at specific wavelengths; this is referred to as MPE. Eye safety can clearly affect both the transmitter and the receiver cross-sectional areas. We briefly compared separate scenarios associated with the choice of aperture size:

i) the laser pulse energy is limited by availability of a suitable laser source,

or

ii) the laser pulse energy is limited by eye safety requirements. We will examine the implications of both models.

Figure 4.1 illustrates the typical aperture requirements for the transmitter/receiver, where D, d are respectively the diameter of the primary mirror and the projected diameter of a mirror which prevent the laser from directly illuminating the detector.

For first case above then the area A of the receiver

$$A = \frac{\pi}{4} (D^2 - d^2) \tag{4.6a}$$

and since the laser pulse energy is independent of d then the total Raman signal is proportional to the receiver area at a given range. The signal and receiver area are both maximum for d = 0, i.e.,

$$A = \frac{\pi D^2}{4} \tag{4.6b}$$

For the second case, the obscured area affects the laser pulse energy E; that is,

$$E = (MPE) \frac{\pi d^2}{4} \tag{4.7a}$$

where MPE is the maximum permissible exposure for eye safety. The Raman signal then is proportional to

$$d^2(D^2 - d^2) \tag{4.7b}$$

which maximizes for the ratio d/D = 0.707 and in this case

$$A = \frac{\pi D^2}{8} \tag{4.7c}$$

So that the two cases described above only differ by at most a factor of 2 in receiver area.

For the 30 cm diameter aperture of the primary, a maximum obscuration of 21 cm is suggested to satisfy the eye safety requirement whereas a small obscuration of up to 5 cm decreases the receiver area by less than 3%.

Laser Figure of Merit

For a given wavelength and laser beam diameter, however, the eye safety limitation can be expressed in terms of a laser figure of merit (refer to Equation 4.3). Table 4.5 summarizes the data for each laser system as a function of wavelength for specific beam diameters.

We note that:

i) for a given wavelength, the maximum eye safe laser figure of merit is proportional to the square of the beam diameter;

ii) the laser figure of merit decreases at longer wavelength. Stated simply, a larger figure of merit is permissible in the UV region than is permitted in the visible or infrared wavelength region.

The laser figure of merit (laser function) was calculated for each of the lasers listed in Table 4.4. The results of the calculation are given in Table 4.6. We note that the laser figure of merit varies by about five orders of magnitude!

The best system performance will be obtained using a laser source with a large figure of merit. However, if we account for eye safety, it is clear that operation in the UV region is preferred because of the larger permissible laser figure of merit. Although more powerful sources are available at 530 or 1060 nm, a beam diameter of 21 cm only permits a laser figure of merit of less than 2E02 nm**-4 sec**-1. Operation between 355 and 266 nm, however, permits a laser figure of merit exceeding 1E06 nm**-4 sec**-1.

For operation in the 266 to 355 nm region using a 5 cm beam, there is an eye safety limitation of ca 2E05 nm**-4/sec. It is evident that most of the lasers shown in Table 4.6 have laser figure of merits which exceed the limitations due to eye safety for a 5 cm beam. The one exception is the nitrogen laser operating at 337 nm which has a figure of merit approximately an order of magnitude less than permissible based on eye safety requirements.

Eye safety limitations are also affected by pulse repetition rate. Figure 4.2 shows the decrease in maximum permissible exposure with pulse repetition rate. For the 10 sec, we have indicated the number of laser pulses that would be obtained at the resulting increase in signal to noise ratio. However, the overall performance is dependent on the product of the two which is shown as the overall gain, G, in the same figure. Clearly, there is no significant variation for repetition rates between 1 and 200 Hz. Since the latter repetition rate would require a rather larger power supply, we are better off with a low repetition rate higher pulse energy source than a low pulse energy high repetition rate source.

In summary use of the Photochemical Research Associates nitrogen laser which has a figure of merit of 6.6 E03 nm**-4 sec**-1, will provide the minimum system performance. The maximum system performance is limited by the eye safety and not by availability of the laser source However, we desire to limit the power consumption (see Table 2.1) of the laser so that this will ultimately limit performance. The salient point is that these other systems must be scaled down to meet the requirement.

4.3 System Performance - Signal Levels and Signal to Noise Ratio Calculations

In this section we provide a detailed evaluation of the system performance with respect to the signal and signal to noise ratio (SNR) calculations. The calculations are based upon the equations for signal and SNR which were derived in Section 4.1. The system parameters are given in Table 4.1. For clarity, the data is presented in graphical form. Details of the computer program and example calculations are provided in Appendix 1.

The system performance is evaluated separately as a function of range and concentration, while the laser figure of merit is treated as an independent system parameter. Although the system performance is dependent upon both the receiver aperture and laser figure of merits, the laser figure of merit is more significant as it can vary by almost two orders of magnitude (Tables 4.5 and 4.6).

Three values of the laser figure of merit are shown for each plot. They correspond to the nitrogen laser figure of merit (F3) of 6.57 E03 nm-4 sec-1 (Table 4.6) and an intermediate figure of merit which is one order of magnitude greater (F3'). In addition, the figure of merit for a source limited by eye safety with a 5 cm beam diameter at 337 nm is also illustrated (F3"). The hatched area above the latter illustrates the unsafe region with respect to eye safety at the 337 nm wavelength region.

4.3.1 Methane

Figures 4.3a and 4.3b depict the system performance versus range at the lower/upper concentration level of 0.20% and 5% respectively. The signal is plotted along the left side of the graph while the signal to noise ratio SNR axis is located at the right. We compare the indicated performance to the desired values (Table 4.3).

We note that the required signal to noise ratios of 5:1 and 25:1 can be obtained (or exceeded) up to a range of 12 m using the nitrogen laser (F3, PRA LN103). For the intermediate source (F3') which is ten times brighter than this nitrogen laser, we can just exceed the desired signal to noise ratios at the 30 m range. While for a system limited by eye safety, signal to noise ratios of 12:1 and 60:1 can be obtained at the 0.2% and 5% concentration levels at the maximum range of 30 m.

Figures 4.4a and 4.4b present the same data versus concentration at two fixed ranges of 3 m and 30 m respectively. The signal to noise at 3 m exceeds the requirements using the nitrogen laser by a factor of 4 for both concentration limits (0.1% and 5%). On the other hand, the SNR at 30 m is poorer than the requirement by a factor of 2.5. The intermediate source just exceeds the requirement whereas the strongest source (limited by eye safety) exceeds the requirement by a factor of 2.4.

4.3.2 Nitrogen

The concentration of nitrogen in the atmosphere is nearly constant and therefore can be used to normalize atmospheric concentration measurements of other gaseous species. The usefulness of the techniques, however depends upon the performance of the system with respect to measuring nitrogen. Figure 4.5 illustrates the performance of the system at nitrogen concentrations of 80% as a function of ranges. The parameters used in the calculation are identical to those used for the previous data. Points worthy of note are:

i) Based upon the nitrogen laser figure of merit the SNR at the 30 meter range is approximately 14:1.

ii) Based upon a laser figure of merit ten times greater than the nitrogen laser (i.e. F3') the SNR at the 30 meter range is approximately 45:1.

Since these signal to noise ratios are substantially larger than the corresponding values for methane, the normalization (Ref. Section 4.1.4) will not substantially increase the overall system noise. In fact, the worst case occurs for 5% methane case where the overall system noise increases by a factor of 1.22.

4.4 System Performance versus Laser Figure of Merit

4.4.1 Requirements of the Laser

Figures 4.6a - 4.6d illustrate the system performance as a function of the laser figure of merit. System performance is represented by the SNR which is the ordinate. The required SNR for the selected concentration and accuracy (from Table 4.3) is shown by a horizontal line.

The laser figure of merit is shown along the horizontal axis. The figure of merit for the nitrogen laser (6.57 E03 nm-4 sec-1) is shown by a point on the plot. The eye safety figures of merit (5 cm beam diameter) for the 337 nm (nitrogen laser) and 355 nm (Nd:YAG laser) wavelengths are also illustrated by points along the plot. It is important to note that currently available Nd:YAG lasers (355 nm) have a figure of merit which exceeds the eye safety requirements at that wavelength and therefore that the system performance at 355 nm is limited by the eye safety figure of merit (Ref. Section 4.2).

Figures 4.6a and 4.6b represent the system performance versus the laser figure of merit at the lower concentration level of 0.2% for ranges of 3 and 30 m respectively.

i) At the lower range of 3 m the minimum laser figure of merit which will yield a SNR of 5:1 is approximately 4 E02 nm-4 sec-1.

ii) At the 3 m range the minimum laser figure of merit is achievable using the currently available nitrogen laser.

iii) At the 30 m range the minimum laser figure of merit which will yield a SNR of 5:1 is approximately 4.5 E04 nm-4 sec-1.

iv) At the 30 m range the nitrogen laser is only capable of a SNR of approximately 2:1, however, a SNR of better than 10:1 can be achieved with lasers operated at the maximum eye safety level.

Identical conclusions can be drawn from Figures 4.6c and 4.6d which illustrate the performance at the 5% concentration level with a 25:1 SNR requirement.

In Section 4.1.2 we noted that under conditions of large background to signal ratio (B/S = 8) a factor of 3 to 4 increase in system performance was required to ensure compliance. Under these circumstances the desired performance would not be obtained using a source at the limit of eye safety (5 cm beam). However, these discrepancies can be overcome by either of two strategies: increasing the integration time or by adjusting the range resolution to compensate. In the latter case the range resolution would be degraded to 4 m to achieve the desired performance.

As we noted above increasing the beam diameter increases the maximum pulse energy so that the 'eye safety' limit is not a hard limit. While increasing the beam diameter from 5 cm to 21 cm increases the limit by a factor of 4 times, the receiver is severely obscured, so that the area is ca 1/2 that of the system described above. Consequently, this alternative can only yield an improvement of a factor of 2.

4.5 Size and Efficiency of Laser Sources

4.5.1 Commercial

The remote sensing of methane requires a laser system which can optimize the figure of merit while at the same time satisfying the customer's requirements with respect to eye safety, range resolution, portability, etc. A review of existing commercial laser systems indicates a field of potential candidates which can at least satisfy the technical requirements of the producing a high figure of merit plus sufficient signal to be detected by a photomultiplier detection system. The characteristics of these different laser systems are presented in Table 4.7.

It is clear, that all the lasers have sufficient power to produce an adequate signal for the range of methane concentrations encountered. However, the nitrogen laser comes closest to fulfilling the specifications.

The XeCl excimer laser is a non-portable system having a typical volume displacement of 2 cubic meters and a weight in excess of 100 kg. It also operates on toxic gases in a flow-through discharge and is generally operated in conjunction with a fume hood in a laboratory or industrial environment. The pulse width of these lasers may be too long for the range resolution required. Lumonics (Ottawa, Ontario) is an internationally recognized supplier of these lasers. They are interested in fabricating the highest average power sources with the result that the Hyperex laser has superseded earlier lower power modules.

The Nd:YAG laser is a solid state laser operating at a fundamental wavelength of 1.06 um, but the output pulses can be frequency doubled or tripled in a nonlinear optical crystals to yield 0.53 and 0.35 um pulses. These systems are used extensively in remote sensing applications and other field uses but are generally not designed for portability. The main factor in the low-efficiency is the flashlamp pumping and the associated large capacitors, inductors, fluid cooling systems, etc., that go with them. International Laser Systems (Orlando, Florida) is a supplier of many of these systems for military and remote sensing applications. A typical size of one of their systems is 0.5 m**3 with a weight of 50 kg. Besides the problems discussed the pulse width of the system is too long for the range resolution required.

The nitrogen laser can operate as a closed system and has the power and the pulse width to satisfy the technical requirements. Its average power is also below the maximum allowed for eye safety. The only point on which the N2 laser fails is its size, although it comes close. PRA International (London, Ontario) manufactures a number of N2 lasers with sizes down to 0.1 m3 and weights of 25 kg. In discussions with them we have established that it might be possible to achieve even smaller figures in these areas, but some research would have to be done on new designs first. The scientific literature also reveals that work is underway by a number of individuals to construct compact N2 lasers. Of all the existing systems, a pulsed N2 laser comes the closest to being suitable for the remote sensing of methane.

4.5.2 Future Sources

The future holds essentially two possibilities for laser systems which can be used for the remote detection of methane. We have already mentioned that with a specifically adapted design it may be possible to construct a N2 laser to be used as a portable system in the field. N2 laser technology is somewhat mature and the technical specifications are not likely to undergo dramatic change in the next few years. On the other hand most N2 lasers built to date are laboratory systems, and manufacturers, by and large, have not been challenged to determine the ultimate size for their systems.

The latest development in laser systems is the semiconductor diode pumped Nd:YAG laser. This is close to being a virgin area of research and development and has created a stir in the scientific and industrial community. This has come about because of the recent (within the last year) development of semiconductor diode arrays (GaAlAs) with average optical power up to 500 mW and with 40% efficiency. These lasers can be tuned to match the absorption bands of Nd:YAG and provide an extremely efficient pump for that laser. Wall-plug to optical power conversion efficiency has been measured to be as high as 15%. As a pump the array would replace the very inefficient xenon flashlamps which are typically used today. Many researchers have demonstrated continuous versions of such lasers with typical output powers at 1.06 um of 30 mW, with frequency doubled (0.53 um) output of 12 mW based on a 200 mW array. The frequency doubling is performed in a special crystal (KTP) useful at these low powers.

A typical continuous system is indicated in Figure 4.7. The diode array end pumps the Nd:YAG rod, to allow the longest absorption length and match the small array to the small end of the rod. It should be noted that the pumping wavelength at 808 nm, the lasing wavelength at 1060 nm and the frequency doubled wavelength 530 nm can be injected, trapped, and extracted by selectively coating mirrors or lenses. A thermoelectric cooler stabilizes the temperature of the array at 10 +/- 0.5 C. The TE cooler power consumption is estimated at 7 watts and in the entire system there is no potential above 2 volts.

It should be possible to use the diode arrays to serve as pumps for pulsed Nd:YAG systems as well, with nearly the same efficiency. As such, these new laser systems will be much more compact than the Nd:YAG lasers discussed above.

Table 4.1: Instrumental Parameters for a Raman Methanometer

Description	Parameter	Value	Comment
Receiver Area	A	707 cm^2	30 cm diameter (assumed independent of range)
Integration Time	τ	10 sec	
Transmittance	$T(\lambda o)T(\lambda_R)$	0.08	
Detector Quantum Efficiency	ε	0.25	
Range Resolution	RN-RF	1 m	
Range	$\frac{RN+RF}{2}$	2-30 m	Evaluate effect on signal and signal to noise ratio
Methane Concentration	C	0.2%-5%	Evaluate effect on signal and signal to noise ratio
Laser Figure of Merit	F3	See Tables	Evaluate effect on signal and signal to noise ratio

Table 4.2: Reduction in Signal to Noise Ratio due to Background

	Stable Background	Alternate Measurement
B/S	F1	F2
0.01	1.005	1.01
0.1	1.05	1.1
1	1.4	1.3
8	3.0	4.1
10	3.3	4.6
100	10.	14.2

Table 4.3 : Alternative Signal to Noise Ratio Requirements for the Desired System

Methane Concentration	Absolute Error	Relative Error	SNR
Alternate #1			
0.2%	+/- 0.04	+/- 20%	5:1
1.25%	+/- 0.10	+/- 8%	12.5:1
5.0%	+/- 0.2	+/- 4%	25:1
Alternate #2			
0.2%	+/- .1	+/- 50%	2:1
1.25%	+/- .25	+/- 20%	5:1
5.0%	+/- .4	+/- 8%	10:1

Table 4.4: Summary of Available Laser Sources

WAVELENGTH (μm)	OUTPUT (J) TEM ∞	MULTI MODE	REP RATE (Hz)	PULSE-LENGTH (μS)	BEAM DIA (mm)	BEAM DIVERGE (mrad)	FEATURES	MANUFACTURER	MODEL#	PRICE ($)
Nitrogen										
.337		$150x10^{-6}$ to	100	.001	2x3	3x5	High PRF	Phase-R Corp.	Micro-T	3,850
.337		$150x10^{-6}$ to	20	.001	2x3	3x5	Low cost, 150kW	Phase-R Corp.	Micro	
.337		.00005	0-100	.0003	2x3	3x7	Low jitter	Photochemical Res	LN-103	
.337		.00005	0-100	.0003	1x2	3x7	Short pulse	Photochemical Res	LN-100	
Xenon Chloride										
.308	$3x10^{-4}$		100	$1x10^{-3}$	3	-1	Md-Lkd,diff Ltd	Multilasers	MOPAX-300M	
.308		.001	1-1000	.005	4x4	5		Quanta-Ray	EXC-410	25,000
.308		.005	1-100	.005	7x7	5		Quanta-Ray	EXC-401	18,000
Xenon Fluoride										
.35		.275	110	.01	6x33		High avg power	Lumonics	TE-860-4	36,000to45,000
Neodymium:YAG	(Quadrupled)									
.266	.02		10	.007	7	.7	Q-switched	Quantel Int'l	YG580-10FHG	34,000
.266	.03		4-40	.004	6.5	.1		Quanta-Ray	DCR2A-30(4)	59,950
.266	.045		3-30	.004	6.5	.1		Quanta-Ray	DCR2A-20(4)	56,450
.266	.045		20	.007	7	.7	Q-switched	Quanta Int'l	YG581-20FHG	49,000
.266		.02-1	50	.008	4-8	.8	HyperYAG	JK Lasers Ltd.	HY Series	
Neodymium:YAG	(Tripled)									
.355	.05		3-30	.005	6.5	.2		Quanta-Ray	DCR-2-20(3)	38,950
.355	.06		1-14	.005	6.4	.2		Quanta-Ray	DCR-11(3)	
.355	.06		2-20	.005	6.5	.2		Quanta-Ray	DCR-2-10(3)	37,450
.355	.06		10	.008	7	.7	Q-switched	Quantel Int'l	YG580-10TH	32,000
.355	.1		3-30	.005	6.5	.2		Quanta-Ray	DCR2A-20(3)	56,450

Table 4.4 (continued)

Neodymium:YAG (Doubled)										
.53		.06-.35	50	.008	4-8	.8	HyperYAG	JK Lasers Ltd.	HY Series	
.532	.07		30	.009	7	.7	Q-switched	Quanta Int'l	YG580-30SHG	36,000
.532		.003	10-100	.015	5	5	Freq double	General Photonics	TWO-45Q2	22,000-30,000
.532		.2	5	.002	50	.25	Cavity dump	General Photonics	TWO-82	160,000
Neodymium:YAG										
1.06		.008	1	.008	12	.8	Miniature	Laser Photonics	MYL-100	
1.06		.2-.85	50	.008	4-8	.8	HyperYAG	JK Lasers Ltd.	HY Series	
1.064	.275		1-14	.008	6.4	.5		Quanta-Ray	DCR-11	
1.064	.28		3-30	.009	6.5	.5		Quanta-Ray	DCR-2-10	34,000
Neodymium:Glass										
1.06	10		.017	.003	25	.3	Silicate	Quanta Int'l	NG34	119,000
1.06	20		.017	.003	44	.3	Silicate	Quanta Int'l	NG44	170,000
1.06	3		.06	.003	16	.3	Silicate	Quanta Int'l	NG24	68,000
Ruby (Doubled)										
.347		.3	.lor1	.125	6-10	1-3	System 2000	JK Lasers Ltd.	DLPR Series	

Table 4.5: Laser Figure of Merit at the Maximum Permissible Exposure

Laser Figure of Merit for Beam Diameter 1 cm

Wave length (nm)	Pulse Energy (J)	Figure of Merit (nm-4/sec)
266	2.360E-003	1.262E+004
337	3.380E-003	8.889E+003
347	3.380E-003	8.143E+003
355	3.380E-003	7.604E+003
530	3.900E-007	2.637E-001
1060	3.900E-006	3.296E-001

Laser Figure of Merit for Beam Diameter 10 cm

Wave length (nm)	Pulse Energy (J)	Figure of Merit (nm-4/sec)
266	2.360E-001	1.262E+006
337	3.380E-001	8.889E+005
347	3.380E-001	8.143E+005
355	3.380E-001	7.604E+005
530	3.900E-005	2.637E+001
1060	3.900E-004	3.296E+001

Laser Figure of Merit for Beam Diameter 5 cm

Wave length (nm)	Pulse Energy (J)	Figure of Merit (nm-4/sec)
266	5.900E-002	3.155E+005
337	8.450E-002	2.222E+005
347	8.450E-002	2.036E+005
355	8.450E-002	1.901E+005
530	9.750E-006	6.592E+000
1060	9.750E-005	8.240E+000

Laser Figure of Merit for Beam Diameter 21.2 cm

Wave length (nm)	Pulse Energy (J)	Figure of Merit (nm-4/sec)
266	1.061E+000	5.672E+006
337	1.519E+000	3.995E+006
347	1.519E+000	3.660E+006
355	1.519E+000	3.418E+006
530	1.753E-004	1.185E+002
1060	1.753E-003	1.481E+002

Table 4.6: Laser Figure of Merit for Selected Lasers

NITROGEN LASER

Wave length (nm)	Pulse Energy (J)	PRF (Hz)	Laser Function (nm-4/sec)
337	1.5E-004	50	1.97E+004
337	1.5E-004	10	3.94E+003
337	5.0E-005	50	6.57E+003
337	5.0E-005	50	6.57E+003

ND:YAG LASER

Wave length (nm)	Pulse Energy (J)	PRF (Hz)	Laser Function (nm-4/sec)
266	2.0E-002	5	5.35E+005
266	3.0E-002	20	3.21E+006
266	4.5E-002	15	3.61E+006
266	4.5E-002	10	2.41E+006
266	1.0E-001	25	1.34E+007
355	5.0E-002	15	1.69E+006
355	6.0E-002	7	9.45E+005
355	6.0E-002	10	1.35E+006
355	6.0E-002	5	6.75E+005
355	1.0E-001	15	3.37E+006
530	3.5E-001	25	5.92E+006
532	7.0E-002	15	7.02E+005
532	3.0E-003	50	1.00E+005
532	2.0E-001	3	4.01E+005
1060	8.0E-003	1	6.76E+002
1060	8.5E-001	25	1.80E+006
1064	2.8E-001	7	1.64E+005
1064	2.8E-001	15	3.51E+005

Xe:Cl LASER

Wave length (nm)	Pulse Energy (J)	PRF (Hz)	Laser Function (nm-4/sec)
308	3.0E-004	100	1.03E+005
308	1.0E-003	500	1.72E+006
308	5.0E-003	50	8.61E+005

ND:GLASS LASER

Wave length (nm)	Pulse Energy (J)	PRF (Hz)	Laser Function (nm-4/sec)
1060	1.0E+001		7.18E+003
1060	2.0E+001		1.44E+004
1060	3.0E+000		7.61E+003

Xe:Fl LASER

Wave length (nm)	Pulse Energy (J)	PRF (Hz)	Laser Function (nm-4/sec)
350	2.8E-001	55	3.62E+007

RUBY LASER

Wave length (nm)	Pulse Energy (J)	PRF (Hz)	Laser Function (nm-4/sec)
347	3.0E-001	1	7.23E+005

Table 4.7: Typical Commercial Laser Characteristics

Laser	Wave-length	Energy/Pulse	Rep. Rate	Pulse-width	Efficiency
N2 Laser	337 nm	50 uJ	50 Hz	< 1 ns	0.1%
XeCl	308 nm	0.3 J	< 300 Hz	> 20 ns	0.1%
Tripled Nd:YAG	353 nm	50 mJ	20 Hz	4 ns	0.05%
Doubled Nd:YAG	530 nm	130 mJ	20 Hz	5 ns	0.15%

Figure 4.1: Schematic Diagram of Transmitter/Receiver Aperture

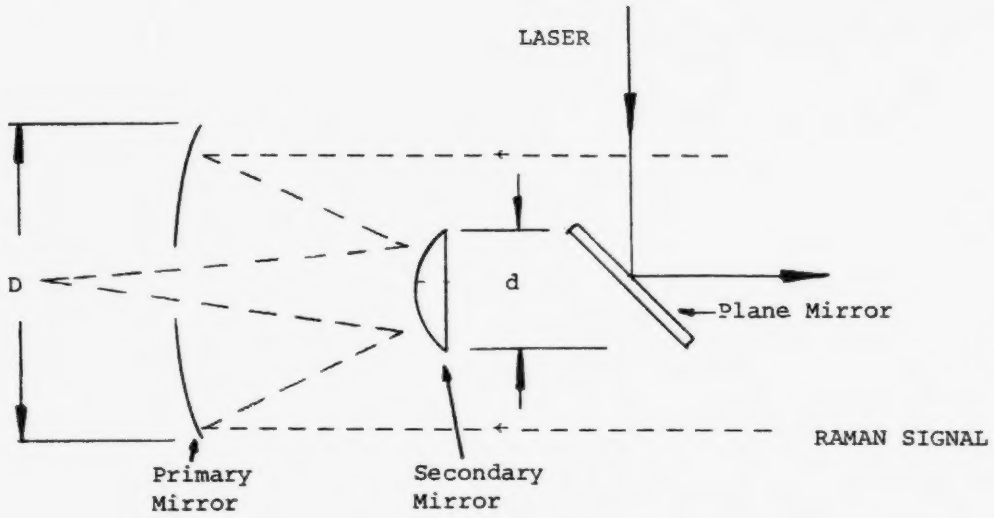
LASER
D
d
Plane Mirror
RAMAN SIGNAL
Primary Mirror
Secondary Mirror

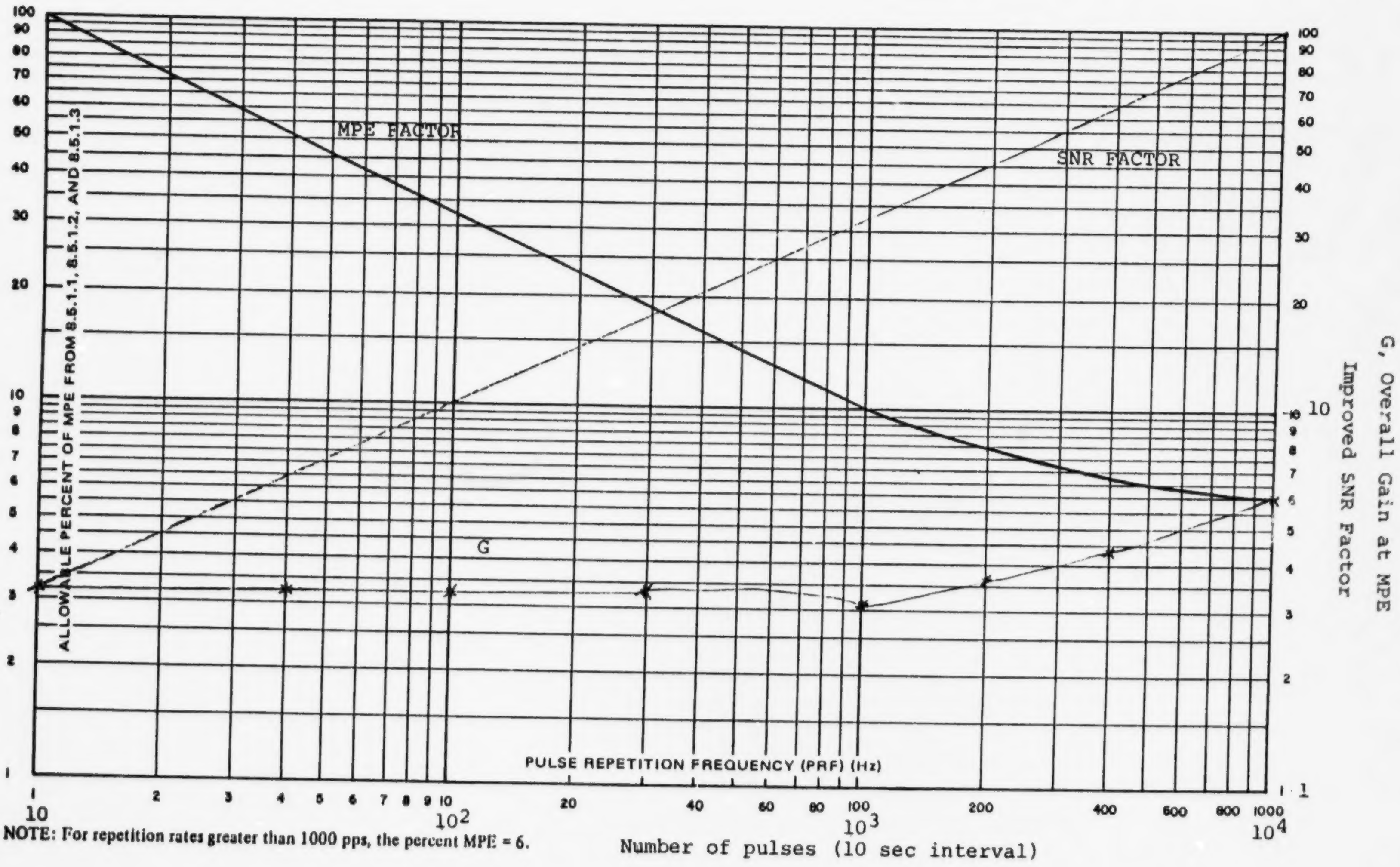

NOTE: For repetition rates greater than 1000 pps, the percent MPE = 6.

Figure 4.2a: Reduction of MPE for Repetitively Pulsed Lasers (Individual Pulse Less Than 10 µs Duration)

4.2b: Overall System Gain

Modified from: Z136.1-1980

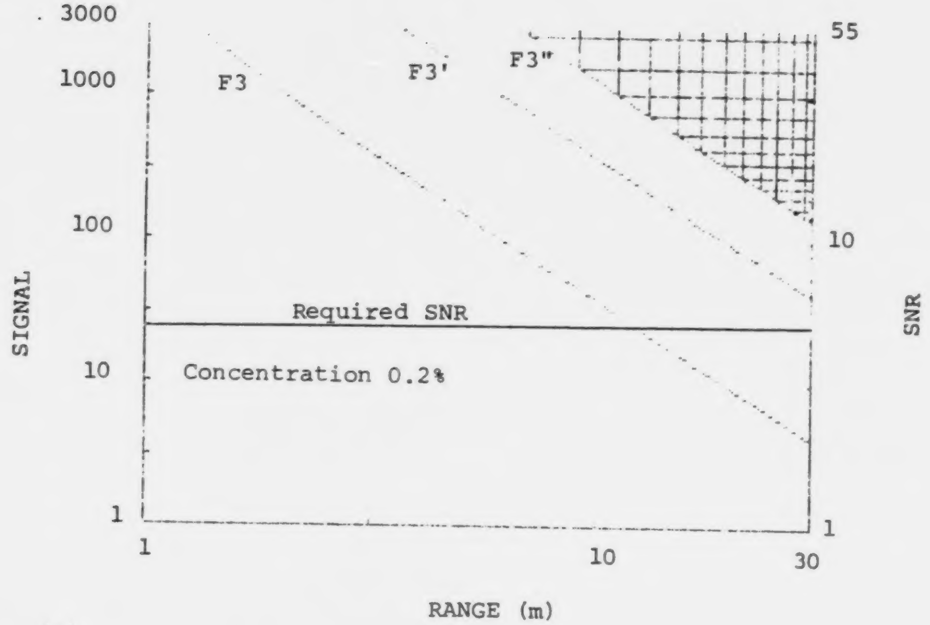

(a)

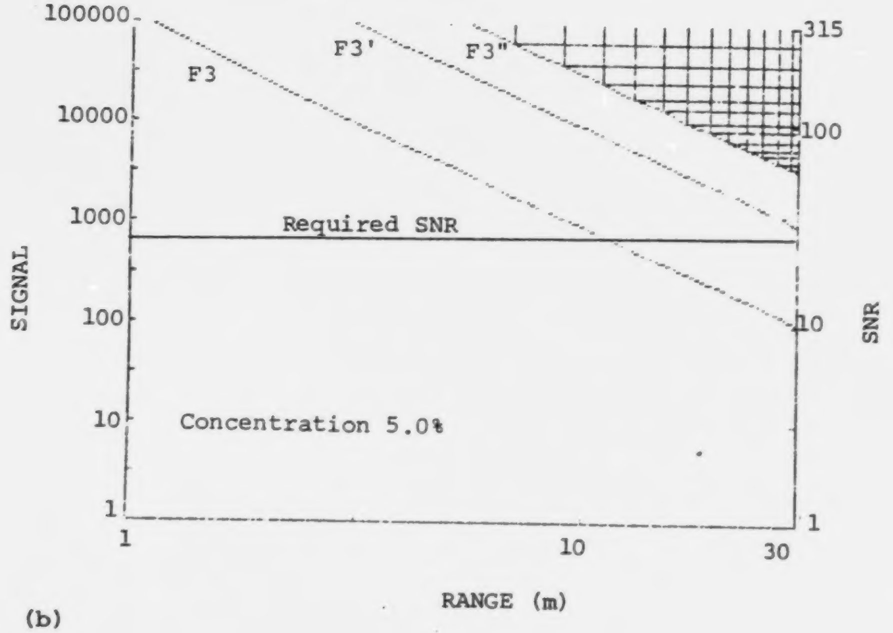

(b)

F3 = Laser Function: 6.570E+003
F3' = Laser Function: 6.570E+004
F3" = Laser Function: 2.222E+005

Figure 4.3: Signal and Signal to Noise Ratio (SNR) versus Range for Methane

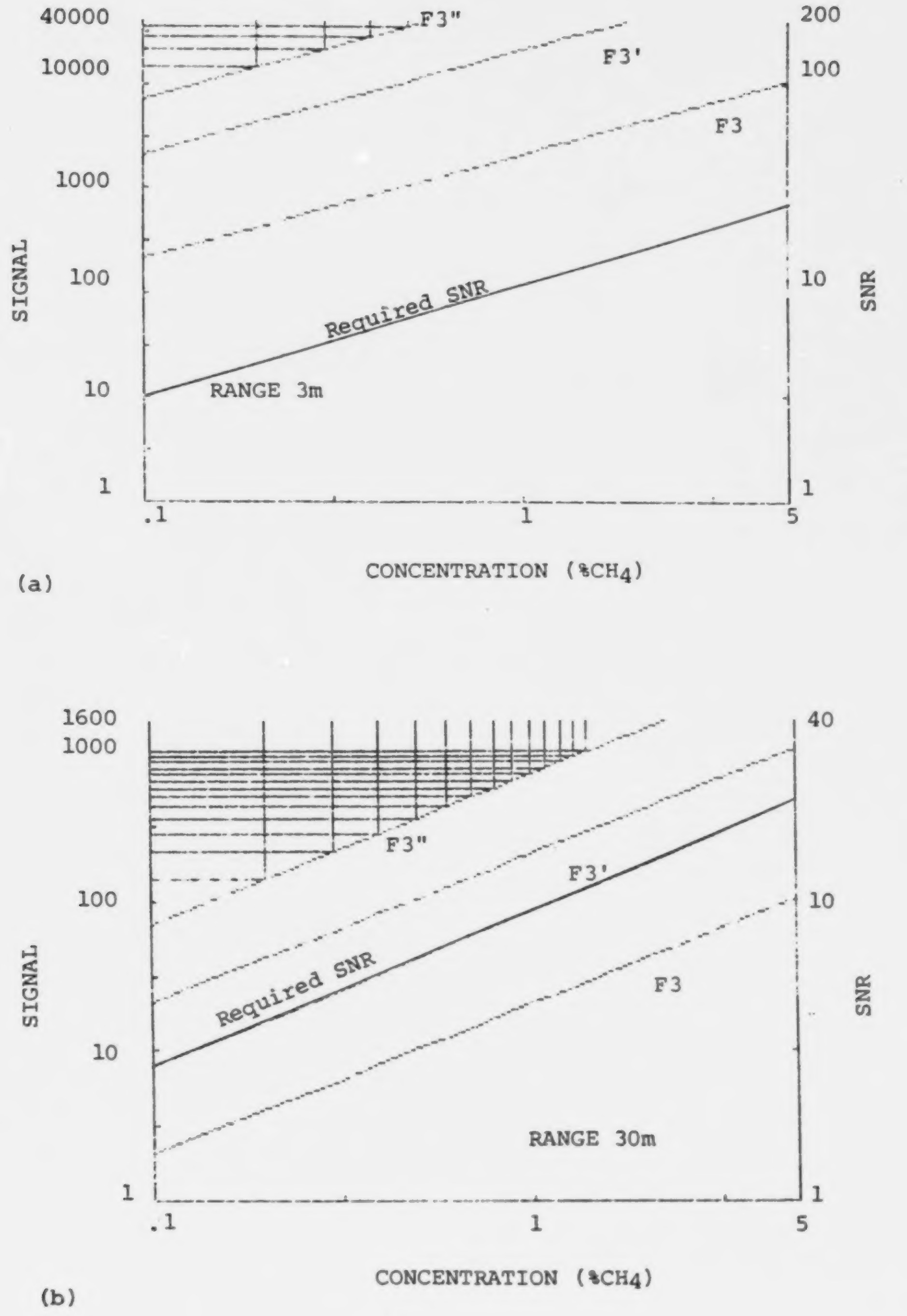

F3 = Laser Function: 6.570E+003
F3' = Laser Function: 6.570E+004
F3" = Laser Function: 2.222E+005

Figure 4.4: Signal and Signal to Noise Ratio (SNR) versus Methane Concentration

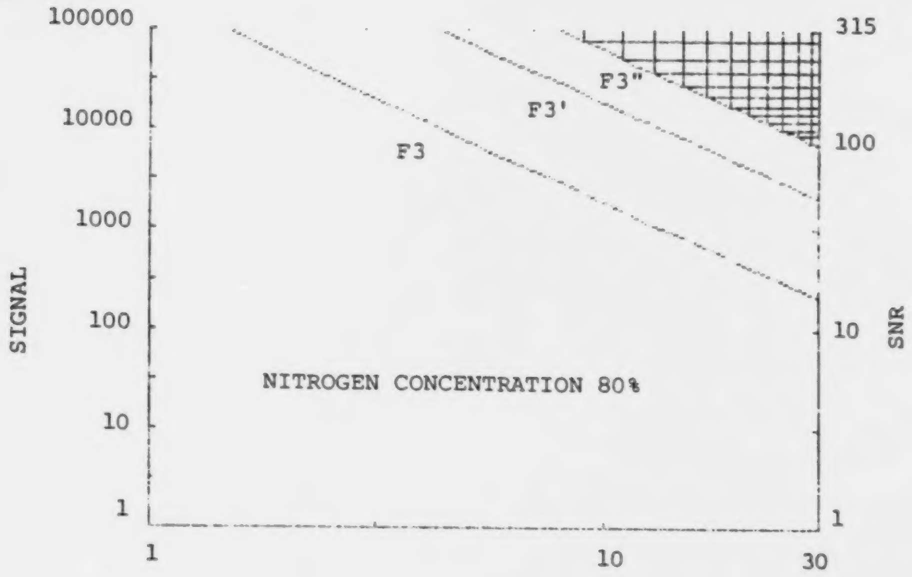

F3 = Laser Function: 6.570E+003
F3' = Laser Function: 6.570E+004
F3" = Laser Function: 2.222E+005

Figure 4.5: Signal and Signal to Noise Ratio (SNR) versus Range for Nitrogen

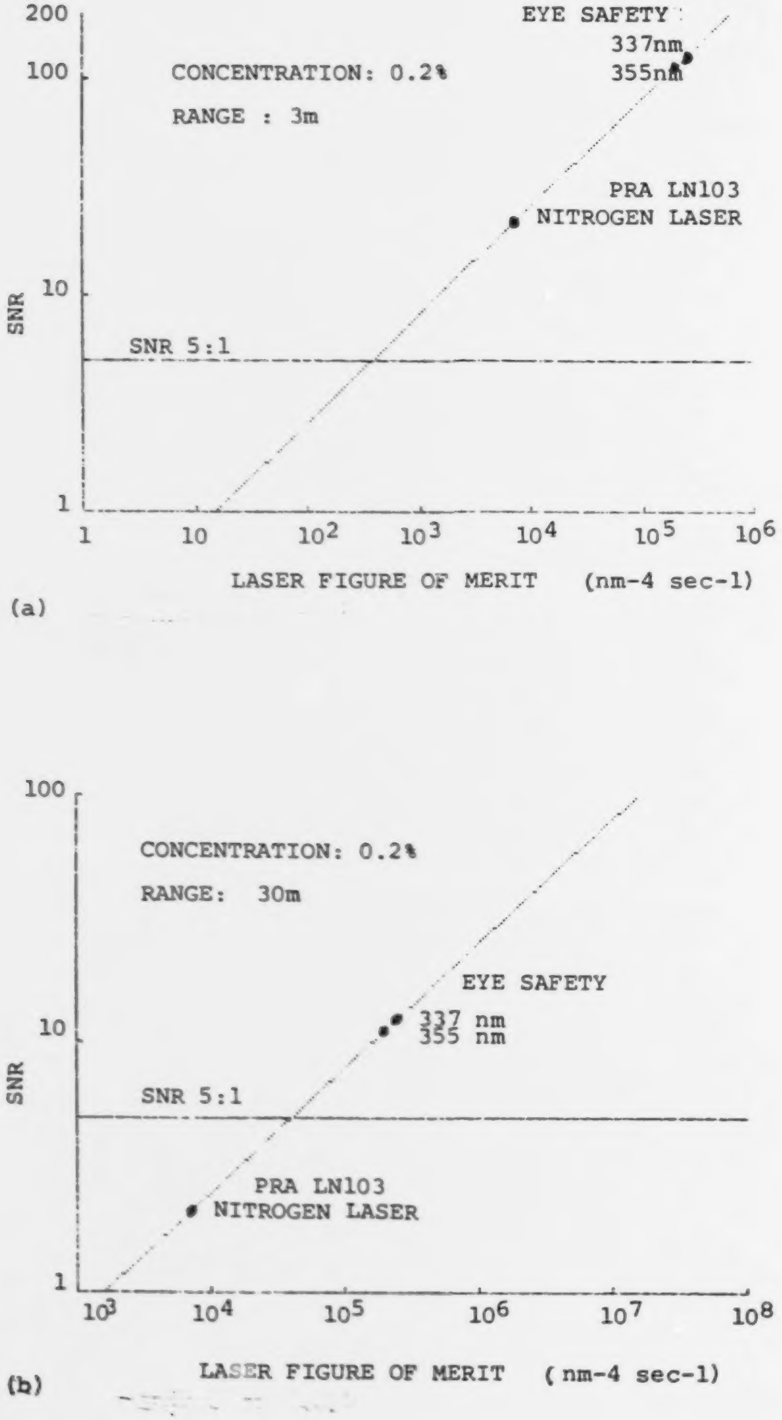

Figure 4.6: System Performance versus Laser Figure of Merit

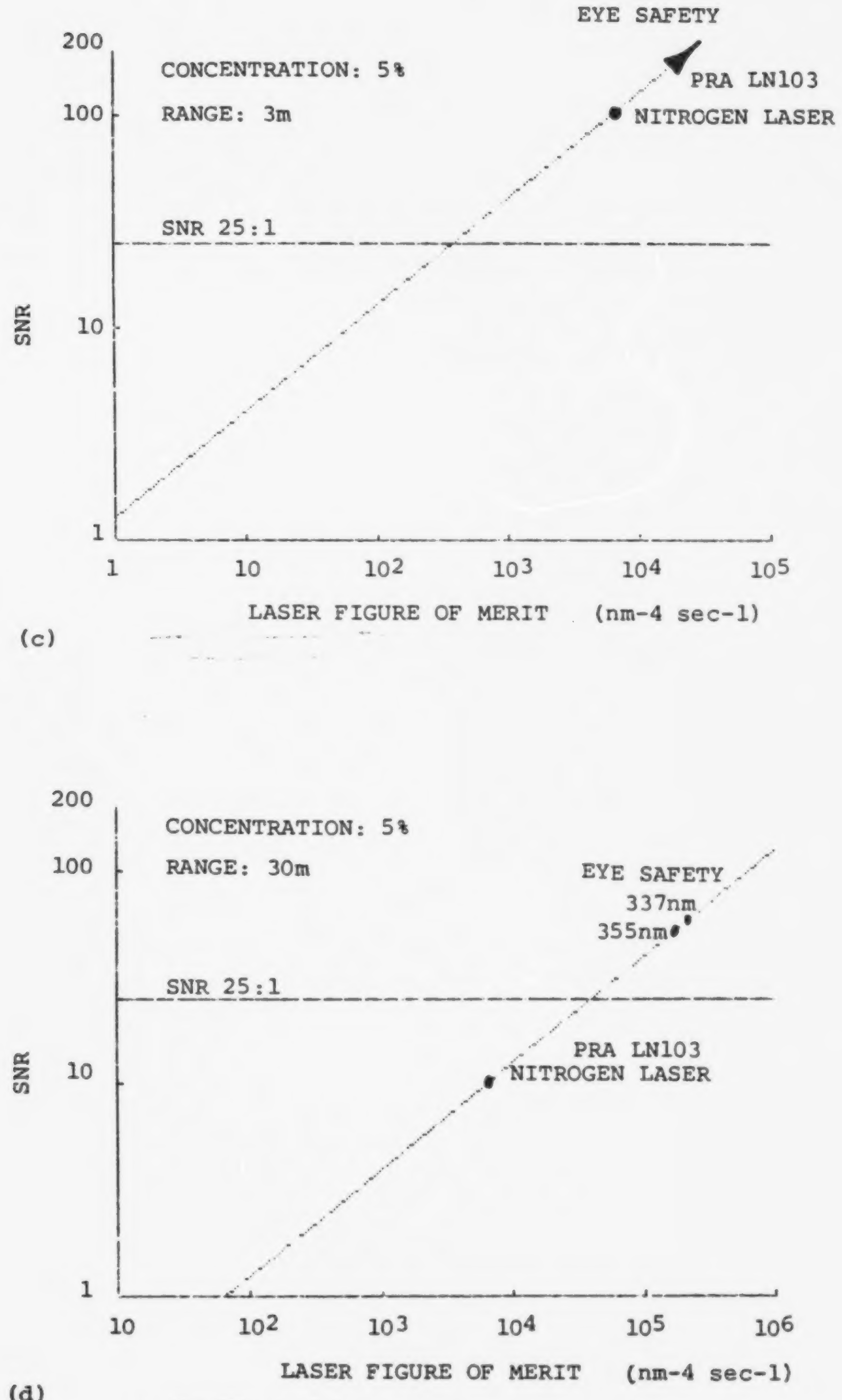

(c)

(d)

Figure 4.6: System Performance versus Laser Figure of Merit (cont'd)

Figure 4.7: Schematic Diagram of Laser Diode Pumped Nd:YAG Laser

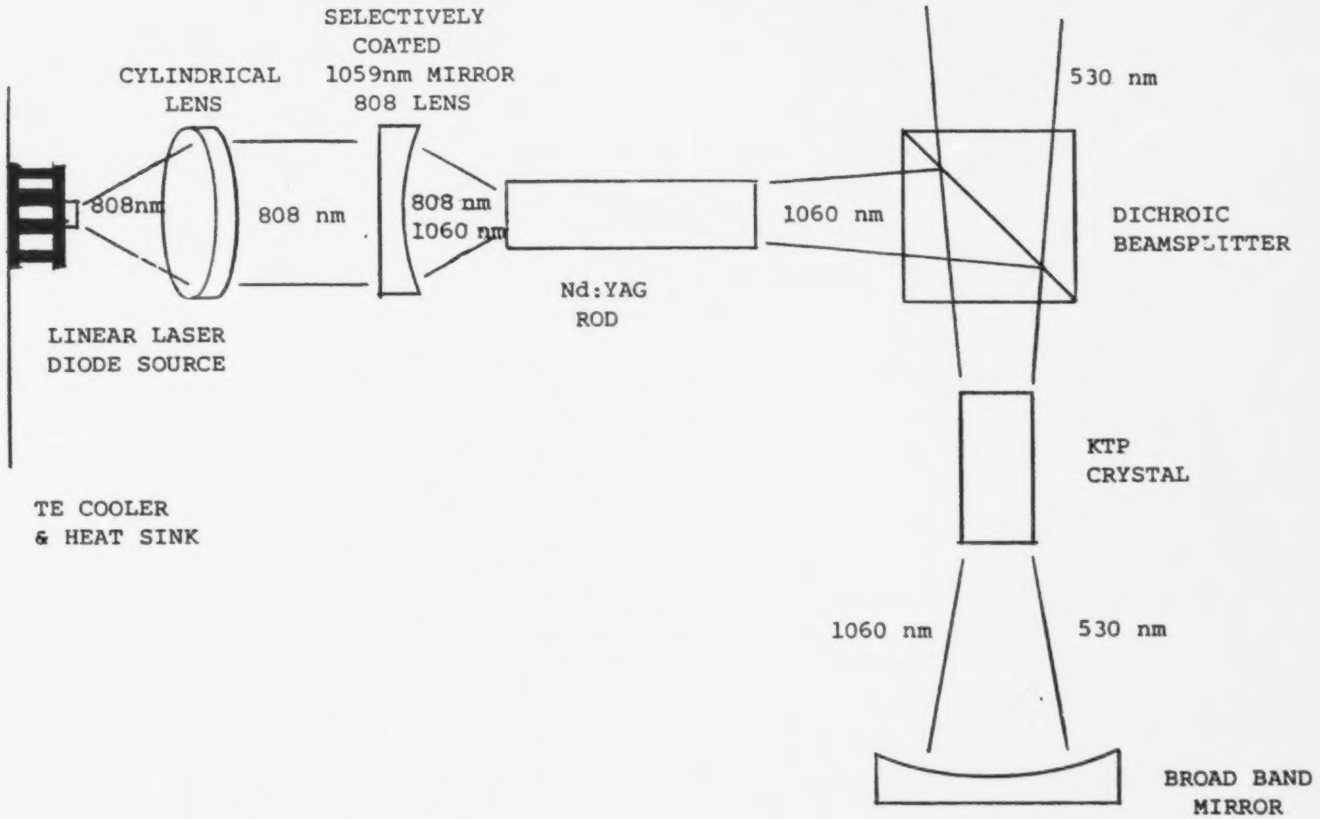
SELECTIVELY
COATED
1059nm MIRROR
808 LENS
CYLINDRICAL
LENS
530 nm
808nm
808 nm
808 nm
1060 nm
1060 nm
DICHROIC
BEAMSPLITTER
Nd:YAG
ROD
LINEAR LASER
DIODE SOURCE
KTP
CRYSTAL
TE COOLER
& HEAT SINK
1060 nm
530 nm
BROAD BAND
MIRROR

5.0 OPTICAL INSTRUMENTATION CONCEPTS

5.1 Optical Overview

A collinear optical design places considerable constraints on the system geometry. The optical train described in the sections following uses a catadioptric collection lens to gather backscattered light from a collimated source beam along the optical axis of the lens. A catadioptric lends itself to this application since its secondary mirror presents a natural place for the source beam; that is, the source does not directly illuminate the receiver while maximizing the target volume. In addition, the entrance pupil is located at the entrance aperture of the lens which maximizes the collection efficiency. Finally optics of this type are typically long focal length collecting over narrow field angles, a desirable feature in this system.

Figure 5.1 shows an overview of a typical optical system. As noted above, certain sources require beam expansion to satisfy limitations of eye safety; that is, the beam can be expanded to match the diameter of the central obscuration in the collection lens. Aside from reducing the sources energy density to eye safe or skin safe levels, we have obtained better collimation of the source beam minimizing its divergence. In addition, beam expansion prevents heating of contaminants on external windows.

The collection optic must have two characteristics. A large entrance pupil is necessary to maximize the signal collected at the greatest range of the instrument. The lens also must have a narrow collection angle and therefore a long focal length. A mirror lens (catadioptric) has its entrance pupil located at the first surface; with a folded path, a long focal length lens can be packed into a small package. In the system discussed here good spatial resolution is secondary to maximizing the radiometric throughput. We can do this by keeping the number of refractive optical elements to a minimum. Section 5.2 examines the range response of the system.

After the light is collected the relevant spectral signals must be isolated. Three signals will be important in this detection scheme. By far the largest signal will be the Mie scattering signal from aerosols in the mine atmosphere. The Mie signal occurs at the laser wavelength. The remaining two signals are both due to the Raman shift from the source wavelength to characteristic wavelengths corresponding to the target gas, methane, and a normal atmospheric constituent, nitrogen. The nitrogen signal will give a normalization factor for the expected range response function and the degradation of the source energy due to absorption or scattering by coal dust or other aerosols.

Each signal can be isolated by using spectral filters. Suffice it to say that there are very stringent requirements on the out of band rejection for both Raman signals since they are many orders of magnitude less than the Mie scattering signal. There are other sources of stray light such as fluorescence and ambient light. Fluorescence in the optical train can be minimized by using fused silica and reflective optics where possible.

Photomultiplier tubes are by far the most sensitive detectors in the spectral region covering the near ultraviolet to blue green. In Section 5.3 we identify the following desirable characteristics of PMTs.

- Fast rise times (< 2 ns) for range resolution.
- High sensitivity, 25% quantum efficiency.
- High inherent gain, (ca 1E06).
- Good linearity.

Reflectance from any solid object can easily exceed the background signals referred to before and its misinterpretation as signal is an item of concern. The principal reason for measurement at the laser wavelength is to establish the operational range for the measurement. The detectors can be gated to collect data only over the interval starting with the laser pulse and ending just before the wall return.

Considering the working environment there may be concern of coal dust on the optical surfaces. Clearly a front window will be necessary to protect the internal optics. This can be protected when not in use by a lens cap, and when in use by either flowing filtered air across the surface, or with periodic cleaning. The effect of small accumulations of coal dust will be minimal since the degradation of the signal is proportional to the fraction of the window actually obscured. Any fluorescence in the coal dust both on the window or in the optical path will likely obscure at longer wavelengths and will be dealt with by the spectral filters.

5.2 Range Response Function

In this section, we specifically address the variation of the receiver aperture with range.

Note that the terms in equation 4.1 can be rewritten (replaced)

$$A\left(\frac{1}{R_N} - \frac{1}{R_f}\right) \sim \frac{A}{R^2}\,\Delta R \sim \int_{R}^{R+\Delta R} \Omega(R)\,dR \qquad (5.1)$$

where ΔR is the range resolution.

Ω is the solid angle collected by the optical system.

There are four distinct regions from which the backscatter signal is collected. Each zone is dominated by obscurations which vignette at a particular range, and by the limiting field angle allowed by the collection optic. Figure 5.2 shows the illuminated cylindrical volume the central obscuration and the outer diameter of the primary mirror. The cones that are illuminated represent the limiting field angle for the receiving optic. Each zone is identified.

Zones 2 and 4 have a very straight forward analysis. In Zone 2 the solid angle of collection is limited only by the area of the central obscuration and the range. The outer angle is limited by the admissible angle for the collection optic. Clearly as the range increases the solid angle of the receiver increases since the solid angle occupied by the central obscuration decreases. Backscatter from Zone 4 is by definition within the allowable angular range. The same effect that allowed the signal to increase now causes the signal to decrease. Only signal that is incident on the receiver is collected, since the receiver subtends a smaller solid angle as range increases the backscatter collected also decreases. In both these cases there is little dependence on the location within the source beam since the areas vary only as the cosine of the off-axis angle. In the system described here, that angle is very small and becomes smaller with range.

Zones 1 and 3, can be thought of as transition regions; in Zone 1 the transition is between no signal (Zone 0), and the Zone 2 signal. The signal here has a strong dependence on the off-axis location since it is dominated by vignetting, the fractional signal loss is large due to the obscuration.

Zone 3 is the transition from a signal that increases with range to one that decreases with range. This section has a large dependence on the radius from the axis; at different radial positions lights lost backscatter because of misses the collection aperture. Although the angle of propagation is within the limiting field angle. In Zone 3 the contribution from the central obscuration is of a lesser importance.

We have evaluated a test case which matches the central obscuration to the source beam at 5 cm diameter radius, and uses a 30 cm diameter collection optic. For these illustrations the full collection angle has been pegged at 2 degrees, and no beam divergence has been included. The extent of the four zones is:

Zone 1 0 - 2.865 m

Zone 2 1.432 - 8.594 m

Zone 3 7.161 - 10.025 m

Zone 4 8.594 - 30 m

Each transition zone is about 3 m long and the signal from each zone must be normalized in order to get quantitative results.

The normalization that has been chosen differs slightly from a strict calculation of Ω (R); rather we have calculated the range response function F(R)

$$F(R) = \frac{\Omega(R)}{4\pi \sin^2 \alpha/2} \text{ ca } \frac{A}{4\pi R^2 \sin^2 \alpha/2} \tag{5.2}$$

where α is the cone half angle (ca 1 degree in our case);

i.e., we normalize to the solid angle accepted by the field stop.

For a receiver of 30 cm diameter, A ca 707 cm**2, F(R)=1 corresponds to a range of 8 m. That is, for range beyond 8 m we expect R**-2 dependence and for ranges less than 8 m we expect serious departures as the field stop limits the maximum aperture.

Figure 5.3 shows both the actual range response function and the R**-2 limit.

Clearly, the system performance (relative to Section 4.3) is unaffected at ranges > 9 m and is maximum at a range of ca 7.5 m. We note that there is substantial degradation in performance at shorter ranges; however, the results of Section 4.3 indicated a safety factor of 4 times at range of 3 m for the nitrogen laser. The figure shows that the response between 1.5 and 9 m is greater or equal to the response at 12 m and in Section 4.3, we had concluded, that satisfactory performance could be obtained at 12 m range (i.e. SNR of 5/25 for 0.2%/5% methane concentration). Consequently, the system performance will be adequate at the shortest range (3 m) that we have considered in that section.

The other point that we note is the reduction in dynamic range relative to Section 4.3 above. In that section the overall dynamic range was about 2500:1; of this a factor of 25 comes about due to the concentration range and a factor of ca 100 due to spatial range. In Figure 5.3 we see that latter factor is clearly reduced to ca 9:1 resulting in an overall dynamic range of ca 225:1.

5.3 Colour Separation and Stray Light

The most important source of stray light is that due to Mie scattering. We estimate the amount of stray light from the transmittance of a column of air and derive the requirements of the filter system.

The wavelengths corresponding to Raman bands from methane and nitrogen are given in Table 5.3. We note that the Raman band of methane is narrower than filter technology will permit. However there is a general reduction in filter transmittance as filter bandwidth decreases. Filters of different construction will be examined.

5.3.1 Laser Rejection Requirement

In this section, we estimate the amount of stray light that is present in the overall system and the effect of careful filter design.

The transmittance, T of a dust laden air column of length R is given by

$$T = e^{-(\alpha + \beta) R} \qquad (5.3)$$

where α and β are the absorption coefficient and the scattering extinction respectively.

The absorption term affects signal and background equally while the scattering term affects the signal to background ratio. Assuming a Beer's Law model and uniform phase function. We can estimate the product of dust density and differential scattering cross-section:

$$\beta R = \rho \left(\frac{d\sigma}{d\Omega}\right)_{\text{Mie}} 4\pi R \qquad (5.4)$$

If the transmittance due to scattering Ts = exp(-βR) then $\left(\rho\frac{d\sigma}{d\Omega}\right)_{\text{Mie}}$ = -2.65 E-05 lnTs cm**-1/sr while the corresponding methane terms are

$$\left(\rho \frac{d\sigma}{d\Omega}\right)_{\text{Methane}} = 7.1 \times 10^{-11} c \text{ cm}^{-1}/\text{Sr}. \qquad (5.5)$$

where c is the gas concentration.

At the Raman wavelength (λR) and the background wavelength (λB), we find a signal to background (S/B) ratio of

$$\frac{S}{B} = -2.7\text{E-06} \left(\frac{\varepsilon(\lambda_R)\ T(\lambda_R)}{\varepsilon(\lambda_B)\ T(\lambda_B)}\right) \frac{c}{\ln T_s} \qquad (5.6a)$$

Furthermore it is reasonable to assume equal quantum efficiencies, i.e.,

$$\frac{\varepsilon(\lambda_R)}{\varepsilon(\lambda_B)} \text{ ca } 1 \qquad (5.6b)$$

Consequently the filter rejection at a concentration of 0.25% is given as:

$$\text{Rejection} = \frac{T(\lambda_R)}{T(\lambda_B)} = -(\frac{S}{B}) \ln T_s \; 1.5E08 \qquad (5.7)$$

where S/B is the desired signal to background ratio. A similar deviation is applicable to the Raman scattering from nitrogen. Since 80% nitrogen in the atmosphere corresponds to an equivalent signal of 10% methane, the rejection for methane is 40 times less. These ratios are given in Tables 5.1 and 5.2.

5.3.2 Interference Filters

Bandpass filters in the 350-400 nm region have a rejection of 1E-04 in collimated light. However such filters have an overall transmittance of only 20%. Referring to Table 5.1, for B/S=0.1, Ts=0.9 we require a rejection of ca 1.6E08, so these two such filters will have an overall transmittance of 4% which is rather small. The low transmittance is due to the use of metal films; all-dielectric bandpass filters are not normally fabricated in this spectral region.

Two alternate proposals are suggested using multi-layer dielectric bandpass coatings. The first employs a filter which reflects at the laser wavelength while transmitting at the Raman wavelength, while the second employs a pair of filters which transmit at the laser wavelength and reflect at the Raman wavelength. Use of both filters, is illustrated in Figure 5.4.

In both cases an absorptive cavity is required to stop the laser beam from reaching the detector. The characteristcs of a Raman Notch filter constructed for the visible is shown in Figure 5.5 and a rejection of 1.8E03 is possible for 2 plates. Use of 4 plates improves the rejection to 3.2E06 at the expense of reduced transmittance. The reflection filter can typically reflect 99.9% of the laser light, (i.e. transmit 0.1% of the laser light) and yet transmit 75% of the Raman light which is > 25 nm away from the laser giving a rejection of ca 750:1.

5.3.3 Long Pass Filters

Color glass filters, plastic filters or liquid filters can be used to provide a cut on filter which rejects the laser radiation. A liquid filter consisting of a water solution of 2,7-dimethyl-3,6-diazcyclohepta-1, dieneperchlorate, has been reported to provide an effective filter for rejecting the returned radiation from a nitrogen laser (337.1 nm) (Ref. 19). The filter, however, is only useful for rejecting radiation below 340 nm and is not, therefore, suitable for use with the tripled Nd:YAG laser (353 nm). It is possible however that an extensive literature search would uncover a liquid filter suitable for use with the tripled Nd:YAG. The tabulation below is tentative since fluorescence characteristics are not available in the literature and experimental evaluation is required. Transmittance curves are given in Appendix 3.

We note that these filters cannot effectively distinguish the Raman signals from methane and nitrogen. Furthermore, that such filters should be placed behind any multi-layer dielectric filter since the fluorescence is reduced by the rejection ratio of the dielectric. If filters are placed in a pseudo collimated region fluorescence is collected over a small solid angle.

Theoretical calculations for a multi-layer dielectric long pass sharp cut on filter have been performed by InterOptics Limited. The long pass cut on filter would behave as a reflection filter with a 15 degree angle of incidence (as opposed to the 45 degree angle shown in Figure 5.4). The transmittance is tabulated below:

Transmittance of a long pass filter at 15 degree incidence:

Description	λ (nm)	Transmittance	Rejection
Laser	353	5E-05	2E04
N2 Raman	378	.01	100
CH4 Raman	394	> 0.75	1

We note that the filter could also be used to reject the nitrogen line if this is required.

At incidence angles of 25 degrees the edge of the filter is not as sharp and the rejection ratio is reduced. Greater detail is provided in Appendix 3.

The design of the long pass dielectric filter is not particularly sensitive to the laser wavelength and will avoid any of the fluorescence difficulties associated with the color filters.

5.3.4 Angle of Incidence Effect

The effects of angle of incidence of the light on the filters can be modelled for the multi-layer dielectric coating. For the 350 nm region an effective index of 2.0 is as large as is practical and 1.45 may in fact be more accurate. We can estimate the cone angle at the filter.

$$\theta = \sin^{-1} \left(\frac{2\eta^2 \Delta\lambda}{\lambda}\right)^{1/2} \qquad (5.8)$$

where θ is the cone angle of the converging/diverging beam, η is the effective index and $\Delta\lambda$, λ are the wavelength shift and centre wavelength respectively. The solid angle of the cone is:

$$\Omega = 4\pi \sin^2 \theta/2 \qquad (5.9)$$

These results are tabulated in the Table 5.4. Since the etendu (area x solid angle) of an optical system is fixed, the larger the cone angle the smaller the filter.

5.3.5 Recommendation

The recommended filter system will consist of a dielectric long pass cut on filter in series with a bandpass filter; one for each Raman band. Bandwidths as narrow as 2 nm appear practical due to the limited field angle.

5.4 Other Sources of Stray Light

5.4.1 Ambient Light

Incandescent bulbs provide little radiation in the spectral region < 400 nm. Since we are using a "Time of Flight" method of detection we are collecting the ambient light only for a short time interval. Most importantly perhaps is the fact that our signals occur in a very narrow passband that serves to minimize the effect of stray light. Everett et al (Ref. 8) estimate ambient sources as contributing ca 1.5 photons; this corresponds to < 0.4 observed photoelectrons for quantum efficiency of ca 0.25.

5.4.2 Fluorescence in Coal Dust

Fluorescence from coal dust has not been studied quantitatively. In their study of spectral fluorescence as a classifier of coalification, Ottenjan et al indicate that absolute intensities are heavily dependent on weathering and handling of their pressed samples. Their experimental work however is relevant since excitation at 365 nm is similar to the wavelengths suggested here. The results indicate fluorescrence which starts at 400 nm and extends to the near infrared. Figure 5.6 is reproduced from their paper (Ref. 17).

However, since Raman signals are very small (25-50 photons) this data is clearly inadequate unless it is quantified by detailed experimental evaluation. We note that the fluorescence will increase with laser power but not with methane concentration so that fluorescence is most important at low concentration.

5.5 Detector Selection

The requirements of the detector that is used to sense range gated Raman signals can be put in three categories: sensitivity, fast response and linearity. High sensitivity is required because of the small signals that are present. The detector must be compatible with narrow band rejection filters and be sensitive in the UV. Fast response is intrinsic to a 'time of flight' measurement; for a 1 m spatial resolution a 3.3 ns response time is required. The pulse response duration is determined by pulse dispersion in the electron multiplier. Linearity is an important characteristic of the detector and preamplifier. If the detector is non-linear a history interpretation would be necessary to extract concentrations of the target gas. This implies that the analog signal chain must operate well below fast return recovery with in between pulses.

There are two physical mechanisms for detecting light: the photoelectric effect and internal quantum conversion. The first effect is utilized in a variety of detectors which all possess a photocathode. All such devices use secondary electron emission to give high amplification without introducing large amounts of noise. This category includes photomultipliers (PMT) and image intensifiers. The second effect is characteristic of semi-conductor detectors. In this case, an electron hole pair is created in the device and electric fields associated with the doping of the detector separates the electron hole pair, suitable detectors in the category correspond to PIN and avalanche photodiode all based on silicon.

Photocathodes are generally quite sensitive and have quantum efficiencies of 10-25% through UV and visible. The silicon devices have very high quantum efficiency (ca 80%) in the red but this degrades rapidly toward the blue so that the quantum efficiency is substantially smaller than that of a photocathode.

Photomultiplier Description and Characteristics

Photocathodes are of two types: opaque (side on) and semi-transparent. Bialkali and trialkali materials are used, both have low work functions which improves their red sensitivity. Figure 5.7 shows the wide variety of photocathodes that are available.

There are three different designs for the electron multipliers. These are circular cage, linear focussed and microchannel plates.

Side on type PMTs have a limited cathode area, however, they are suited to slits of spectrographic instrumentation. The spatial uniformity of the photocathode is poor varying between 50-100% of the nominal sensitivity. This type of PMT uses a circular cage electron multiplier but can only incorporate opaque photocathodes. These photocathodes have quantum efficiency of 10-25% at wavelengths beyond 300 nm although the quantum efficiency can exceed 25% below 300 m. The circular cage can give quite fast rise times comparable to the linear focussed devices.

End on type PMTs utilize semi-transparent photocathodes which are available in circular, square, hexagonal shapes. These photocathodes are very uniform, sensitivity varies spatially from 90-100% of the nominal value. This type of photocathode is available in diameters from 10 mm to 127 mm in diameter. However the rise times vary as a function of diameter from 0.8 ns at 10 mm, 1.3 ns at 51 mm, 3.4 ns at 127 mm due to the pathlength associated with the electron trajectories from the photocathode to the first dynode. There is a choice of dynode arrangements. The conventional dynode is linearly focussed which gives very fast rise times, and very fast fall times. Box and grid electron multipliers generally give slower rise times and are not recommended. The fastest rise times and fall times are available from microchannel plates which of course provides minimum pulse FWHM. Microchannel plates are limited to 18 mm diameter photocathodes.

The semi-transparent photocathode materials have higher quantum efficiency in the 300-400 nm region than at shorter wavelength; the quantum efficiency exceeds 25% for K-Cs-Sb and is optional.

Table 5.5 summarizes information for one manufacturer's data for suitable PMTs and indicates asymmetry in the pulse shape.

5.6 Receiver Focal Length

To estimate the focal length of the optical train, we note that the field stop should be imaged on the PMT. Consequently a +/- 1 degree circular field stop will imply the effective focal lengths given in Table 5.6. The focal ratio is calculated for a 300 mm diameter receiver.

Table 5.1: Rejection Ratio for Methane vs Atmospheric Transmittance

T_s	.995	.95	.90	.50	.10
$\frac{B}{S}$					
.01	$7.5x10^{7}$	$7.6x10^{8}$	$1.6x10^{9}$	$1x10^{10}$	$3.4x10^{10}$
.1	$7.5x10^{6}$	$7.6x10^{7}$	$1.6x10^{8}$	$1x10^{9}$	$3.4x10^{9}$
1	$7.5x10^{5}$	$7.6x10^{6}$	$1.6x10^{7}$	$1x10^{8}$	$3.4x10^{8}$
10	$7.5x10^{4}$	$7.6x10^{5}$	$1.6x10^{6}$	$1x10^{7}$	$3.4x10^{7}$
100	$7.5x10^{3}$	$7.6x10^{4}$	$1.6x10^{5}$	$1x10^{6}$	$3.4x10^{6}$

*T_s - Transmittance due to scattering

Table 5.2: Rejection Ratio for Nitrogen vs Atmospheric Transmittance

T_s	.995	.95	.90	.50	.10
$\frac{B}{S}$					
.01	$1.9x10^{6}$	$1.9x10^{7}$	$4x10^{7}$	$2.5x10^{8}$	$8.5x10^{8}$
0.1	$1.9x10^{5}$	$1.9x10^{6}$	$4x10^{6}$	$2.5x10^{7}$	$8.5x10^{7}$
1	$1.9x10^{4}$	$1.9x10^{5}$	4.10^{5}	$2.5x10^{6}$	$8.5x10^{6}$
10	$1.9x10^{3}$	$1.9x10^{4}$	$4x10^{4}$	$2.5x10^{5}$	$8.5x10^{5}$
100	$1.9x10^{2}$	$1.9x10^{3}$	$4x10^{3}$	$2.5x10^{4}$	$8.5x10^{4}$

*T_s - Transmittance due to scattering

Table 5.3: Centre Wavelength(s) and Absorptive Filters

Laser Source	Filter	Laser		Nitrogen Raman		Methane Raman	
		λo (nm)	Transmittance	λ (nm)	Transmittance	λ (nm)	Transmittance
Quadrupled Nd: YAG	None	265		282.4		287.2	
Nitrogen	KV370	337	$<10^{-5}$	365.7		373.0	
Doubled Ruby	Plexiglass	347	<.01	377.5	NA	386.1	>0.7
	UVA-3						
	KV370		$<10^{-3}$		0.8		>0.95
	KV380		$<10^{-4}$				0.8
Tripled Nd: YAG	Plexiglass	353		384.7		394.0	
	UVA-3		<.01		0.72		.85
	KV370		8×10^{-3}		>.95		>.95
	KV380		$<10^{-4}$		>.95		>.95
Doubled Nd: YAG	OG590	530	$<10^{-5}$	604.7	0.8	626.8	>.95
	OG610		$<10^{-5}$		0.20		>.90

NA - Not Applicable

Table 5.4: Wavelength Shift

Shifts (nm)	Nominal Centre Wave-length	Cone Angle		Solid Angle (sr)		Maximum Demagnification at the Filter	
		Effective Index 1.45	2.0	Effective Index 1.45	2.0	Effective Index 1.45	2.0
2	390	8.44	11.7	6.8x10-2	0.13	8.2	11.4
5	390	13.4	18.7	0.17	0.33	13	18

Table 5.5: Hamamatsu Photomultiplier Tubes

R2051 2 inch O BiAlkali	Rise Time FWHM	1.3 ns 3 ns
12 dynode linear focus	Fall Time	7.4 ns
R2287U 18 mm O BiAlkali	Rise Time FWHM	0.3 ns 1.5 ns
MCP 3 stage	Fall Time	.7 ns

Table 5.6: Effective Focal Length

PMT Diameter (nm)	Focal Length (mm)	Focal Ratio
18	515	1.7
25	716	2.3
50	1432	4.8

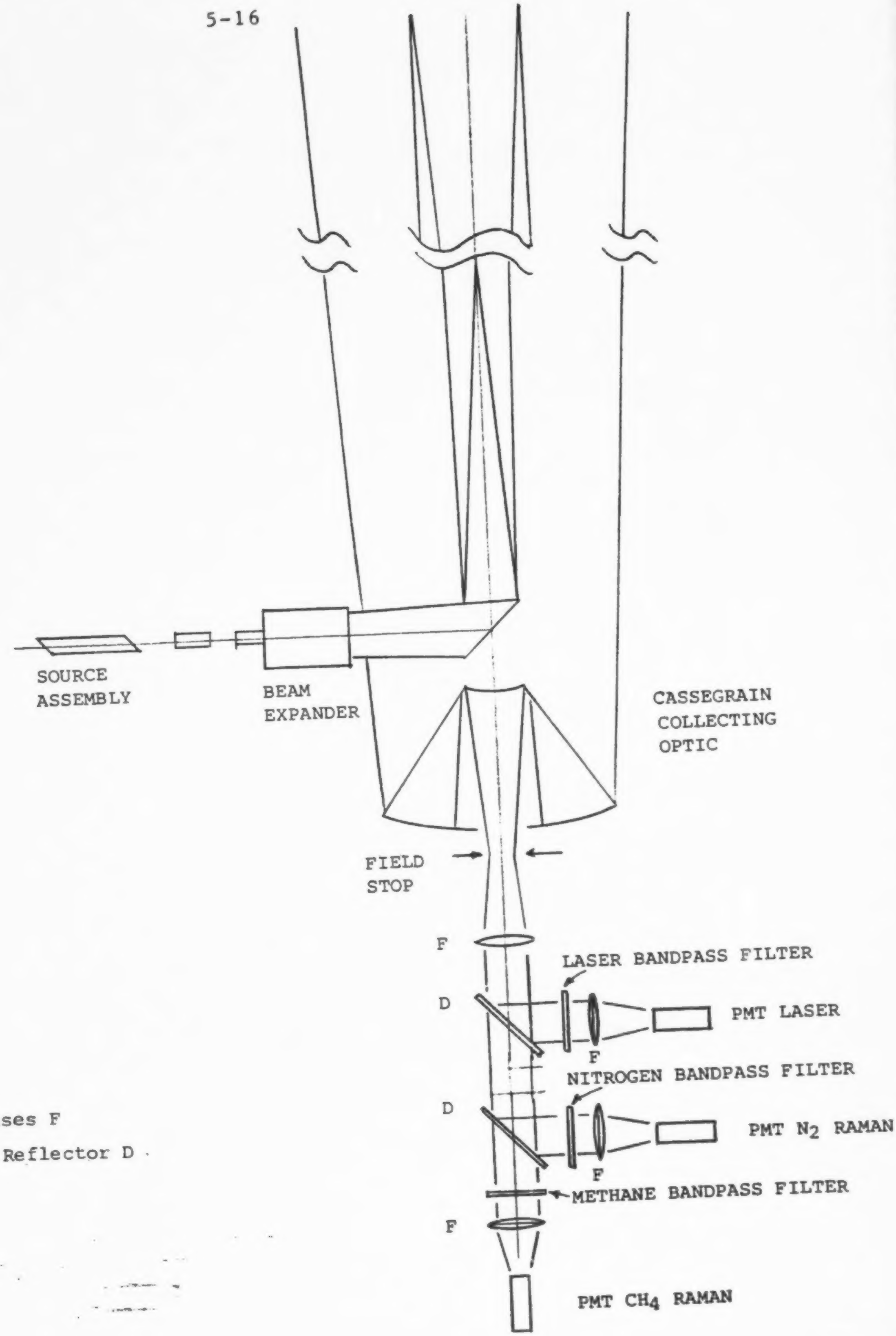
SOURCE ASSEMBLY
BEAM EXPANDER
CASSEGRAIN COLLECTING OPTIC
FIELD STOP
F
LASER BANDPASS FILTER
D
PMT LASER
F
NITROGEN BANDPASS FILTER
D
PMT N_2 RAMAN
F
METHANE BANDPASS FILTER
F
PMT CH_4 RAMAN

- Field Lenses F
- Dichroic Reflector D

Figure 5.1: Overview of a Typical Optical System

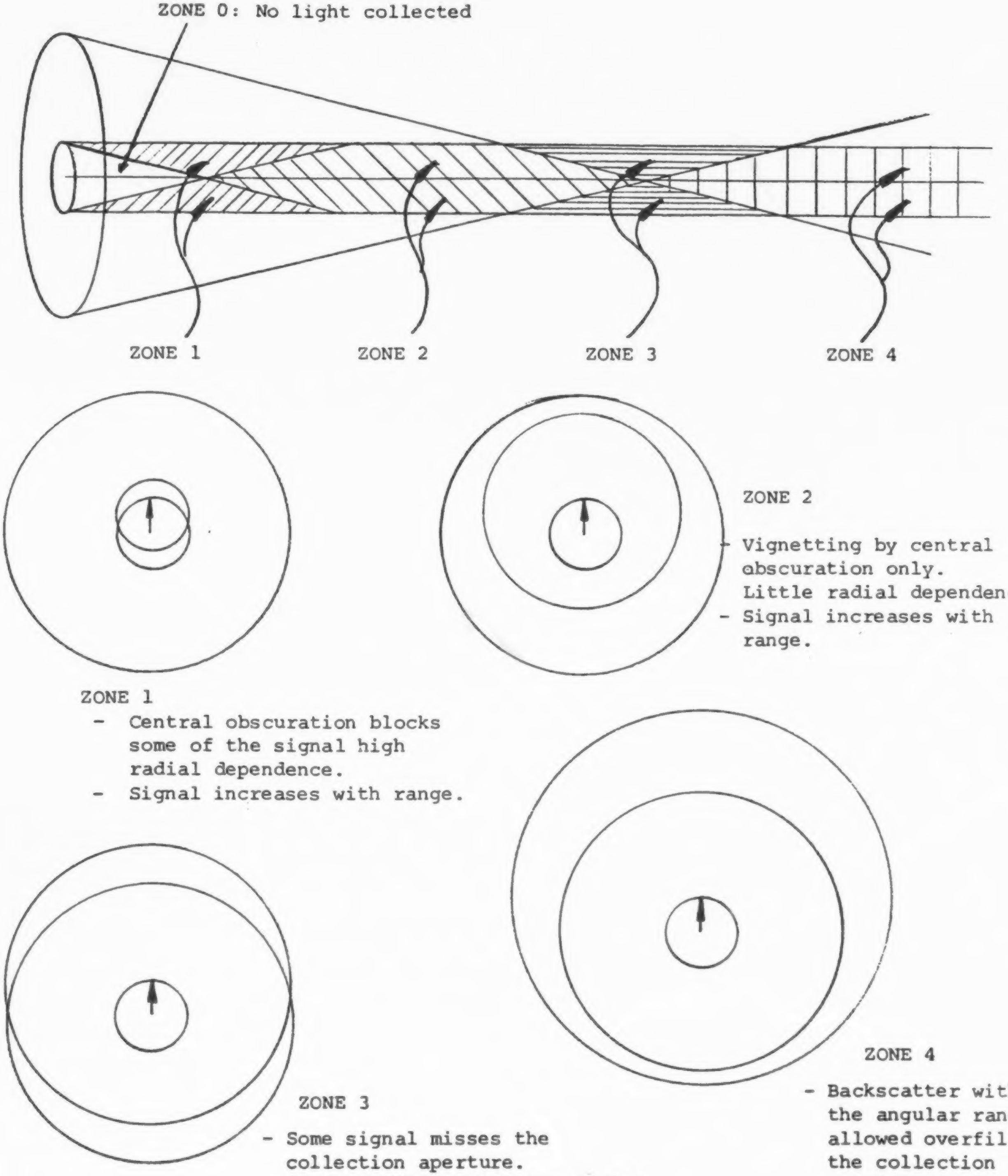

ZONE 2

- Vignetting by central obscuration only. Little radial dependence.
- Signal increases with range.

ZONE 1

- Central obscuration blocks some of the signal high radial dependence.
- Signal increases with range.

ZONE 4

- Backscatter within the angular range allowed overfills the collection aperture.
- Signal varies as $\frac{\text{collection Area}}{(\text{range})^2}$

ZONE 3

- Some signal misses the collection aperture. Central obscuration has little influence strong radial dependence.
- Signal decreases with range.

Figure 5.2: Zones of Different Range Response

Figure 5.3: Normalized Range Response

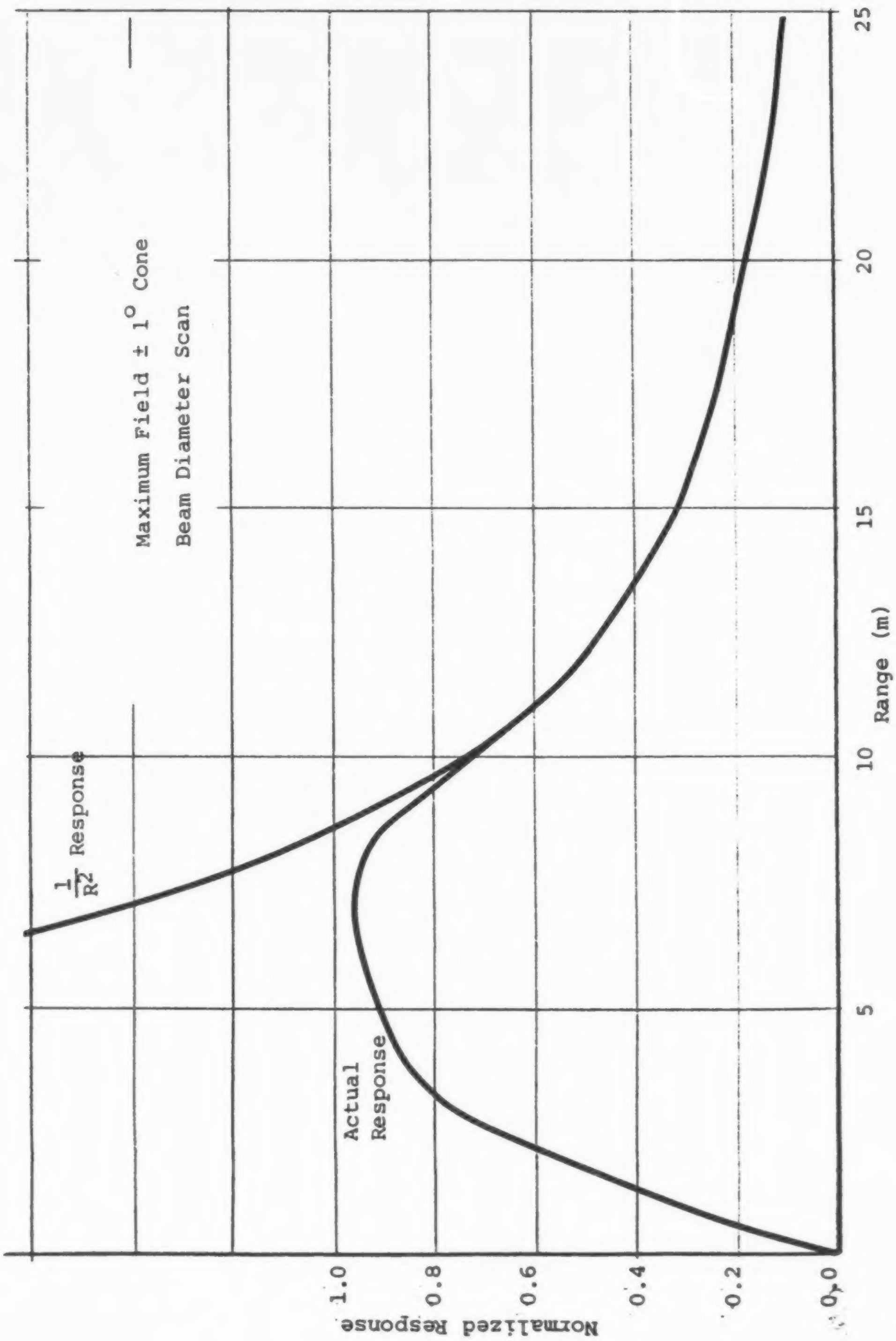

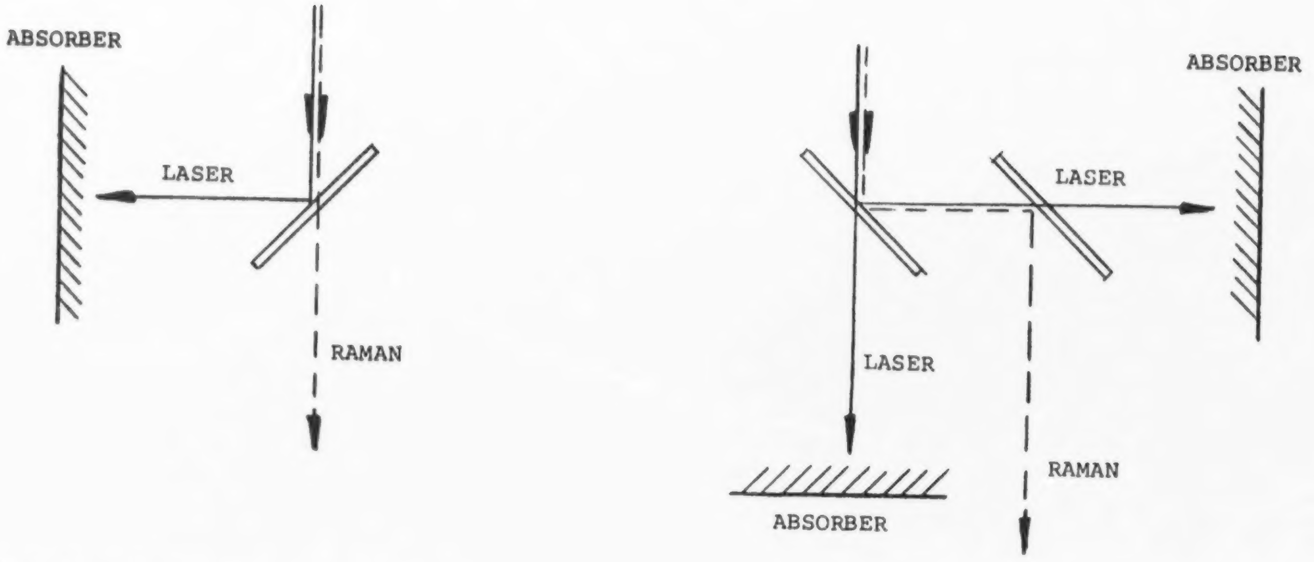
ABSORBER
LASER
RAMAN
LASER
ABSORBER
LASER
ABSORBER
RAMAN

a) Reflection Filter

b) Raman Notch

Figure 5.4: Alternate Interference Filter Deployment Scenarios

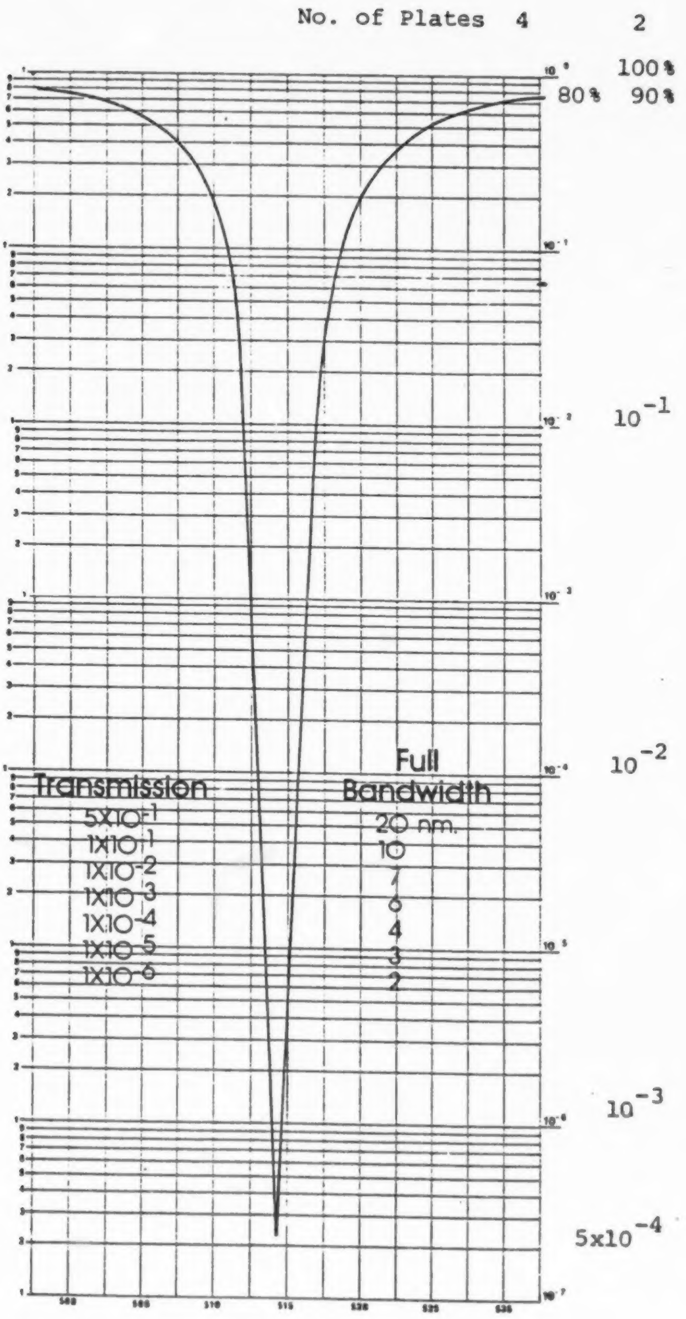

Figure 5.5: Raman Notch Filter

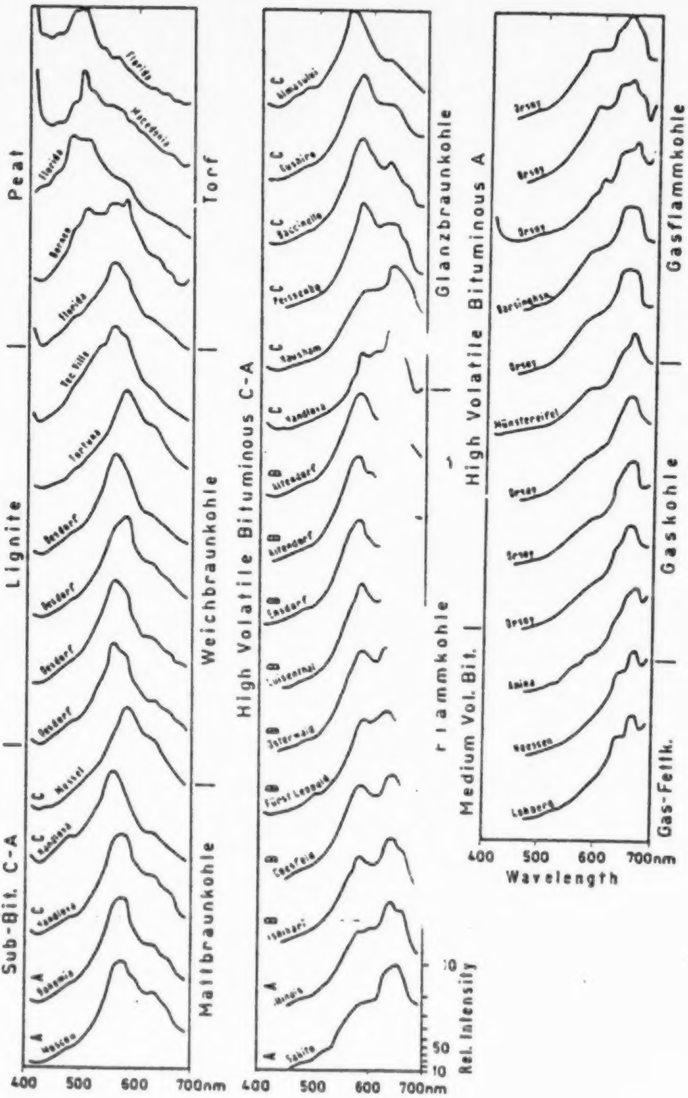

Figure 5.6: Fluorescence from Coals

Change of average sporinite fluorescence spectra with increasing rank of coal (related to the ASTM classification, USA and the German coal classification.

Reproduced from Ottenjaun et al

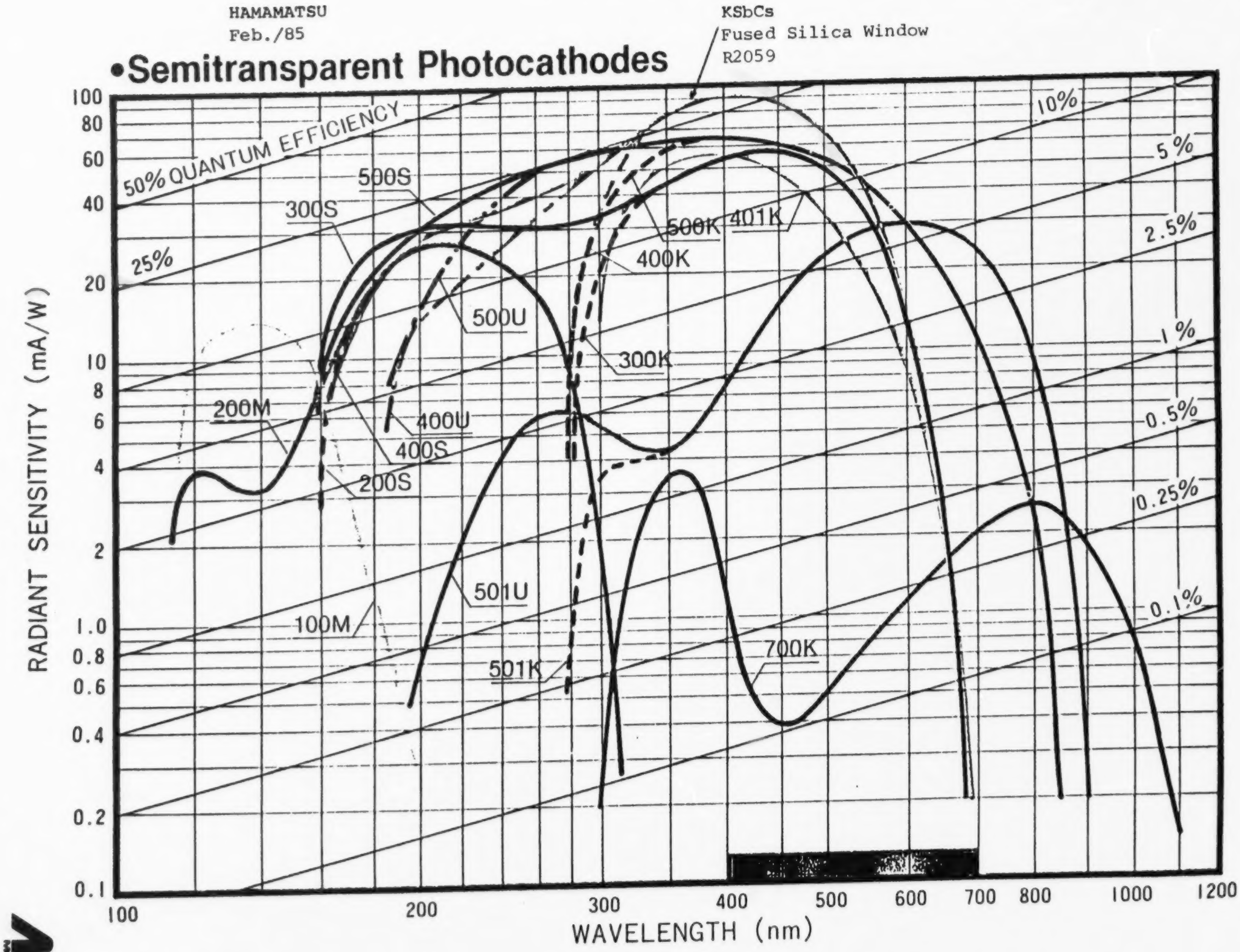

Figure 5.7: Quantum Efficiency and Radiant Response of Photocathodes

6.0 ELECTRONICS SUBSYSTEM

6.1 Electronics Overview

The system electronics processes the output of the PMT and ultimately produces methane gas concentration as a function of distance from the instrument. The electronics must be able to cope with the expected signal levels so that no useful signal information is discarded, and it must also meet the required range resolution specifications. The electronics also provides control and sychronization of the instrument as a whole.

A simplified block diagram of the electronic data processing section for a laboratory evaluation system is shown in Figure 6.1. A personal computer such as an IBM PC can control and read a digitizer through an IEEE 488 bus interface. Synchronizing hardware is required to ensure capture of the Raman return signals after a start pulse (or perhaps the laser pulse) is detected. A simple parallel interface from the PC is used to program the synchronization hardware. The laser itself is given a logic command causing it to pulse from the same interface.

The raw data is accumulated over a 10 second period; the signals will then be averaged and corrected. For a field instrument, the processing and control would be done by a dedicated microprocessor system instead of the personal computer.

We will briefly discuss the expected signal levels and the instrument performance goals. We consider the impact on the electronic instrumentation requirements and the availability of commercially available instrumentation. Various approaches which could be used to customize the electronic subsystem will also be covered.

The single most important factor in the electronic design is the requirement to digitally sample the return signal in intervals of a few ns. Considerable attention and detail must be paid to achieve a net system time resolution of 6.6 ns. If it were not for this requirement the electronics of the instrument would be a relatively minor, straight-forward technicality. It should be borne in mind that the most commonly available high speed logic family, ECL, has propagation and set-up times of 1 to 2 ns. Gallium arsenide is a faster logic 'family' but is not readily available except on a custom chip basis. Consequently, digital sampling in the few ns domain is near state-of-the-art.

6.2 System Accuracy and Dynamic Range Requirements

Although the laser probe attributes and PMT characteristics are discussed elsewhere we discuss the expected output of the PMT. Given the requirements for system portability, and the difficulty of achieving adequate laser output power, we assume that the signal at the PMT will marginally satisfy the S/N requirements needed to achieve the design specifications.

The design goals are to measure methane concentrations from 0.2% with +/- 0.04% accuracy to 5% with +/- 0.1% accuracy with a range resolution of one metre measured over the span of 2 to 30 metres from the instrument. The PMT is governed by shot noise since it detects and responds to quantum events with little other additional noise sources. Each measurement interval will last 200 E-09 sec which corresponds to the travel and return time for an object 30 m away. The laser will likely have a maximum pulse repetition frequency (PRF) of 60 Hz which over the 10 sec measurement period would yield a total measurement time of 120 E-06 sec. PMTs suffer from dark current photoelectron events of typically one per millisecond. These events will be indistinguishable from the true Raman signal photoelectrons. Given these assumptions we would observe less than one dark event in 8 measurements. This variation is very small compared to the shot noise in any range bin. Thus photomultiplier dark events (not to be confused with a background signal) are not a major concern.

The signal processing algorithm to extract methane concentration is:

$$(CH_4) = \left(\frac{S_{CH_4} - K_1\, S_{Laser}}{S_{N_2} - K_2\, S_{Laser}}\right) K_3 \qquad (6\text{-}1)$$

Where S(laser) is the signal observed at the laser wavelength in each range bin and similarly S(CH4), S(N2) correspond to the signals at the Raman wavelengths for methane and nitrogen respectively. The coefficients K1, K2 remove the laser background contribution to the Raman measurement and are a property of the filter isolation. K3 is a scalar which depends on the normal atmospheric concentration of nitrogen (80%) and the relative sensitivity of the two Raman channels. The normalization removes all dependence on the geometry of illumination and collection.

Since the laser signal is many orders of magnitude greater than the Raman signals, errors are independent of the terms involving S(laser). So that the fractional error in measurement is as given in Section 4.1.4 above. Alternatively a direct measurement of the background contribution could be made.

Since the relative cross-section and density of nitrogen relative to methane is such that 80% nitrogen corresponds to 10% methane, we can construct simple estimates of the signal and noise on each channel to give the desired fractional error.

Tables 6.1a and 6.1b provide detailed estimates of the signal in the absence of background (B/S = 0); the signal levels are sufficient to determine 0.2% +/- 0.04% concentration of methane at the maximum range (minimum signal) bin. These assumptions are consistent with a SNR of 5 as discussed in Section 4.1 above. However, in Section 5.2, we noted that the receiver optics modify the 1/R**2 dependence for the near and for ranges so that the maximum range factor is 9:1 rather than 225. We further note that the signals are integrated over a 10 sec period and that the laser can be expected to have a pulse repetition rate (PRF) of at least 1/sec. Table 6.1a and 6.1b only differ with respect to the assumption of background stability (see Section 4.1). Subsequent sections of the table calculate the effect of background on the number of photoelectrons detected in each range bin. We note that for a background to signal ratio of 1, there is a small change in the precision of measurement which is only significant for the lowest concentration at the farthest range. On the other hand, if we assume alternating backgrounds (Table 6.1b) and background to signal ratio of 10, this same measurement is marginal since the signal to noise ratio is only slightly greater than one.

The dynamic range of the measurement is dependent on the shot noise per measurement and the largest signal that is detected. The dynamic range is largest in the absence of background since the shot noise increases with the background level. We note that this is a consequence of permitting a degradation in system performance as the background increases and that if the system precision was maintained the dynamic range requirements would be greater in the presence of increasing background.

However, the background signal is essentially due to fluorescence, so that given a particular sensor implementation, increased background will degrade performance. The tables also indicate the reduction in dynamic range with increasing PRF. Increasing the PRF reduces the dynamic range because the number of photoelectrons per measurement are reduced linearly whereas the shot noise decreases as the square root of the PRF. Clearly an 8 bit digitizer will provide satisfactory performance at a PRF of 5/sec.

The nitrogen measurement would double the dynamic range requirement if the system had to accommodate both nitrogen and methane without modifying the signal processing. However, if the nitrogen measurement is made on its own, the dynamic range measurements is in fact less. One can include a two times attenuator in the analog signal chain to process nitrogen signals while otherwise using the same detector/processing system.

6.3 Time Resolution Requirements

In order to achieve range resolution of one metre the total response time of the methanometer should be less than 6.7 ns. To estimate the methanometer response it is considered to have of four contributions:

i) the laser pulsewidth;

ii) the PMT (photomultiplier tube) response characteristic;

iii) the analog system bandwidth prior to the analog to digital converter; and

iv) the digitization time of the analog to digital converter.

For mathematical simplicity the first three elements can be considered to have Gaussian impulse responses r(t) of the form:

$$r(t) = e^{-t^2/2\sigma^2} \tag{6-2}$$

where σ is the variance which is related to the full width at half maximum (FWHM, Γ) by:

$$\sigma = \frac{\Gamma}{2\sqrt{2\ln 2}} \tag{6-3}$$

In fact, the PMT response will have a somewhat skewed Poisson-like distribution while the analog electronics is likely to have an exponential response and the analog to digital converter response is box-like.

Since the overall pulse response is a convolution of the individual terms described above, we find that our mathematical model yields a Gaussian with a FWHM that is given by:

$$\Gamma^2 = \Gamma_1^2 + \Gamma_2^2 + \ldots \Gamma_n^2 \tag{6.4}$$

Table 6.2 illustrates the effects of system time constants and Gaussian gas plume distributions upon the overall pulse response.

In columns 2 and 3, we assume a negligible size to the gas plume and calculate the response time for lasers with pulse widths of 2.5 and 5.0 ns respectively. For a laser with negligible pulse width the system response time is only 4.1 ns and this rises only marginally for the short pulse time of 2.5 ns. However, the laser contribution dominates the response time when the laser pulse is as long as 5 ns. The effect of a 1 metre plume is illustrated in columns 4 and 5. If one assumes a one metre Gaussian and a negligible laser pulse, the overall system response is 7.8 ns. This response time increases to 9.3 ns using a laser with a 5 ns response time. The Nyquist sampling rate is assumed to be twice the response time in accordance with the sampling theorem.

Two Gaussian plumes each 1 m wide (FWHM) and separated by 2 m are shown in Figure 6.2. Pulse broadening to 10 ns (cf col. 5 Table 6.2) degrades the positional resolution and introduces a delay; however, the signal level shows two peaks and valley. Since the signal is sampled every 5 ns, at least three measurements would occur to permit definition of the two separate plumes. That is, a Nyquist sampling rate of 200 million samples per sec (MSPS) would be sufficient to minimally identify one plume from the other.

The laser, PMT, and analog electronics system timing elements can permit deconvolution of the raw data. It is not necessary to limit the bandwidth of the signal to be digitized as there are not expected to be any frequencies in the signal higher than the Nyquist rate. The Nyquist sampling rate is only important from a ranging point of view.

If the analog electronics were to have a Gaussian response characteristic, the -3dB corner frequency, f_c , would be given by:

$$f_c = \frac{\sqrt{2}\,\ln(2)}{\pi\Gamma} \qquad (6\text{-}5)$$

where Γ is the FWHM of the input pulse. We note that the -3db point of the analog electronics would be 104 MHz and 62.4 MHz for 3 ns and 5 ns Gaussian impulse response curves. The analog electronic response is more likely to be characterized by a first order exponential rather than a second order exponential as in the Gaussian response. Therefore the above estimates of the -3dB corner frequency are likely to be conservative rather than optimistic.

6.4 Digitizer Recommendations

In summary, an 8 bit dynamic digitizer is required with a sample rate > 200 MSPS. We now address the fulfillment of the digitizer requirements using commercial transient recorders and custom designs.

6.4.1 Commercial Transient Recorders

The fastest waveform recorders generally use one of two techniques to capture and digitize a transient event. The first method, and by far the most common, uses flash A/D converters to directly convert the analog signal to a digital equivalent. The method employs 2**n (where n is the converter's number of bits) comparators with each comparator sampling a reference voltage formed from one corresponding element of a 2**n element resistor divider chain. The output of the comparators are fed to a binary encoder which produces the desired output. From a data throughput point of view, transient recorders based upon this method are limited by the buffer readout speed, not the conversion process. Currently available waveform digitizers using this technique have a maximum sampling rate of 200 MSPS with an 8 bit dynamic range.

The other conversion process uses an analog technique to store an image of the transient event on a solid state imaging device. After the event occurs, the image is readout at a leisurely pace, digitized, and properly analysed to represent the analog input.

Some commercial transient recorders incorporate an inaccessible analog front end. The analog input bandwidth is normally reduced from 1/2 (Nyquist frequency) to 1/6 of the digitizing rate to avoid aliasing of high frequency signals into the bandwidth below the Nyquist frequency. Since the Raman signal will be characterized by a white noise spectrum, it is undesirable and not necessary to limit the analog bandwidth to the A/D converter. As mentioned earlier the Nyquist limit is only relevant from a ranging point of view.

Several manufacturers were contacted to determine the availability of transient waveform digitizers. As expected, we found flash converters provide 200 MSPS digital sampling with 8 or 6 bits resolution.

In the future there will be less of a distinction between transient waveform recorders and digitizing oscilloscopes. There now are some digitizing scopes on the market that sample at 200 MSPS, they are capable of signal processing, and can download their information by an IEEE 488 port. This capability is provided by an internal 16 or 32 bit microprocessor and a digital scope is a good solution for a laboratory-phase system evaluation. In addition, most digital scopes are capable of sampling simultaneously on two channels. This is important since it may be necessary to acquire simultaneously the Raman methane signal, the Raman nitrogen signal, and the laser output signal.

Tektronix has fabricated a transient recorder based on scan conversion techniques. The device (TEK 7912AD) utilizes a photodiode array matrix. However the instrument is limited by its inability to perform successive readouts any faster than 10 per second. Since it is expected that a laser in the methanometer system can exceed this repetition rate, the Tektronix instrument would not be suitable. However, if the laser PRF were below 10 Hz and/or the repetition rate of the TEK 7912AD were improved then this method could be considered for a laboratory feasibility study. The TEK 7912AD is capable of 9 bit resolution with a maximum 100 GHz 'equivalent' sampling rate. The analog bandwidth of this instrument is limited to a maximum of 500 MHz.

LeCroy has very recently introduced an 8 bit 1.3 GS/SEC digitizer with an 8 bit resolution (Model #6880). It uses a technology similar to the TEK 7912AD. It too suffers from a slow system cycle time, but has programmable front end filters ranging from 150 Mhz to 300 Mhz. Its triggering error is +/- 1/2 sample.

The Biomation Model 6500 is purported to sample at 500 MSPS, but is no longer available. Some possibility exists that a similar instrument may be reintroduced by Gould-Biomation.

Table 6.3 summarizes the characteristics of the commercial digitizers available.

6.4.2 Custom Digitizer Implementations

There are now fast (8 bit-50 MSPS, 6 bits-100MSPS) commercial monolithic A/D converters available. The 6 bit A/D, TDC1029, and a similiar 8 bit device TDC1025, are both available from TRW. With these one could construct (using two or more of the devices in parallel) a 200 MSPS A/D conversion system. Accurate phase timing of the multiple converters used in this technique would be essential to maintain the effective number of bits available from each single converter. Since there are no 'high density' memory components capable of storing data at 5 ns intervals it would be necessary to store data from the A/D conversion process in parallel and dump this data at a slower pace into Schottky or high speed CMOS memory. This memory would then be read out at an even slower pace by the controlling microprocessor.

For a limited number of sequential samples, we can also use a number of fast sample and holds equal to the number of desired samples (30 in this case). The sample and holds capture the signal at fixed time intervals. This could be generated by an accurately tapped delay line; each tap corresponding to incremental delays in time following the laser pulse. After the signal sampling period the sample and held signals are digitized by a relatively slow A/D by an appropriate multiplexing scheme . An advantage of this conversion method is that the sampling time chain is started by the actual laser emission time, thus there are no synchronization problems as in a direct A/D conversion approach.

6.4.3 Custom Design - Power, Size Requirements

The approximate power and size (board space) of two possible 200 MSPS digitizing schemes are roughly estimated in Table 6.4. The first design uses four 8-bit flash A/Ds to achieve a 200 MSPS rate. The second design uses multiple (30) fast sample and hold bridges to achieve an effective 200 MSPS capture speed.

6.4.4 Summary

A laboratory model of a methanometer should be based on the 8 bit transient recorder TR8828 or 6880. However, given the great cost of such a system we believe that a credible performance evaluation can be developed using a cheaper system based on a digital oscilloscope such as the HP Model 54200A/D. By switching the input gain of the oscilloscope a full evaluation of different concentration levels can be made. The analog bandwidth can be increased by using a different preamplifier than the normal one provided if this becomes necessary. A custom design will be required for a deployable system.

6.5 Synchronization

Whereas the relative system timing must be kept accurate to within a few ns (or better) to maintain range resolution, all timing aspects of the system would have to be measured accurately and adjusted by the addition or deletion of time delays. One method of doing so would be to continually and very accurately activate the timing chain by a psuedo laser pulse. Critical timing would be measured by either a fast analog scope or an averaging digital scope with a high analog bandwidth.

Transient recorders based on a scan conversion technique are easily triggered by the laser pulse and can compensate for laser jitter. However, synchronization is a serious problem for instruments using clocked flash A/D conversion since there is an inherent uncertainty of at least one clock cycle with respect to the command to convert and the beginning of digitization. This occurs because the transient recorder converts synchronously (internally) using a high speed clock (200 MHz). Since the laser cannot be expected to emit at a fixed time relative to a start pulse, the laser pulse will be asynchronous with respect to the digitizer. If this remains uncorrected a minimum uncertainty of 5.0 ns would result. This problem also occurs in the design of a customer A/D flash arrangement. Compensation could be provided using clocks of different phases relative to the master clock; in this way the delay of the conversion process relative to the laser emission time can be determined.

Table 6.1a: Detailed Signal Estimates

```
SIGNAL LEVELS AND CONCENTRATION ERRORS

BACKGROUND/SIGNAL (B/S)         A STABLE BACKGROUND IS ASSUMED
RATIO IS GIVEN FOR .2% METHANE                                                 MINIMUM         MAXIMUM
                                            RANGE FACTOR 9.00                  SIGNAL          SIGNAL
 B/S        0
                                            MAXIMUM
METHANE    MINIMUM PHOTOELECTRONS           PHOTOELECTRONS       METHANE   RELATIVE CONC.      CONC.
CONC.      PER RANGE BIN                    PER RANGE BIN        CONC.     ERROR    ERROR      ERROR
==========================================================================================================
           PER         PER         SHOT NOISE  PER
  %        10 sec      MEASUREMENT PER         MEASUREMENT          %         %        %          %
           Interval    @PRF= 1/sec MEASUREMENT @PRF= 1/sec
----------------------------------------------------------------------------------------------------------
 .20        25.00       2.50        1.58        22.50                .20       20.00    .04        .01
 1.25       156.25      15.62       3.95        140.62               1.25      8.00     .10        .03
 5.00       625.00      62.50       7.91        562.50               5.00      4.00     .20        .07
 10.00      1250.00     125.00      11.18       1125.00              10.00     2.83     .28        .09
                                                                               MINIMUM         MAXIMUM
 B/S        1.00                                                               SIGNAL          SIGNAL
                                            MAXIMUM
METHANE    MINIMUM PHOTOELECTRONS           PHOTOELECTRONS       METHANE   RELATIVE CONC.      CONC.
CONC.       PER RANGE BIN                   PER RANGE BIN        CONC.     ERROR    ERROR      ERROR
==========================================================================================================
           PER         PER         SHOT NOISE  PER
  %        10 sec      MEASUREMENT PER         MEASUREMENT          %         %        %          %
           Interval    @PRF= 1/sec MEASUREMENT @PRF= 1/sec
----------------------------------------------------------------------------------------------------------
 .20        50.00       5.00        2.24        45.00                .20       28.28    .06        .02
 1.25       181.25      18.12       4.26        163.12               1.25      8.62     .11        .04
 5.00       650.00      65.00       8.06        585.00               5.00      4.08     .20        .07
 10.00      1275.00     127.50      11.29       1147.50              10.00     2.86     .29        .10
                                                                               MINIMUM         MAXIMUM
 B/S        10.00                                                              SIGNAL          SIGNAL
                                            MAXIMUM
METHANE    MINIMUM PHOTOELECTRONS           PHOTOELECTRONS       METHANE   RELATIVE CONC.      CONC.
CONC.       PER RANGE BIN                   PER RANGE BIN        CONC.     ERROR    ERROR      ERROR
==========================================================================================================
           PER         PER         SHOT NOISE  PER
  %        10 sec      MEASUREMENT PER         MEASUREMENT          %         %        %          %
           Interval    @PRF= 1/sec MEASUREMENT @PRF= 1/sec
----------------------------------------------------------------------------------------------------------
 .20        275.00      27.50       5.24        247.50               .20       66.33    .13        .04
 1.25       406.25      40.62       6.37        365.62               1.25      12.90    .16        .05
 5.00       875.00      87.50       9.35        787.50               5.00      4.73     .24        .08
 10.00      1500.00     150.00      12.25       1350.00              10.00     3.10     .31        .10

DYNAMIC RANGE FOR METHANE (0.2 - 5 %)                      DYNAMIC RANGE FOR NITROGEN (= 10% METHANE)
==========================================================================================================
PRF (/SEC)  1.00        5.00        10.00       20.00       1.00       5.00       10.00    20.00
 B/S
----------------------------------------------------------------------------------------------------------
 0          355.76      159.10      112.50      79.55       100.62     45.00      31.82    22.50
 1.00       261.62      117.00      82.73       58.50       101.62     45.45      32.14    22.72
 10.00      150.17      67.16       47.49       33.58       110.23     49.30      34.86    24.65
```

Table 6.1b: Detailed Signal Estimates

```
SIGNAL LEVELS AND CONCENTRATION ERRORS

BACKGROUND/SIGNAL (B/S)          ALTERNATING BACKGROUND MEASUREMENTS ARE ASSUMED
RATIO IS GIVEN FOR .2% METHANE                                              MINIMUM          MAXIMUM
                                             RANGE FACTOR 9.00              SIGNAL           SIGNAL
 B/S        0
                                             MAXIMUM
METHANE    MINIMUM PHOTOELECTRONS            PHOTOELECTRONS      METHANE    RELATIVE CONC.   CONC.
CONC.      PER RANGE BIN                     PER RANGE BIN       CONC.      ERROR    ERROR   ERROR
==========================================================================================================
           PER         PER          SHOT NOISE  PER
 %         10 sec      MEASUREMENT  PER         MEASUREMENT      %          %        %       %
           Interval    @PRF= 1/sec  MEASUREMENT @PRF= 1/sec
----------------------------------------------------------------------------------------------------------

 .20        25.00        2.50        1.58        22.50           .20        20.00    .04     .01
 1.25       156.25       15.62       3.95        140.62          1.25       8.00     .10     .03
 5.00       625.00       62.50       7.91        562.50          5.00       4.00     .20     .07
 10.00      1250.00      125.00      11.18       1125.00         10.00      2.83     .28     .09
                                                                            MINIMUM          MAXIMUM
 B/S        1.00                                                            SIGNAL           SIGNAL
                                             MAXIMUM
METHANE    MINIMUM PHOTOELECTRONS            PHOTOELECTRONS      METHANE    RELATIVE CONC.   CONC.
CONC.       PER RANGE BIN                    PER RANGE BIN       CONC.      ERROR    ERROR   ERROR
==========================================================================================================
           PER         PER          SHOT NOISE  PER
 %         10 sec      MEASUREMENT  PER         MEASUREMENT      %          %        %       %
           Interval    @PRF= 1/sec  MEASUREMENT @PRF= 1/sec
----------------------------------------------------------------------------------------------------------

 .20        75.00        7.50        2.74        67.50           .20        34.64    .07     .02
 1.25       206.25       20.62       4.54        185.62          1.25       9.19     .11     .04
 5.00       675.00       67.50       8.22        607.50          5.00       4.16     .21     .07
 10.00      1300.00      130.00      11.40       1170.00         10.00      2.88     .29     .10
                                                                            MINIMUM          MAXIMUM
 B/S        10.00                                                           SIGNAL           SIGNAL
                                             MAXIMUM
METHANE    MINIMUM PHOTOELECTRONS            PHOTOELECTRONS      METHANE    RELATIVE CONC.   CONC.
CONC.       PER RANGE BIN                    PER RANGE BIN       CONC.      ERROR    ERROR   ERROR
==========================================================================================================
           PER         PER          SHOT NOISE  PER
 %         10 sec      MEASUREMENT  PER         MEASUREMENT      %          %        %       %
           Interval    @PRF= 1/sec  MEASUREMENT @PRF= 1/sec
----------------------------------------------------------------------------------------------------------

 .20        525.00       52.50       7.25        472.50          .20        91.65    .18     .06
 1.25       656.25       65.62       8.10        590.62          1.25       16.40    .20     .07
 5.00       1125.00      112.50      10.61       1012.50         5.00       5.37     .27     .09
 10.00      1750.00      175.00      13.23       1575.00         10.00      3.35     .33     .11

DYNAMIC RANGE FOR METHANE (0.2 - 5 %)               DYNAMIC RANGE FOR NITROGEN (= 10% METHANE)
==========================================================================================================
PRF (/SEC) 1.00      5.00      10.00     20.00      1.00      5.00      10.00    20.00
 B/S
----------------------------------------------------------------------------------------------------------

0          355.76    159.10    112.50    79.55      100.62    45.00     31.82    22.50
1.00       221.83    99.20     70.15     49.60      102.62    45.89     32.45    22.95
10.00      139.74    62.49     44.19     31.25      119.06    53.24     37.65    26.62
```

Table 6.2: Response Time and Sampling Rate

SYSTEM ELEMENT	IMPULSE RESPONSE (FWHM) ns			
LASER	2.5	5.0	5.0	5.0
PMT	2.5	2.5	2.5	2.5
ANALOG ELECTRONICS	3.3	3.3	3.3	5.0
GAUSSIAN PLUME	<0.1	<0.1	6.6	6.6
NET SYSTEM RESPONSE TIME	4.8	6.5	9.3	10.0
NYQUIST SAMPLING INTERVAL	2.4	3.3	4.7	5.0
SAMPLING RATE (MSPS)	417	303	213	200

Table 6.3: Commercial Transient Recorders and Digital Oscilloscopes

MANUFACTURER	MODEL #	INSTRUMENT TYPE	MAX DIGITIZING RATE	# OF BITS	# OF CHANNELS	ANALOG BANDWIDTH	CONVERSION METHOD	COMPUTER INTERFACE	REMARKS	COST
LeCroy	TR8828B MM8103A	Transient Recorder	200 MSPS	8	1	>100MHZ	Flash A/D	CAMAC	modular & expandable >60watts	$18,000 + rack~ $7,000
Tektronix	7912AD	Transient Recorder	100GSPS effective	9	1	500MHZ	Scan Conversion	IEE 488	<10Hz rep rate 300watts 19"x7"x27"	$46,268
LeCroy	9400	Digital Oscilloscope	100MSPS	8	2	125MHZ	Flash A/D	IEE 488	8"X15"x19" 30lbs Random sample capability	
Tektronix	7612D	Transient Recorder	200MSPS	8	2	200MHZ	Flash A/D	IEE 488	Accepts modular pre-amps rack mount 55lbs	$48,065
Hewlett Packard	HP54200A/D	Digital Oscilloscope	200MSPS	6	2	50MHZ	Flash A/D	IEE 488	200watts 18"x17"x8" 25lbs	$9,000

Table 6.4: Custom Digitizer Designs - Power Consumption and Size

a) PARALLEL A/D METHOD

COMPONENT	# REQUIRED	POWER/DEVICE	NET POWER REQ'D	ca SPACE
8-BIT, 50MSPS A/D CONVTR TDC1025(TRW)	4	3.8 WATTS	15.2 WATTS	8 sq in
FAST STORAGE MEMORY F10422(FC) 256X4-BIT	8	1.0	8.0 WATTS	8 sq in
ECL GLUE & SYNCHRO LOGIC	8	1.0	8.0	6 sq in

APPROXIMATE TOTAL DIGITIZER POWER = 31 WATTS
APPROXIMATE TOTAL BOARD SPACE = 22 Square inches

b) MULTIPLE SAMPLE AND HOLD

COMPONENT	# REQUIRED	caPOWER/DEVICE	ca POWER	ca SPACE REQ'D
SAMPLE & HOLD (HTS-0010)	30	1 Watt	30 Watts	30 Sq in
DIGITIZER	1	1 Watt	1 Watt	2 Sq in
SUPPORT LOGIC	8	.25 Watt	2 Watt	6 Sq in

APPROXIMATE TOTAL POWER = 33 WATTS
APPROXIMATE TOTAL BOARD SPACE = 38 Square inches

PMT = Photomultiplier Tube
AMP = Analog Electronic Chain
APD = Avalanche Photodiode

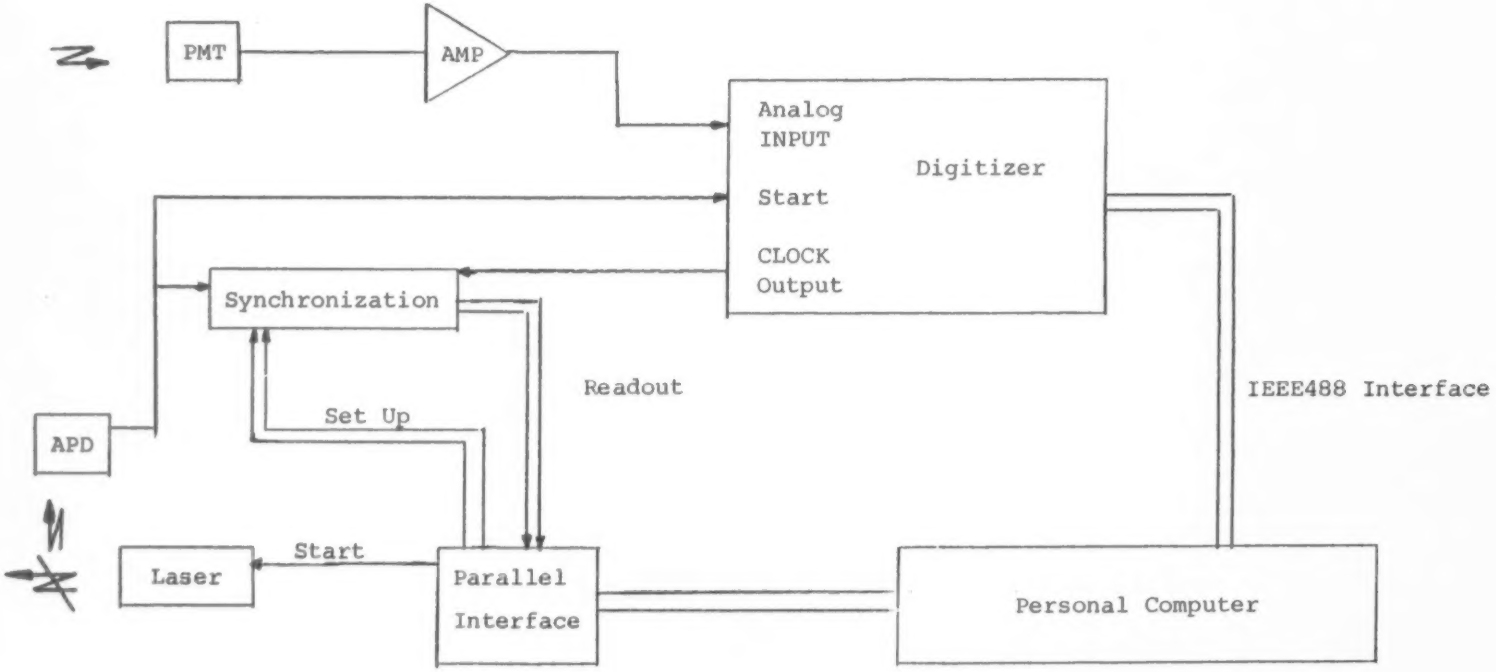
PMT
AMP
Analog INPUT
Start
CLOCK Output
Digitizer
Synchronization
Readout
Set Up
IEEE488 Interface
APD
Laser
Start
Parallel Interface
Personal Computer

Figure 6.1: Electronics System Block Diagram

IMPULSE RESPONSE TO TWO GAS PLUMES

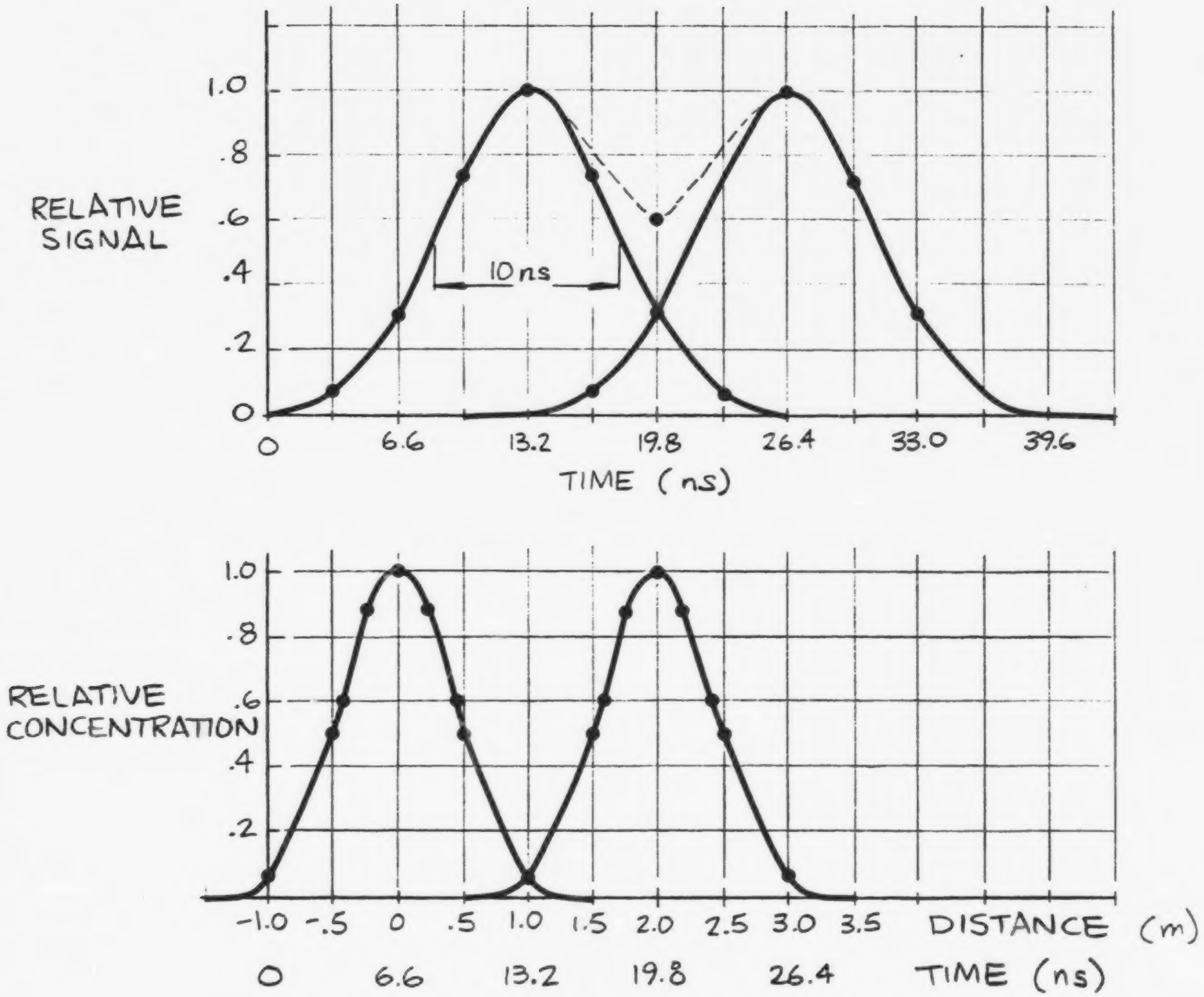

Figure 6.2: Response to Two Gaussian Gas Plumes

7.0 RECOMMENDATIONS FOR FURTHER WORK

This section will describe two different scenarios for implementing a laboratory based breadboard system and will provide a summary of the system specifications. The two scenarios are based on different perceptions of the critical performance requirements of the different system components.

As we have indicated in Section 4, the laser performance is the single most important element in the system. We have noted, however, that the existing nitrogen laser can provide only marginal performance in the most exacting conditions. In any engineering development, it is important to have a concrete demonstration of the system performance. That is, the development of a Raman methanometer based on the nitrogen laser would permit a full experimental evaluation of both the laser performance and of the background contributions to the analysis of concentration errors. This approach establishes an experience base by pursuing system implementation.

The alternative approach would develop a laser source based on the tripled Nd:YAG laser. This route potentially has the greatest risk and payoff. The risk is associated with the development of a source without the parallel development of a test facility for the evaluation of suitability in the mine methane environment. The approach has its greatest payoff if the laser source that is developed provides a reduction in size, weight and power without sacrificing performance. In this case, the systems aspects would be developed after the laser source had been fabricated. This approach is likely to be very costly and involves the funding of state of the art technology. It may have the greatest spinoff value since a technology base for the fabrication of such sources could provide a commercial facility.

A systems approach will allow a more thorough specification of a laser system based on the diode pumped tripled Nd:YAG laser. The substitution of the Nd:YAG based laser for the nitrogen laser would occur at a future time after such sources have been developed commercially. This scenario would of course require that various custom filters be refabricated since the source and receiver wavelengths would have changed. We note that this approach is very similar to that adopted by the U.S. Bureau of Mines; that is, the USBM work could also utilize this alternate source. In this regard, we have some reservations with certain aspects of the optical design but the major difference between the USBM work and the laboratory facility which CANMET could develop lies in the greater range capability that is desired. If this maximum range is reduced to 10 m as in the USBM case, then there is no need for a CANMET development, rather, one should concentrate on developing the newer source.

A third alternative exists - the development of a path averaging sensor. As we noted above such a device could be based on infrared differential absorption. An auxiliary method of range determination would be required and the system would average over the 4-5 m path to a wall; the operation of such an instrument assumes that the optical path is uniformly filled with methane. Further discussion of this alternative is beyond the scope of the current report.

7.1 System Specifications and Implementation

Table 7.1 summarizes the performance characteristics of a Raman methanometer. The critical parameters affecting system performance are the range, range resolution and integration time. Since measurements are required for both methane and nitrogen, a specification on each measurement is given. The overall measurement time depends on the need to make these and/or other measurements in sequence. The specification for atmospheric transmittance affects overall system performance. This is not restrictive since extrapolation of a visible transmittance (Ref. 18) of 38% through a 22 cm column containing a dust concentration of 200 mg/liter to the indicated values should give a transmittance in excess of 97%. There appears to be no difficulty in meeting the eye safety standards.

The optical system components are detailed in Table 7.2. Two options are presented one for a nitrogen laser and one for a tripled Nd:YAG system. We have selected specifications based on a source that is 10 times the power of the currently available PRA LN103 since this is a conservative approach to demonstrating feasibility. The pulse energy is different for the Nd:YAG and nitrogen systems and compensates for the variation in pulse repetition rate. The laser figure of merit has been calculated with the same assumptions used in Section 4 above. The risks and advantages of the two sources have already been described. We note that a laboratory evaluation system based on a nitrogen laser should use an available or slightly modified source which will probably not reach the specification given below; this reflects the emphasis on system development activities rather than on laser development.

The transmitter and receiver have also been specified in Table 7.2. The critical specifications are those relating to beam diameter. In the case of the transmitter, this is necessary to satisfy the eye safety requirement, while the receiver diameter determines the signal level that is received. In both cases non-fluorescing materials must be used; the only optical materials which can be assumed to be non-fluorescing are either reflective or utilize fused silica (e.g. Suprasil). All other materials must be checked for fluorescence. The angular resolution of the optical system is not particular onerous and a telescope design based on an electroformed primary mirror may prove cost effective.

Colour separation should use one customized filter for each channel that is monitored. To assess the influence of background fluorescence from coal dust an additional channel will be required at a wavelength midway between the methane and nitrogen channels. All other characteristics are identical to those of the methane channel. The laser signal itself can be easily monitored using an avalanche photodiode to pickup the laser light from the long pass cut-on filter. The three filters must be inserted sequentially in the beam since the use of beamsplitters will likely introduce too large an attenuation.

The detector characteristics are given in Table 7.3. The detector is based on a UV sensitive photomultiplier tube; a variety of manufacturers can produce suitable devices.

The specifications for the electronics are given in Table 7.4. The recommended implementation for an evaluation system is based on a digital oscilloscope. We note that a substantial experience base can be developed by using the variable gain input amplifier of a lower dynamic range system. This will permit evaluation of system performance for a uniform concentration of methane and require re-adjustment for different concentration ranges. Customization will be required for a deployable system. An evaluation system will likely require a GPIB interface to a data logging and analysis computer based on a personal computer. The deployable system would require the development of a dedicated microcontroller to perform synchronization, calibration and data logging functions.

Table 7.1: Proposed System Performance

Range: 2 - 30 meters. Best performance @ 8 meters.

Range Resolution: 1 m

Integration time: 10 seconds for each measurement

Concentration Sensitivity and Precision:

Methane %	R.m.s. Error %
.20	<.07
1.25	<.11
5.00	<.21
Nitrogen	<2.3

Environmental and Safety:

Transmittance at the laser wavelength >92% over 30 meter path. Coal dust < 40 mg/m**3

Satisfies ANSI Z136.1-1980 with respect to eye safety

Table 7.2: Proposed Optical System Components

LASER SOURCES

	Nitrogen	Tripled Nd: YAG
Operating Wavelength :	337 nm	353 nm
Pulse Energy:	>5E-04 Joules	>6E-03 Joules
Pulse Repetition Frequency	>50 Hz	>5 Hz
Pulse width at 50% maximum power	<5 ns	<5 ns
Laser Figure of merit	>6.6E04	>6.6E04
Wall plug effeciency	>.1%	>1%
Estimated Average Power Consumption	50W	6W

TRANSMITTER

Beam diameter: 5 cm

Transmittance: >0.95 at the laser wavelength

RECEIVER

Cassegrain type Telescope

Aperture:	30 cm
Central Obscuration:	5 cm
Effective Focal Length:	72 cm
Field of View	+/-1 degree
Etendue	0.17 cm**2 sr

Table 7.2 (continued)

Color Separation:

Filter sets required for both Methane and Nitrogen Channels.

Filters should incorporate an all dielectric long-pass (cut-on) and metal induced dielectric bandpass filter respectively.

Bandwidth at 50% transmittance	2 nm
In band transmittance	>0.1

Channel	Methane	Nitrogen
Out of band transmittance	<5 E-09	<1.3E-07
Fluorescence	<5 E-08	<1.3e-06
Centre Wavelength		
Nitrogen laser	373.7 nm	365.7 nm
Tripled Nd:YAG	393.5 nm	384.6 nm

Table 7.3: Proposed Detector Specifications

End-On Photomultiplier Tube	
Linearly focussed	
Photocathode K Cs Sb	
Quantum Efficiency	from 360 - 390 nm >0.25
Photocathode diameter	25 mm minimum may be as large as 50 mm
Pulse Response Time (FWHM)	<3.3 ns

Operating Voltage as recommended by the manufacturer
Typically -1800V cathode potential; anode near ground potential.

Manufacturers : Hamamatsu, RCA

Table 7.4: Proposed Electronics Specifications

Analog Bandwidth (3db)	100 MHz
Sampling Rate	2E08 Samples/sec
Duty Factor	Determined by laser PRF >5 Hz
Dynamic Range	<8 bits @5 Hz PRF

APPENDIX 1: DESCRIPTION OF PROGRAM USED FOR SNR CALCULATION

A listing and description of the computer program used to calculate the laser function and the SNR versus concentration and range is shown below.

The SNR equation is defined on line 160 of the program and definitions of symbols is presented on line 200 to 290. This is the same as equation (4.1) which was defined earlier. Line 300 introduces the laser function, equation (4.3), which is part of the SNR equation. The symbols for the laser function are defined in lines 320 to 390.

There are two methods by which the laser function is calculated. The first, program lines 530 to 840, is used to determine the maximum laser function with respect to the eye safety standards. The values are calculated from equation (4.3), line 800 of the program. A sample calculation is detailed below.

F3 = E9.E8.T9.T8.P8/(H9.L8^3)

where

$E8 = 0.25$: quantum efficiency
$T9 = 0.80$: transmittance at laser frequency
$T8 = 0.10$: transmittance at Raman frequency
$P8 = 1$ (Hz) : PRF of laser
$H9 = 1.987 \times 10^{-16}$ (J nm) : product of Plancks constant and speed of light
$L8 = 337$ (nm) : laser wavelength
$E9 = 3.38 \times 10^{-3}$ (J) : laser pulse energy for 1 cm diameter beam
$F3 = 8.889 \times 10^{3}$ nm^{-4} sec^{-1} : laser function

The second method, program lines 2743 to 2990, is used to calculate the laser function based on manufacturers data of laser specifications. The values are also calculated from equation (4.3), line 2930, and the previous sample calculation is valid.

Having calculated values for the laser function the program allows the SNR to be calculated as a function of range (lines 1100 to 1750) or as a function of concentration (lines 1820 to 2450). In either case the SNR value is calculated using equation (4.1), which is the square root of S defined on program line 160. A sample calculation is shown.

S = F3.A.R9.P9.D9.F9^4.T

where

F3 = 8.889×10^{3} ($nm^{-4} sec^{-1}$) : laser function
A = 707 (cm^{2}) : area of receiving optics
R9 = 1/950-1/1050 (cm^{-1}) : 10 m range for a 1 m resolution
P9 = $2.7 \times 10^{19} \times .05$ ($mol\ cm^{-3}$) : for a 5% methane concentration
D9 = 2.64×10^{-30} ($cm^{2} sr^{-1} mol^{-1}$) : absorption coefficient for methane
F9 = 488 (nm) : reference wavelength
T = 10 (sec) : integration time

S = 1273.4 and the square root of S = SNR = 36.

The values of S are computed for various laser functions (F3) at various concentrations or ranges. The computed values are stored in an array and subsequently used to graph the data. The square root S (SNR) is plotted versus either concentration or range. The different laser function values are represented by individual lines on the graph.

```
1 ! ***************************
  *
2 ! ***************************
  *
3 !        RAMPLT [9999=4212]
4 ! REV  FEB 9/86 12:30
5 ! log plot: S vs conc & rang
  e
6 ! ***************************
  *
7 ! ***************************
  *
10 ! W= # OF WAVELENGTHS
20 ! B= BEAM DIAMETER (cm)
30 ! B9=# OF BEAM DIA USED
40 ! Z5=# of plots on graph
50 ! I =count used in eqn array
60 DIM S(5,50)
70 DIM F3(18)
80 DIM L8(18)
90 DIM E9(18)
95 DIM L$[10]
100 DIM P8(18)
110 Z7=0 @ Z8=0 @ Z9=0
120 ! ***************************
130 !  PROGRAM FOR RAMAN CALC
140 ! ***************************
150 !
160 ! S=F3*A*R9*P9*D9*F9^4*T
170 !
180 ! ******** WHERE ***********
190 !
200 ! T =tau=10 sec for measure
210 ! F9=lambda reference=488 nm
220 ! D9=cross sec.[cm^2/sr mol]
230 !  =2.64*10^-30 for methane
240 !  =3.31*10^-31 for nitrogen
250 ! P9=rho=2.7*10^19*(CH4 CON)
260 !  =units of mol/cm^3
270 ! R9=rang=1/Rnear-1/Rfar=cm
280 ! A =area of receiv.=707cm^2
290 ! F3=LASER PARAM=nm^-4/sec
300 ! F3=E9*E8*T9*T8*P8/(H9*L8^3
  )
310 ! ******** WHERE ***********
320 ! L8=laser wavelength nm
330 ! H9=hc=1.987*10^-16 J*nm
340 ! P8=laser PRF in Hz
350 ! T8=trans at raman = .1
360 ! T9=trans at laser = .8
370 ! E8=quantum eff = .25
380 ! E9=laser pul energy=joules
390 ! C9=CH4 CONC  mole frac.
400 !
410 ! ***************************
420 ! CALCULATE LASER FUNCTION
430 ! ***************************
440 CLEAR @ DISP USING 450
450 IMAGE 5/,2X,"DO YOU WISH TO
    CALCULATE",/, "  THE LASER F
    UNCTION:F3 [Y/N]"
460 INPUT Z$
470 IF Z$="Y" THEN GOTO 490
480 GOTO 880
490 DISP "FOR EYE SAFE[1] OR LAS
    ER TYPE[2]"
500 INPUT J5
510 IF J5=1 THEN GOTO 530
520 GOTO 2750
530 W=6 ! # OF WAVELENGTHS
540 B=1 ! BEAM DIA (cm)
550 CLEAR
560 FOR I=1 TO W
570 DISP "INPUT λ % P ENERGY FOR
     1cm BEAM"
575 DISP "  (nm)         (J)"
580 INPUT L8(I),E9(I)
590 NEXT I
600 CLEAR
610 DISP "ENTER # OF BEAM DIA TO
     PROCESS"
620 INPUT B9
630 FOR J=1 TO B9
640 DISP "ENTER BEAM DIA (cm)"
650 INPUT B
660 PRINT USING 670
670 IMAGE 4/
675 PRINT "   LASER FIGURE OF ME
    RIT          "
680 PRINT "   FOR BEAM DIAMETER"
    ;B;"cm"
690 PRINT "---------------------
    -----------"
700 PRINT !
710 PRINT " WAVE         PULSE
    FIGURE OF"
720 PRINT "LENGTH        ENERGY
      MERIT  "
730 PRINT " (nm)          (J)
    (nm-4/sec)"
740 PRINT !
750 FOR I=1 TO W
760 L8=L8(I)
770 E9=E9(I)*B^2 ! BEAM DIA FAC
780 H9=1.987*10^-16 ! J nm
790 P8=1 @ T8=.1 @ T9=.8 @ E8=.2
    5
800 F3=E9*E8*T9*T8*P8/(H9*L8^3)
810 PRINT USING 820 : L8,E9,F3
820 IMAGE DDDD,3X,D.DDDE,3X,D.DD
    DE
830 NEXT I
840 NEXT J
850 !
860 !
870 ! ***************************
880 ! INPUT VARIABLES & CONST.
890 ! ***************************
900 !
910 CLEAR @ DISP USING 920
920 IMAGE 8/,   "CALCULATE FOR C
    H4 [1] OR N2 [2]"
```

```
930 INPUT Z9
940 DISP !
950 DISP "CALCULATE S[1]..OR..RO
    OT S[2] ?"
960 INPUT Z3
970 !
980 T=10
990 F9=488
1000 IF Z9=1 THEN D9=2.64*10^-30
1010 IF Z9=2 THEN D9=3.31*10^-31
1020 IF Z9>2 THEN GOTO 910
1030 A=707 ! cm^2
1040 CLEAR @ DISP USING 1050
1050 IMAGE 10/,   "PLOT VERSUS C
     ONC.[1] OR RANGE[2]"
1060 INPUT Z8
1070 IF Z8=1 THEN GOTO 1820
1080 IF Z8=2 THEN GOTO 1110
1090 IF Z8>2 THEN GOTO 1040
1100 ! *************************
1110 ! **** VARIABLE RANGE *****
1120 ! *************************
1130 !
1140 CLEAR @ DISP USING 1150
1150 IMAGE 3/,"INPUT CONCENTRATI
     ON IN MOLE FRAC"
1160 INPUT C9
1170 P9=2.7*10^19*C9
1180 DISP !
1190 DISP "INPUT # OF F3 VALUES"
1200 INPUT Z5
1205 IF Z5>5 THEN GOTO 1200
1210 FOR I=1 TO Z5
1220 DISP !
1230 DISP "INPUT F3 VALUE [P/nm^
     4 sec]"
1240 INPUT F3(I)
1250 F3=F3(I)
1260 !
1270 !
1280 !
1290 FOR R5=1 TO 30
1295 R4=R5*100 ! CHG TO cm
1300 R1=R4-50 ! NEAR RG
1310 R2=R4+50 ! FAR  RG
1320 R9=1/R1-1/R2
1330 S(I,R5)=F3*A*R9*P9*D9*F9^4*
     T
1340 IF Z3=2 THEN S(I,R5)=SQR(S(
     I,R5))
1350 NEXT R5
1360 NEXT I
1370 !
1380 !
1390 !
1400 !
1410 ! ********** PLOTTING *****
1420 !
1430 DISP "INPUT UPPER LIMIT ","
     FOR THE YAXIS"
1440 INPUT L2
1441 L1=LGT(1)
1442 L2=LGT(L2)
1450 !
1460 GOSUB 2500 ! PRINT ROUTINE
1470 !
1480 GCLEAR
1490 SCALE LGT(1),LGT(30),L1,L2
1500 XAXIS L1,.5
1510 YAXIS LGT(1),.5
1515 YAXIS LGT(30),! ! snr axis
1520 !
1530 !
1540 !
1550 !
1560 FOR I=1 TO Z5
1570 L9=LGT(S(I,2))
1580 MOVE LGT(1),L9
1590 FOR R5=1 TO 30
1600 L9=LGT(S(I,R5))
1610 PLOT LGT(R5),L9
1620 NEXT R5
1630 NEXT I
1631 !
1632 FOR R5=1 TO 30 STEP 2
1633 L9=LGT(S(Z5,R5))
1634 MOVE LGT(R5),L9
1635 PLOT LGT(R5),L9
1636 PLOT LGT(R5),L2
1637 MOVE LGT(R5),L9
1638 PLOT LGT(R5),L9
1639 PLOT LGT(30),L9
1640 NEXT R5
1650 PAUSE
1660 CLEAR @ DISP USING 1670
1670 IMAGE 6/,"CHANGE AXIS ?[Y/N
     ]"
1680 INPUT Z$
1690 IF Z$="Y" THEN GOTO 1410
1700 GRAPH
1710 COPY
1720 PRINT USING 1730
1730 IMAGE 5/
1740 !
1750 END
1760 !
1770 !
1780 !
1790 !
1800 !
1810 !
1820 ! ************************
1830 ! VARIABLE CONCENTRATION
1840 ! ************************
1850 !
1860 CLEAR @ DISP USING 1870
1870 IMAGE 3/,"INPUT RANGE (m)"
1880 INPUT R5
1890 R5=R5*100 ! CHG TO cm
1900 R1=R5-50 ! NEAR RG
```

```
1910 R2=R5+50 ! FAR  RG
1920 R9=1/R1-1/R2
1930 !
1940 DISP !
1950 DISP "INPUT # OF F3 VALUES"
1960 INPUT Z5
1970 FOR I=1 TO Z5
1980 DISP "  INPUT F3 VALUE [P/n
     m^4 sec]"
1990 INPUT F3(I)
2000 F3=F3(I)
2010 !
2020 FOR C1=1 TO 50
2030 C9=C1/1000 ! CHG TO MOLE FR
     AC
2040 P9=2.7*10^19*C9
2050 S(I,C1)=F3*A*R9*P9*D9*F9^4*
     T
2060 IF Z3=2 THEN S(I,C1)=SQR(S(
     I,C1))
2070 NEXT C1
2080 NEXT I
2090 !
2100 ! ******** PLOTTING *******
2110 CLEAR
2120 DISP "INPUT UPPER LIMIT ","
      FOR YAXIS"
2130 INPUT L2
2131 L1=LGT(1)
2132 L2=LGT(L2)
2140 !
2150 GOSUB 2500 ! PRINT ROUTINE
2160 !
2170 GCLEAR
2180 SCALE LGT(.1),LGT(5),L1,L2
2190 XAXIS L1,.5
2200 YAXIS LGT(.1),.5
2205 YAXIS LGT(5),1 ! snr axis
2210 !
2220 !
2230 !
2240 !
2250 FOR I=1 TO Z5
2260 L9=LGT(S(I,1))
2270 MOVE LGT(.1),L9
2280 !
2290 FOR C1=1 TO 50
2300 L9=LGT(S(I,C1))
2310 PLOT LGT(C1/10),L9
2320 NEXT C1
2330 NEXT I
2331 !
2332 FOR C1=1 TO 50
2333 L9=LGT(S(Z5,C1))
2334 MOVE LGT(C1/10),L9
2335 PLOT LGT(C1/10),L9
2336 PLOT LGT(C1/10),L2
2337 MOVE LGT(C1/10),L9
2338 PLOT LGT(C1/10),L9
2339 PLOT LGT(1/10),L9
2340 NEXT C1
2350 PAUSE
2360 CLEAR @ DISP USING 2370
2370 IMAGE 5/,"CHANGE AXIS [Y/N]
     "
2380 INPUT Z$
2390 IF Z$="Y" THEN GOTO 2100
2400 GRAPH
2410 COPY
2420 PRINT USING 2430
2430 IMAGE 5/
2440 !
2450 END
2460 !
2470 !
2480 !
2490 !
2500 ! ***********************
2510 ! ***  PRINT SUBROUTINE ***
2520 ! ***********************
2530 !
2540 IF Z9=1 THEN PRINT "*******
      PLOT FOR METHANE *******"
2550 IF Z9=2 THEN PRINT "*******
      PLOT FOR NITROGEN ******"
2560 PRINT !
2570 IF Z8=1 THEN PRINT "** VARI
     ABLE CONC        [.10%-5%]"
2580 IF Z8=1 THEN PRINT "** FIXE
     D RANGE OF :  ";R5/100;"MET
     ERS"
2590 IF Z8=2 THEN PRINT "** VARI
     ABLE RANGE       [1m - 30m]"
2600 IF Z8=2 THEN PRINT "** FIXE
     D CONCENTRATION: ";C9*100;"
     %"
2610 PRINT !
2620 FOR I=1 TO Z5
2630 PRINT USING 2640 ; F3(I)
2640 IMAGE "** LASER FUNCTION :"
     ,3X,D.DDDE
2650 NEXT I
2660 PRINT !
2670 PRINT USING 2690 ; 10^L1,10
     ^L2
2690 IMAGE "** YAXIS :",1X,D.DE,
     1X,"TO",1X,D.DE,3/
2700 IF Z3=1 THEN PRINT ".......
     ....  PLOT OF S ..........."
2710 IF Z3=2 THEN PRINT ".......
     . PLOT OF ROOT S ........"
2720 PRINT USING 2730
2730 IMAGE 4/
2740 RETURN
2741 !
2742 ! **********************
2743 ! LASER FUNC AS TYPE
2744 ! **********************
2750 CLEAR
2810 CLEAR
```

```
2820 DISP "# IN THIS GROUP [999]
      to exit "
2830 INPUT G
2940 IF G=999 THEN GOTO 880
2850 DISP "ENTER 10 WORD LASER I
     D"
2860 INPUT L$
2861 PRINT USING 2962 ; L$
2862 IMAGE 2/,"******  ",10A," L
     ASER  ******",/
2863 PRINT !
2870 !
2871 PRINT "WAVE  ! PULSE  !PRF
      !  LASER   "
2872 PRINT "LENGTH! ENERGY !
      !FUNCTION  "
2873 PRINT " (nm) !  (J)   !(Hz)
      !(nm-4/sec)"
2874 PRINT "--------------------
     ------------"
2875 PRINT !
2880 E8=.25 @ T9=.9 @ T8=.1 @ H9
     =1.987*10^-16
2890 !
2900 FOR J=1 TO G
2910 DISP "  λ(nm)   P.ENERGY(J)
        PRF(Hz)"
2920 INPUT L8(J),E9(J),P8(J)
2930 F3(J)=E9(J)*E8*T9*T8*P8(J)/
     (H9*L8(J)^3)
2940 NEXT J
2950 FOR J=1 TO G
2960 PRINT USING 2970 ; L8(J),E9
     (J),P8(J),F3(J)
2970 IMAGE 1X,DDDD,2X,D.DE,X,DDD
     ,3X,D.DDE
2980 NEXT J
2990 GOTO 2810
```

APPENDIX 2: SUMMARY OF OPTO-ELECTRONICS LTD. PHOTODIODES

Model	Type	Area	NEP	Risetime	FWHM
CD20	Ge	.1x.13mm		250 ps	400 ps
GD20	Ge	.1x.13mm	5.7x10-13W/Hz	100 ps	
GD10	Ge	.5x.5mm	1.8x10-12W/Hz	180 ps	
GD8	Ge	1.0x1.0mm	2.5x10-12w/Hz	250 ps	

The above are sensitive in the 500-1800 nm range with peak sensitivity at 1500 nm.

APPENDIX 3: LONG PASS FILTER CHARACTERISTCS

ABSORPTION FILTER TRANSMITTANCE

FIGURE 4. ULTRAVIOLET TRANSMITTANCE CURVES-PLEXIGLAS MOLDING PELLETS*

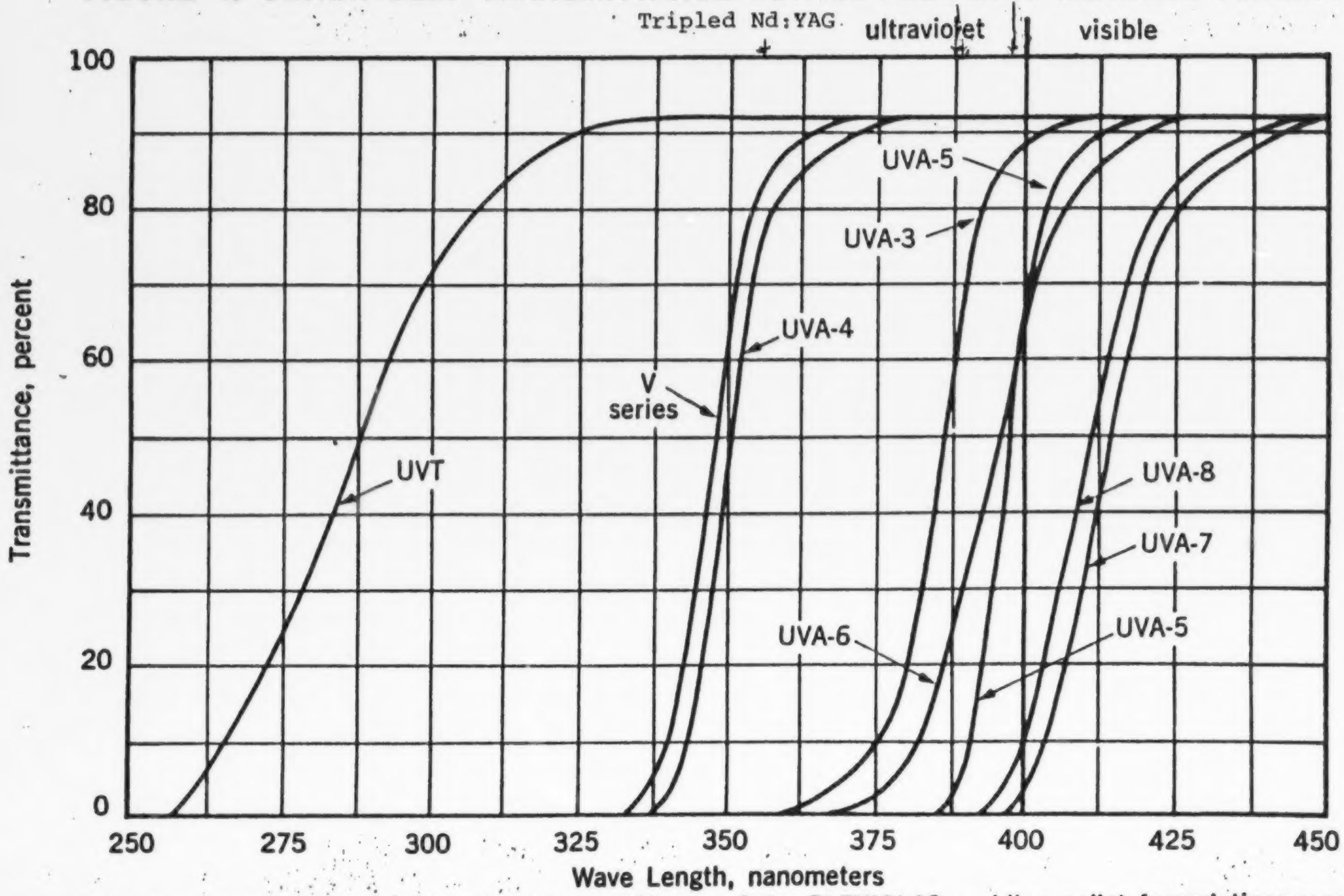

*Curves are for .125" thick samples. Ultraviolet transmittance of the PLEXIGLAS molding pellet formulations vary with thickness. UVA-7 in .060" thickness has the same ultraviolet transmittance as .125" thick UVA-8.

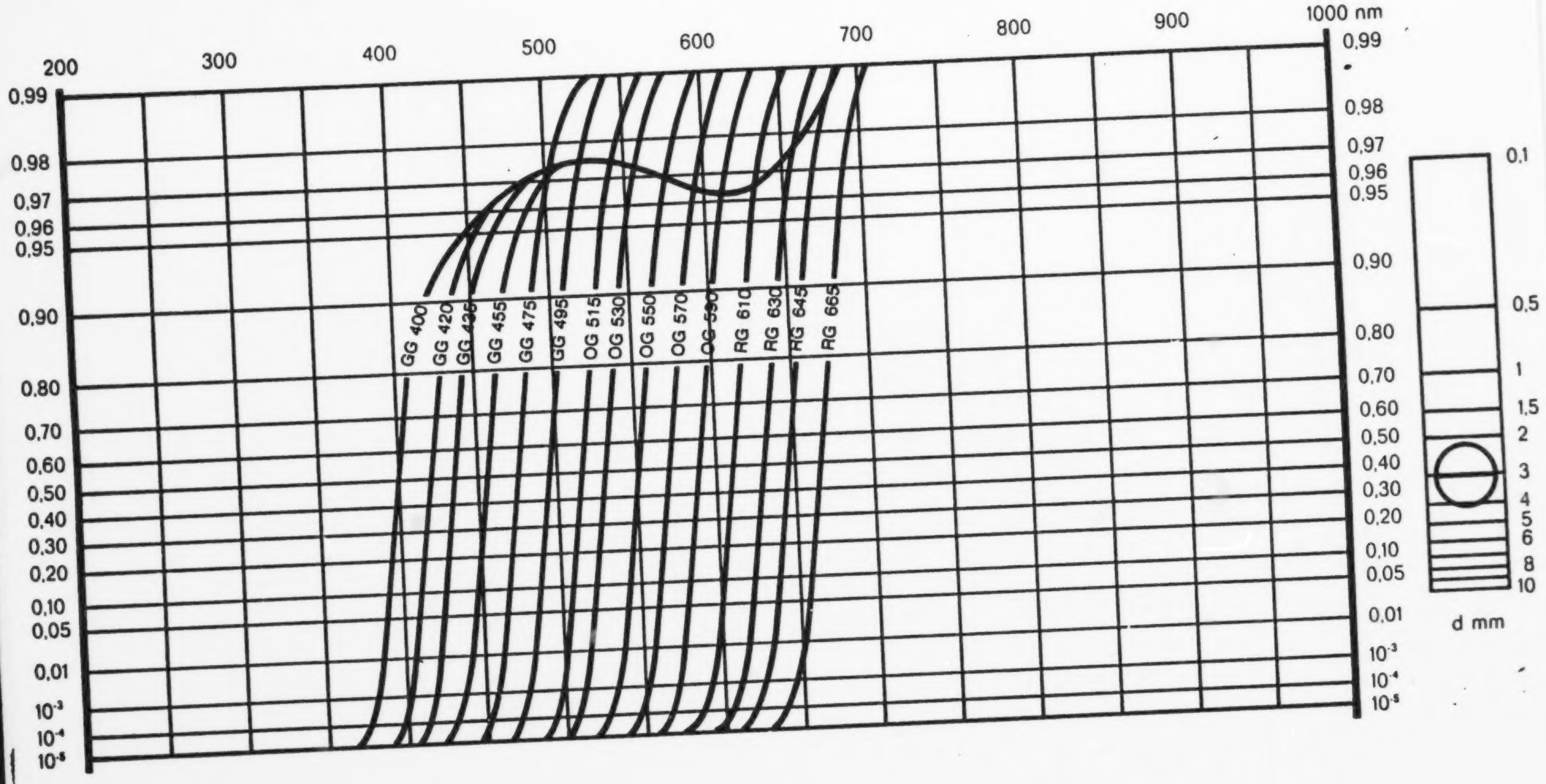
200
300
400
500
600
700
800
900
1000 nm
0,99
0,98
0,97
0,96
0,95
0,90
0,80
0,70
0,60
0,50
0,40
0,30
0,20
0,10
0,05
0,01
10^{-3}
10^{-4}
10^{-5}
GG 400
GG 420
GG 435
GG 455
GG 475
GG 495
OG 515
OG 530
OG 550
OG 570
OG 590
RG 610
RG 630
RG 645
RG 665
0,1
0,5
1
1,5
2
3
4
5
6
8
10
d mm

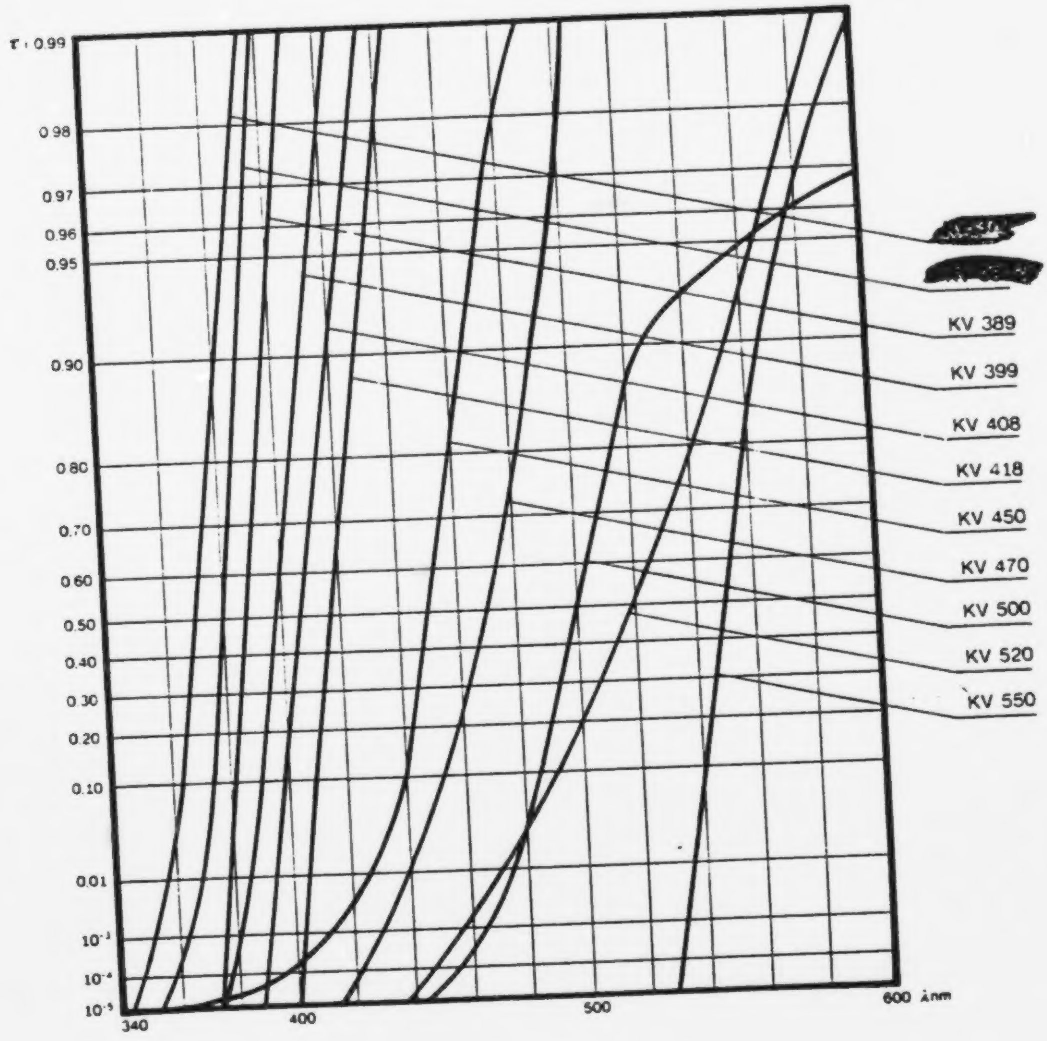
τ: 0.99
0.98
0.97
0.96
0.95
0.90
0.80
0.70
0.60
0.50
0.40
0.30
0.20
0.10
0.01
10⁻³
10⁻⁴
10⁻⁵
340
400
500
600 λnm
[redacted]
[redacted]
KV 389
KV 399
KV 408
KV 418
KV 450
KV 470
KV 500
KV 520
KV 550

DIELECTRIC LONG PASS FILTER

interoptics limited 17 GRENFELL CRESCENT, OTTAWA, ONTARIO, CANADA K2G 0G3 TELEPHONE: (613) 224-4868

February 12, 1986

Mr. A. Hollinger
Moniteq Limited
630 Rivermead Road
Concord, Ontario
L4K 2H7

RECEIVED FEB 17 1986

Dear Mr. Hollinger:

As we discussed by telephone please find the enclosed data for a long wave pass filter.

If more information is needed, please do not hesitate to contact me.

Yours truly,

J R Wimperis

J. R. Wimperis,
President.

25° "S"

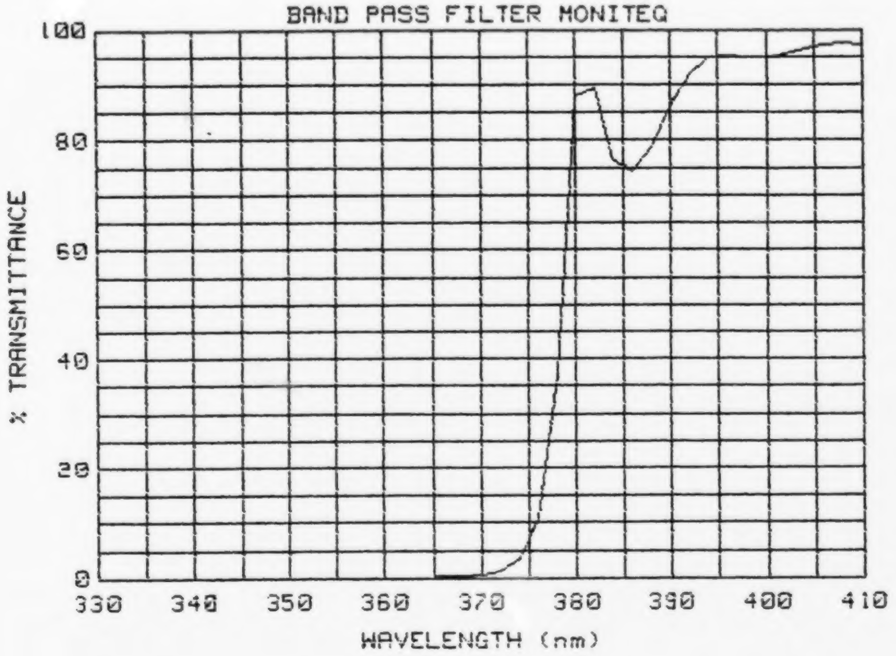
BAND PASS FILTER MONITEQ
% TRANSMITTANCE
100
80
60
40
20
0
330
340
350
360
370
380
390
400
410
WAVELENGTH (nm)

25° "S"

```
WAVE(nm)    %R       %T       Rphase     Tphase
  330.0   100.00    0.00    -138.97     -39.13
  332.0   100.00    0.00    -136.54     -36.33
  334.0   100.00    0.00    -134.08     -33.51
  336.0   100.00    0.00    -131.58     -30.69
  338.0   100.00    0.00    -129.03     -27.82
  340.0   100.00    0.00    -126.40     -24.91
  342.0   100.00    0.00    -123.68     -21.94
  344.0   100.00    0.00    -120.87     -18.89
  346.0   100.00    0.00    -117.93     -15.75
  348.0   100.00    0.00    -114.86     -12.50
  350.0   100.00    0.00    -111.62      -9.13
  352.0    99.99     .01    -108.19      -5.60
  354.0    99.99     .01    -104.53      -1.90
  356.0    99.99     .01    -100.62       2.01
  358.0    99.98     .02     -96.39       6.17
  360.0    99.97     .03     -91.79      10.62
  362.0    99.95     .05     -86.73      15.43
  364.0    99.92     .08     -81.08      20.71
  366.0    99.85     .15     -74.70      26.57
  368.0    99.71     .29     -67.32      33.21
  370.0    99.40     .60     -58.54      40.96
  372.0    98.63    1.37     -47.64      50.40
  374.0    96.43    3.57     -33.20      62.65
  376.0    89.14   10.86     -11.86      80.36
  378.0    62.77   37.23      25.29     109.92
  380.0    11.80   88.20     103.83     157.91
  382.0    10.55   89.45    -105.07    -157.03
  384.0    23.33   76.67     -52.87    -127.11
  386.0    25.77   74.23     -19.39    -103.61
  388.0    21.17   78.83      12.51     -81.49
  390.0    13.92   86.08      48.22     -59.14
  392.0     7.93   92.07      91.60     -36.61
  394.0     5.10   94.90     143.61     -14.63
  396.0     4.75   95.25    -165.28       6.23
  398.0     5.13   94.87    -123.49      25.90
  400.0     5.10   94.90     -88.40      44.65
  402.0     4.40   95.60     -55.41      62.76
  404.0     3.41   96.59     -20.58      80.53
  406.0     2.63   97.37      18.74      98.02
  408.0     2.45   97.55      61.13     115.17
  410.0     2.89   97.11      99.97     131.89
```

25° "S"

Tmin 0.004%   Tmax 0.012%   Tave 0.008%   (350 - 356 nm)

15° "P"

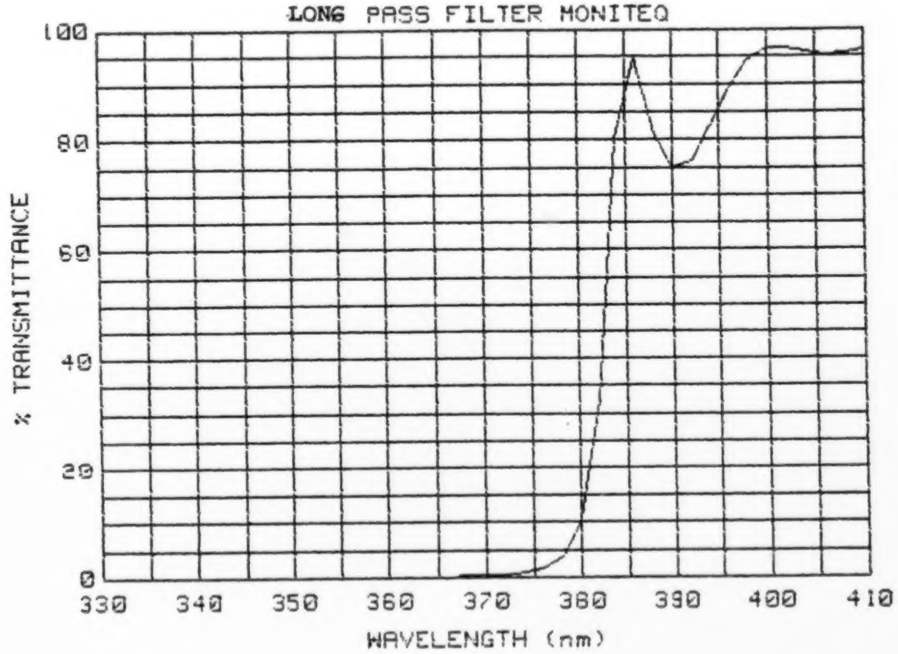
LONG PASS FILTER MONITEQ
100
80
60
40
20
0
% TRANSMITTANCE
330
340
350
360
370
380
390
400
410
WAVELENGTH (nm)

15° "p"

WAVE(nm)	%R	%T	Rphase	Tphase
330.0	99.99	.01	-145.00	-47.90
332.0	99.99	.01	-142.21	-44.69
334.0	99.99	.01	-139.45	-41.53
336.0	99.99	.01	-136.72	-38.43
338.0	100.00	0.00	-133.97	-35.34
340.0	100.00	0.00	-131.19	-32.25
342.0	100.00	0.00	-128.37	-29.14
344.0	100.00	0.00	-125.49	-26.00
346.0	99.99	.01	-122.54	-22.81
348.0	99.99	.01	-119.50	-19.55
350.0	99.99	.01	-116.36	-16.22
352.0	99.99	.01	-113.07	-12.79
354.0	99.99	.01	-109.64	-9.23
356.0	99.99	.01	-106.04	-5.54
358.0	99.98	.02	-102.22	-1.69
360.0	99.98	.02	-98.17	2.36
362.0	99.97	.03	-93.82	6.64
364.0	99.95	.05	-89.12	11.20
366.0	99.92	.08	-83.99	16.11
368.0	99.87	.13	-78.33	21.45
370.0	99.79	.21	-71.98	27.34
372.0	99.61	.39	-64.73	33.98
374.0	99.24	.76	-56.22	41.64
376.0	98.38	1.62	-45.82	50.83
378.0	96.13	3.87	-32.37	62.54
380.0	89.46	10.54	-13.27	78.86
382.0	67.78	32.22	17.83	104.63
384.0	19.75	80.25	76.23	146.34
386.0	4.96	95.04	-131.52	-168.51
388.0	18.74	81.26	-64.57	-136.79
390.0	25.20	74.80	-31.46	-113.26
392.0	23.69	76.31	-3.16	-92.30
394.0	17.70	82.30	26.26	-71.57
396.0	10.69	89.31	60.26	-50.42
398.0	5.56	94.44	102.94	-29.18
400.0	3.43	96.57	156.52	-8.50
402.0	3.47	96.53	-151.18	11.13
404.0	4.19	95.81	-110.36	29.73
406.0	4.59	95.41	-77.24	47.50
408.0	4.38	95.62	-46.94	64.71
410.0	3.72	96.28	-16.32	81.57

15° "P"

Tmin 0.006%   Tmax 0.012%   Tave 0.009%   (350 - 356 nm)

15° "S"

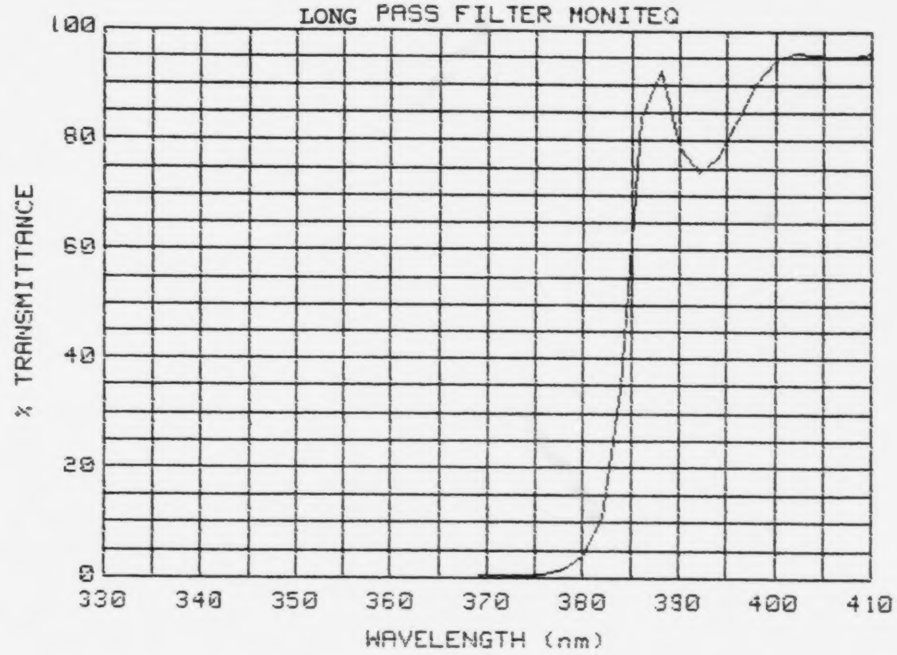
LONG PASS FILTER MONITEQ
100
80
60
40
20
0
% TRANSMITTANCE
330
340
350
360
370
380
390
400
410
WAVELENGTH (nm)

15° "S"

WAVE(nm)	%R	%T	Rphase	Tphase
330.0	100.00	0.00	-145.87	-48.09
332.0	100.00	0.00	-143.32	-45.10
334.0	100.00	0.00	-140.79	-42.16
336.0	100.00	0.00	-138.27	-39.26
338.0	100.00	0.00	-135.74	-36.36
340.0	100.00	0.00	-133.17	-33.47
342.0	100.00	0.00	-130.57	-30.55
344.0	100.00	0.00	-127.91	-27.60
346.0	100.00	0.00	-125.18	-24.61
348.0	100.00	0.00	-122.37	-21.55
350.0	100.00	0.00	-119.46	-18.43
352.0	100.00	0.00	-116.43	-15.21
354.0	99.99	.01	-113.26	-11.89
356.0	99.99	.01	-109.94	-8.45
358.0	99.99	.01	-106.43	-4.87
360.0	99.99	.01	-102.71	-1.11
362.0	99.98	.02	-98.74	2.84
364.0	99.97	.03	-94.46	7.04
366.0	99.96	.04	-89.82	11.52
368.0	99.94	.06	-84.74	16.36
370.0	99.90	.10	-79.11	21.64
372.0	99.82	.18	-72.77	27.49
374.0	99.66	.34	-65.47	34.09
376.0	99.31	.69	-56.86	41.76
378.0	98.48	1.52	-46.26	51.03
380.0	96.24	3.76	-32.38	62.94
382.0	89.26	10.74	-12.31	79.83
384.0	65.56	34.44	21.33	107.16
386.0	15.84	84.16	87.71	151.52
388.0	7.33	92.67	-118.28	-163.31
390.0	21.10	78.90	-59.67	-132.57
392.0	25.87	74.13	-26.71	-109.27
394.0	23.01	76.99	2.81	-88.01
396.0	16.35	83.65	34.47	-66.75
398.0	9.56	90.44	71.94	-45.11
400.0	5.30	94.70	118.84	-23.62
402.0	3.98	96.02	172.29	-2.99
404.0	4.29	95.71	-140.51	16.54
406.0	4.80	95.20	-102.99	35.06
408.0	4.76	95.24	-70.58	52.84
410.0	4.15	95.85	-39.20	70.16

15° "S"

Tmin 0.003%   Tmax 0.007%   Tave 0.005%   (350 - 356 nm)

5° "R"

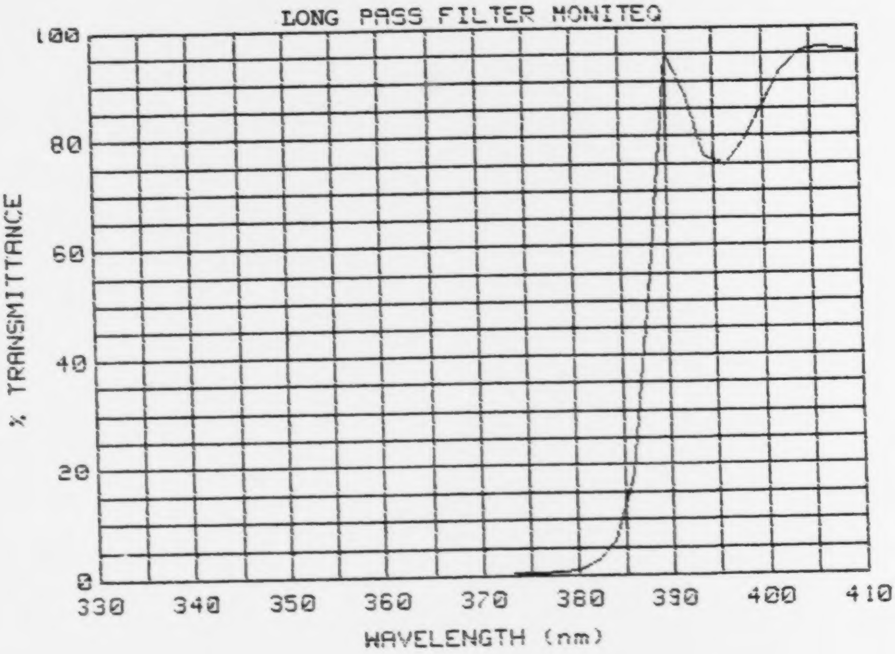
LONG PASS FILTER MONITEQ
% TRANSMITTANCE
100
80
60
40
20
0
330
340
350
360
370
380
390
400
410
WAVELENGTH (nm)

5° "R"

WAVE(nm)	%R	%T	Rphase	Tphase
330.0	99.99	.01	.04	-.03
332.0	99.99	.01	.07	-0.00
334.0	99.99	.01	.10	.03
336.0	99.99	.01	.13	.05
338.0	100.00	0.00	.15	.07
340.0	100.00	0.00	.17	.09
342.0	100.00	0.00	.20	.12
344.0	100.00	0.00	.22	.14
346.0	100.00	0.00	.24	.16
348.0	100.00	0.00	.27	.18
350.0	100.00	0.00	.29	.20
352.0	100.00	0.00	.32	.22
354.0	99.99	.01	.34	.25
356.0	99.99	.01	.37	.27
358.0	99.99	.01	.40	.30
360.0	99.99	.01	.43	.32
362.0	99.99	.01	.47	.35
364.0	99.98	.02	.50	.39
366.0	99.97	.03	.54	.42
368.0	99.96	.04	.59	.46
370.0	99.94	.06	.65	.51
372.0	99.91	.09	.71	.56
374.0	99.85	.15	.79	.63
376.0	99.73	.27	.89	.72
378.0	99.48	.52	1.02	.84
380.0	98.94	1.06	1.22	1.00
382.0	97.59	2.41	1.53	1.27
384.0	93.82	6.18	2.09	1.74
386.0	81.77	18.23	3.26	2.70
388.0	45.34	54.66	5.85	4.36
390.0	4.89	95.11	17.47	4.56
392.0	12.58	87.42	5.84	2.98
394.0	23.62	76.38	3.15	2.16
396.0	25.46	74.54	2.61	1.89
398.0	21.16	78.84	2.59	1.83
400.0	14.23	85.77	2.82	1.82
402.0	7.97	92.03	3.35	1.78
404.0	4.45	95.55	4.13	1.69
406.0	3.61	96.39	4.17	1.58
408.0	4.11	95.89	3.45	1.48
410.0	4.66	95.34	2.91	1.39

5° "R"

Tmin 0.004%   Tmax 0.006%   Tave 0.005%   (350 - 356 nm)

25° "P"

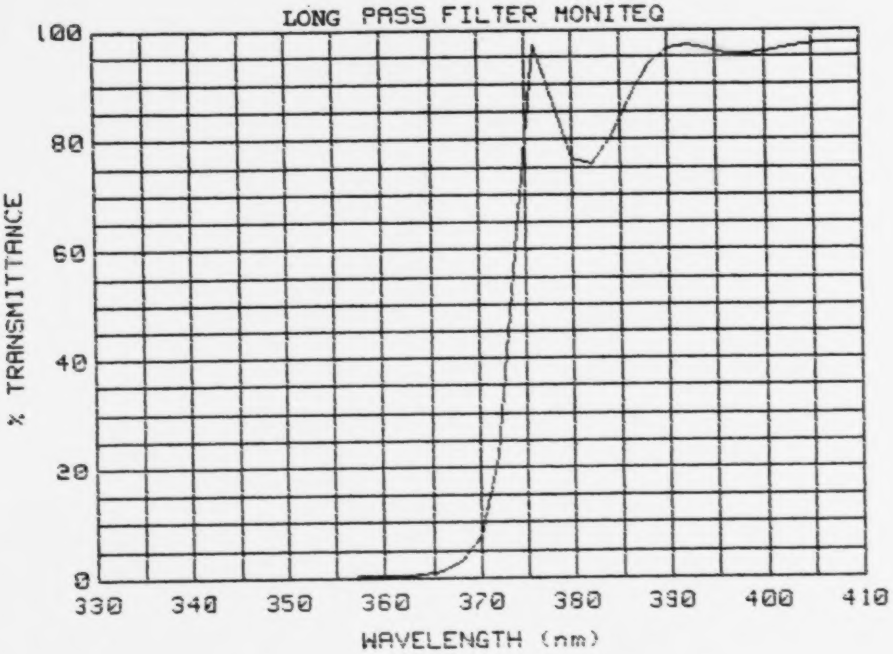
LONG PASS FILTER MONITEQ
% TRANSMITTANCE
100
80
60
40
20
0
330
340
350
360
370
380
390
400
410
WAVELENGTH (nm)

25° "P"

WAVE(nm)	%R	%T	Rphase	Tphase
330.0	99.99	.01	-134.22	-36.54
332.0	99.99	.01	-131.17	-33.17
334.0	99.99	.01	-128.09	-29.79
336.0	99.99	.01	-124.97	-26.41
338.0	99.99	.01	-121.78	-22.99
340.0	99.99	.01	-118.50	-19.50
342.0	99.99	.01	-115.12	-15.94
344.0	99.99	.01	-111.60	-12.27
346.0	99.98	.02	-107.92	-8.49
348.0	99.98	.02	-104.06	-4.56
350.0	99.97	.03	-99.98	-.45
352.0	99.96	.04	-95.61	3.89
354.0	99.95	.05	-90.93	8.48
356.0	99.92	.08	-85.85	13.40
358.0	99.88	.12	-80.29	18.71
360.0	99.80	.20	-74.12	24.53
362.0	99.65	.35	-67.13	31.01
364.0	99.35	.65	-59.03	38.42
366.0	98.67	1.33	-49.33	47.15
368.0	97.01	2.99	-37.11	57.98
370.0	92.34	7.66	-20.47	72.49
372.0	77.59	22.41	5.10	94.30
374.0	36.72	63.28	50.26	130.18
376.0	2.84	97.16	163.89	176.88
378.0	13.48	86.52	-78.70	-146.73
380.0	23.44	76.56	-41.18	-121.09
382.0	24.47	75.53	-12.68	-99.53
384.0	19.72	80.28	15.36	-78.76
386.0	12.64	87.36	46.64	-57.65
388.0	6.50	93.50	85.03	-36.21
390.0	3.25	96.75	136.19	-15.06
392.0	2.73	97.27	-165.20	5.22
394.0	3.50	96.50	-118.35	24.44
396.0	4.25	95.75	-82.91	42.72
398.0	4.41	95.59	-52.34	60.33
400.0	3.97	96.03	-22.72	77.50
402.0	3.26	96.74	8.25	94.33
404.0	2.63	97.37	42.01	110.93
406.0	2.30	97.70	77.87	127.23
408.0	2.30	97.70	112.76	143.21
410.0	2.48	97.52	143.79	158.83

25° "P"

Tmin 0.025%   Tmax 0.076%   Tave 0.047%   (350 - 356 nm)

APPENDIX 4: COLLECTED LITERATURE (Separate Volumes)

A: Articles Related to Raman Scattering Techniques

B: Articles Related to Acousto-optic Tunable Filters

C: Articles Related to Differential Absorption Techniques

D: Information on Laser Sources

E: Information on UV/IR Detectors

F: Information Concerning Properties of Methane and Coal

G: Miscellaneous Systems and Techniques

REFERENCES

1) Herzberg, G., Molecular Spectra and Moleculin Structure II.

2) Bermejo, D., et al, J. Mol. Spect., Vol. 65, 345, (1977).

3) Grant, W.B., Private Communication (1984).

4) Chan, K., et al, App. Optics, Vol. 23, 3415 (1984).

5) Chan, K., et al, App. Optics, Vol. 22, 3802 (1983).

6) Infrared Handbook.

7) Litton, C.D., Remote Measurement of Methane in Underground Mines, Presented at the Topical Meeting on Remote Sensing of the Atmosphere (1985).

8) Everett, P., A. Flushberg, I. Itzkhan, H. Kent, Raman Scattering for Measuring Methane at a Coal Face, Avco Everett Research Laboratory, Everett, MA. (1981).

9) Ryan, F., Westinghouse Electric Corp., Private Communication.

10) DeFrey, R.K., Remote Dial Measurements of Methane in Coal Mines, Presented at the Topical Meeting on Optical Remote Sensing of the Atmosphere (1985).

11) Byer, R.L., Garbuny, M., Pollutant Detector by Absorption Using Mie Scattering and Topographic Targets as Retroreflectors, App. Optics, Vol. 12, 1496, (1973).

12) McClatchie, E.A., The Development of a Methane Monitor for Use in Electric Face Equipment in Underground Mines, Bo Mines OFR 80-78, Andros Inc., (1976).

13) Smith, R., A.I. Carswell, App. Optics, Vol. 25, 398, (1986).

14) Lamberts, C.W., I.H. Dekkler, Raman Lidar a Feasibility Study, Physics Laboratory of the National Defense Research Organization, Report No. PH21975-49, (1975).

15) Laser Focus/Electrooptics Buyers Guide, Pennwell Publishing Co., Littleton, MA., (1985).

16) American National Standard for the Safe Use of Lasers, ANSI Z136-1-1980.

17) Ottenjann, K., M. Teichmuller, M. Wolf, Coll. Ont. Petrographic de la matiere organiqu des sediment.

18) Hershberg, M., K.L. Cashdollar and J.L. Opferman, The Flammability of Coal Dust - Air Mixtures, Bureau of Mines Report of Investigation 8360 (1979); described in Avco Everett Report (Ref. 8), p87.

19) Hoge, F.E., R.N. Swift, Oil Film Thickness Measurement Using Airborne Laser-Induced Water Raman Backscatter, App. Optics, Vol. 19, 3269 (1980).